The influence of land subsidence on pluvial flooding in Rotterdam

J.H. Vleugels

TU Delft

The influence of land subsidence on pluvial flooding in Rotterdam

MSC. THESIS

by

J.H. Vleugels

to obtain the degree of Master of Science
at the Delft University of Technology,
to be defended publicly on Friday August 9, 2019

Student number:	4224221	
Project duration:	October , 2018 – August , 2019	
Thesis committee:	Dr. ir. J. A. E. ten Veldhuis,	TU Delft, Water Resources Management
	Prof. dr. ir. R. F. H. Hanssen,	TU Delft, Geoscience and Remote Sensing
	Dr. ir. F. H. M. van de Ven,	TU Delft, Water Resources Management
	Ir. J. N. Pieneman,	City of Rotterdam
	Msc. A. van 't Veld,	Nelen & Schuurmans

This thesis is confidential and cannot be made public until September 1, 2019.

An electronic version of this thesis is available at `http://repository.tudelft.nl/`.

TU Delft

Abstract

In the Netherlands, the Delta Programme aspires to adjust spatial planning climate-proof and water-resilient, in order to be prepared for extreme weather in 2050. To achieve this ambition, municipalities, provinces, regional water authorities and central governments conduct stress tests to map out the vulnerabilities in their areas of authority by no later than 2019. The stress tests comprise four themes: pluvial flooding, drought, heat and floods. In addition, the Delta Programme 2019 acknowledges the mitigation of and adaptation to land subsidence as an important tasking. The municipality of Rotterdam faces the challenge of adding land subsidence as stress test theme and assessing its influence on pluvial flooding. Contrary to the stress test pluvial flooding, no consended methodology exist on how to map out vulnerabilities concerning land subsidence. In addition, only few studies have numerically investigated the spatial-temporal effect of land subsidence on pluvial flooding in urban areas. However, the advent of techniques to measure ground level (LiDAR) and land subsidence (InSAR) and advances in high resolution flood modelling (3Di) enable the numerical modelling of urban pluvial flooding influenced by land subsidence. This research explores the investigation of the influence of land subsidence on pluvial flooding in Rotterdam by supplementing the conducted stress test pluvial flooding with a land subsidence assessment. The conducted stress test pluvial flooding in Rotterdam is based on a 3Di-simulation of standardised rain events, based on a DEM 2016.

To asses the current influence of land subsidence on pluvial flooding, a Digital Elevation Model (DEM) that approximates the sub-neighbourhood Tuinenhoven at design level is created and used as 3Di-input. When comparing 3Di-results based on this design DEM to the stress test pluvial flooding, it becomes clear that the total volume of water during extreme rainfall stored on the streets is not affected by land subsidence. The bathymetry of the DEM does affect the water's distribution however. The Tuinenhoven case-study demonstrates that currently land subsidence increases the severity of the impact of pluvial flooding but that the main cause of pluvial flooding during extreme rainfall is the limited capacity of the drainage system.

Land subsidence in Rotterdam complex. The conducted land subsidence analysis based on an InSAR data-set supports this complexity. It illustrates that the subsidence behaviour of Rotterdam is influenced by foundation type, land use classification, the presence of dredge in the anthropogenic layer and top soil type. This respectively indicates the occurrence of pole rot and shallow foundations, anthropogenic compression and compaction of shallow soft layers caused by loading, landfill subsidence as a result of land fillings that contain dredging spoil and consolidation of the Holocene clay layer as a result of drainage. However, the land subsidence analysis failed to identify location-specific dominant land subsidence processes. This failure was primarily caused by the limitation to only one linear subsidence rate between 2009 and 2014 per point. To demonstrate how land subsidence can be translated to pluvial flooding based on a land subsidence analysis, land use classification was selected as the most dominant influencing factor and used in a linear land subsidence prognosis until 2030. The linear assumptions largely obstructs results to be interpreted location-specific.

The IJsselmonde case-study shows that land subsidence is expected to decrease the passability of roads and decrease the risk per building in the future. These decreases are caused by the fact that roads relatively subside fast and buildings relatively slow. The biggest influence on the risk per building classification is the assumed threshold value per building. Simulated road maintenance results in an increase of the passability of roads and an increase of buildings at risk of water nuisance. The loss of the water-storing function of the road after reconstruction increases the water levels in gardens and puts buildings at an increasing risk.

In conclusion, the most challenging part of investigating the influence of land subsidence on pluvial flooding is the crucial identification of the different occurring land subsidence processes. It is demonstrated that the possibilities with InSAR-data are promising, when used with sufficient competency, although the available InSAR data should be divided in shorter intervals to detect the subsidence rate trends. Land subsidence rate trends are crucial in the identification of land subsidence processes and assessing influences like groundwater variations and increased loading due to maintenance or construction works. When the land subsidence analysis is improved, so will the land subsidence and threshold height per building prognosis. When the relative prognosed decrease of the threshold value per building is improved, it can be quickly assessed whether buildings classified at risk in the stress test pluvial flooding are at future increasing risk during extreme rainfall, without conducting a full 3Di-simulation.

Preface

This report is produced in the context of a Master Thesis by Jef Vleugels as a conclusion of the Msc. Civil Engineering (track Water Management) at Delft University of Technology. Guidance is provided by the municipality of Rotterdam, by Jorg Pieneman, together with consultancy firm Nelen & Schuurmans, by Arnold van 't Veld. I would like to thank both for giving me the opportunity for this double internship. Their expertise and attitude helped me a lot during my thesis and I always liked our meetings. Jorg helped me to unravel the political context of my subject and by demanding a structured approach, especially in the beginning of my thesis. Arnold taught me a lot in the programming part of my thesis and how to be inventive. I want to thank them especially for giving me the trust to move around freely between Utrecht, Rotterdam and Delft. This triple cooperation was new to them and I believe that I answered their trust with discipline. Next to leaving out work-place-restrictions, it was possible for me to visit conferences, presentations and additional classes in 3Di and InSAR. Additionally, I would like to thank all colleagues of Jorg and Arnold. In the absence of Jorg and Arnold they were always helpful, interested and, above all, gezellig. On top of my thesis, this double internship taught me a lot with regard to my future career.

The chair of the TU Delft assessment committee is Marie-Claire ten Veldhuis. Just like her previous guidance during a previous internship of mine, I would like to thank Marie-Claire for her help and her critical feedback. She helped me to translate a practical problem in a practical-oriented internship in a scientific paper. I learned a lot from her about scientific writing and critically regarding the stress test scenarios. The assessment committee is completed by Frans van de Ven and Ramon Hanssen. Being team leader of the living lab land subsidence in the city centre of Gouda, Frans' expertise matched this thesis perfectly. His comments and feedback during the kick-off-, mid-term- and green-light-meeting were very useful. Ramon helped me most with the use of InSAR-data and assessing it scientifically. This method was totally new to me and remote-sensing is not a working field extensively addressed in my Master's curriculum. Being a pioneer in the development of InSAR data, his expertise was immense and of great help.

Help that appeared half-way through this thesis came from SkyGEO, who processed and delivered InSAR data to the city of Rotterdam. Questions per mail about this data-set resulted in several welcoming meetings where Martijn Houtepen, Johannes Smit and Hanno Maljaars helped me with all my questions.

Furthermore, I would like to thank my roommates for their support and, not in the last place, keeping me fed. Additionally, my fellow-students in hokje 1 deserve a word of thank. Moments of coffee, laughing and sparring were very much appreciated. It goes without saying that I am thankful to my parents and family. Without them, studying in Delft would not have been as carefree as my past 7 years. My last word of thank goes out to Eva. Who had to endure my moments of rancour and dullness. It was inspiring how she helped me and tried to ease my mind unconditionally.

With pride I present to you my Msc. thesis. I hope you enjoy reading it.

J.H. Vleugels
Delft, August 2019

Contents

List of Figures

List of Tables

1 Introduction

1.1. Background

More than half of the world's population, built assets and economic activities are located in urban areas (Revi et al., 2014). Severe rainstorms have demonstrated that the impact of local high-intensity rainfall to cities can be large (Spekkers et al., 2015) and in many parts of the world, pluvial flooding is one of the most common natural hazards with a potential of significant societal concern (Ahern et al., 2005; Westra et al., 2014; Yin et al., 2016). Primary cause of floods are storm events that lead to overloading of rivers and urban water infrastructures (Delta Program, 2017; ten Veldhuis, 2011). Besides increasing precipitation due to climate change (Van den Hurk et al., 2014), cities are getting increasingly prone to urban flooding due to denser populations, increasing imperviousness and ageing infrastructure (Ashley et al., 2005; Gaitan et al., 2016; Revi et al., 2014; ten Veldhuis et al., 2011). In addition, increasing pluvial flood risks in cities are affiliated with land subsidence (Chan et al., 2012; Delta Program, 2017; Erkens et al., 2015; Koster et al., 2018; Yin et al., 2016). Land subsidence causes significant economic losses in the form of structural damage and high maintenance costs for (infra)structure. The total damage worldwide induced by land subsidence is estimated at billions of dollars per year (Erkens et al., 2015). It is estimated that in the Dutch urban area, the extra costs and damage to infrastructure caused by soil consolidation in the period up to 2050 will amount to between 1.7 and 5.2 billion euros, and that the extra costs related to the restoration of inadequate foundations in weak soils will add up to at least 16 billion euros (Delta Program, 2018; van den Born et al., 2016).

The spatial-temporal effect of land subsidence on pluvial floods has not been fully understood (Delta Program, 2018; Yin et al., 2016). Only few studies have numerically investigated the relationship between land subsidence and pluvial flooding in complex urban communities, largely due to the lack of high accuracy and multi-temporal ground-level data (Yin et al., 2016). However, the advent of Light Detection And Ranging (LiDAR) techniques to measure ground level, combined with the geodetic techniques (InSAR) to measure land subsidence and advances in high resolution flood modelling techniques (3Di) enable the numerical modelling of dynamic urban pluvial flood risks in the context of land subsidence (Dahm et al., 2014; Higgins, 2016; Sampson et al., 2012; Stelling, 2012; Volp et al., 2013). Yin et al. (2016) performed a numerical analysis of pluvial flooding to evaluate the impact of land subsidence on flood risks in Downtown Shanghai using a hydraulic model. He showed that much of the subsiding area shows minor to moderate changes (< 5 cm) in water depth and in some parts of the city risk even decreases. However, it is suspected that the results of this case study of Downtown Shanghai were site-specific and therefore Yin et al. (2016) recommends to perform comparable case studies in different urban environments, preferably including adaptation modelling. This allows decision-makers, like the city of Rotterdam, to prioritise adaptation investments.

Next to technical possibilities also political demand motivates the urge of this research. Pluvial flooding and land subsidence are important topics in Dutch policy and are nationally addressed in the Delta Decisions on spatial adaptation (Delta Program, 2018). Insight into the vulnerability to weather extremes constitutes the basis for spatial adaptation. That is why municipalities, provinces, regional water authorities and central governments have agreed to conduct stress tests in order to map out the vulnerabilities in areas under their responsibility by no later than 2019 (Delta Program, 2018). These stress tests cover four main themes, these being: pluvial flooding, drought, heat and floods. In the Delta Program (2018), a further analysis of the causes and effects of land subsidence is dictated and land subsidence is added as a fifth stress test-theme.

1.2. Research' structure and questions

This research tries to asses the influence of land subsidence on urban pluvial flooding in Rotterdam, now and in the future. The main research question is as follows:

What is the current and expected future influence of land subsidence on urban pluvial flooding in Rotterdam?

To answer the main research question, the impact of pluvial flooding in Rotterdam is firstly investigated. Currently, this impact is addressed in the performed stress test prescribed in the Delta Program (2018). The calculated impact of pluvial flooding and the method behind this calculation of the Rotterdam stress test on pluvial flooding is analysed. Since the results of stress tests are established values in the the current policy (City of Rotterdam, 2019), their method is continued in this research to estimate the impact of urban flooding. A crucial aspect of the performed stress test's method in Rotterdam is the use of the hydrodynamic model 3Di, of which a Digital Elevation Map (DEM) is one of the most important inputs (Nelen & Schuurmans, 2018). To estimate the influence of past land subsidence on urban pluvial flooding a fictional DEM is created that represents Rotterdam at design level. 3Di-calculations based on this DEM illustrate a situation where subsidence has never occurred. The difference between simulation-output and the stress test results estimates the extent of the current influence of land subsidence on flooding.

1. To what extent is the impact of current pluvial flooding induced by land subsidence?
    (a) How is the impact of urban pluvial flooding expressed and determined?
    (b) What is the current expected impact of pluvial flooding in Rotterdam?
    (c) What is the expected impact of urban flooding based on the design level?

To investigate the influence of future land subsidence on urban flooding in Rotterdam, land subsidence and its influence on the future surface level of Rotterdam needs to be understood. The available data, processes, consequences and Rotterdam's maintenance policy concerning land subsidence is studied and analysed to make an estimation of land subsidence in the future. Based on this analysis, it is estimated how the surface of Rotterdam will develop in the coming years, in- and excluding the maintenance policy and expressed in two prognosed Digital Elevation Maps for the year 2030, one in- and one excluding Rotterdam's maintenance policy.

2. What is the expected future surface level influenced by land subsidence with/without the planned maintenance?
    (a) What is the current rate of subsidence and how is this measured?
    (b) What are the causes of land subsidence in Rotterdam?
    (c) What is the prognosed 2030 DEM in- and excluding adaptive measures?

Land subsidence directly influences a DEM and therefore 3Di functions as the translator between land subsidence and pluvial flooding. The two prognosed 2030 DEM's in sub question 2c are used as a 3Di input and the expected pluvial flooding is calculated for a theoretical DEM for the year 2030 in- and excluding maintenance work. Comparing these results reciprocally and to the results of the conducted stress test, indicates the future expected influence of land subsidence on urban flooding and assesses the effectiveness of the current policy in Rotterdam.

3. What will be the influence of land subsidence on urban pluvial flooding in the future?
    (a) How will land subsidence influence the expected future urban flooding?
    (b) What is the effect of the current strategy to compensate for land subsidence in Rotterdam on future urban flooding?

To answer the research questions satisfactory, first, the theoretical background is studied and documented in chapter 2. Before assessing the influence of land subsidence on pluvial flooding, both processes are studied separately. Secondly, chapter 3 presents the used data in this research. In addition, available data was processed and filtered out, based on its applicability and accuracy. Chapter 3 also includes the case-study

selection and the motivation behind this. How this data is used to optimally answer the research questions is described in chapter 4. Fourthly, the data presented in chapter 3 is implemented in the method described in chapter 4 and the results of this implementation are presented in chapter 5. This chapter also includes whether the results corresponds with the theory described in chapter 2. Fifthly, chapter 6 discusses critical assumptions and other factors that constrain direct applicability of the results presented in chapter 5. Sixthly, taking all preceding chapters in account, the research question are answered concludingly in chapter 7. Finally, this research presents its recommendations for future research and policy-making in chapter 8.

2

Theoretical background

To investigate the influence of land subsidence on pluvial flooding, the theoretical background of both elements is assessed in this chapter. Firstly, the causes and consequences of pluvial flooding in the Netherlands are described. Additionally, the motive, method and results of the conducted stress test on pluvial flooding in Rotterdam are documented. Secondly, the processes, causes, damage, prediction, measurement and Rotterdam's counter-policy of land subsidence are illustrated.

2.1. Pluvial Flooding

2.1.1. Pluvial flooding in the Netherlands

In the Netherlands, short extreme rain events have a large impact in cities (Delta Program, 2017; Spekkers et al., 2015). The densely built-up and largely paved urban areas drain most of the rainwater via sewers and public roads. The capacity of the sewer system is insufficient for draining short extreme rain events. In addition, urban water systems are susceptible to component failure and human error (ten Veldhuis et al., 2011). During extreme rainfall, excess water flows to lower-lying locations, where it can cause damage such as obstruction of roads inundation of buildings. Over the period from 2003 up to and including 2015, regional water authorities have spent some 1.5 billion euros on water system measures to combat pluvial flooding. In 2015 alone, municipalities spent a total of 1.56 billion euros on urban water management, of which 225 million euros to tackle pluvial flooding (Delta Program, 2017). Despite these investments, urban flooding is expected to occur more frequent and fiercely due to future climate change, as is explained in appendix A. Climate change and different patterns of precipitation is an important factor that increases the vulnerability of cities to pluvial flooding but not the only one (Ashley et al., 2005; Willems, 2013; Yin et al., 2016). Cities are expected to become increasingly prone to urban flooding due to denser populations, augmenting imperviousness, and ageing infrastructure (Ashley et al., 2005; Delta Program, 2017; Gaitan et al., 2016; Revi et al., 2014; ten Veldhuis, 2011). In addition, there is a general awareness that land subsidence causes an increasing pluvial flood risks in cities (Chan et al., 2012; Delta Program, 2018; Erkens et al., 2015; Yin et al., 2016).

2.1.2. Stress test pluvial flooding

The essence of the Delta Decision on Spatial Adaption is collaboration among government authorities, companies and civic society organisations aimed at climate proofing and achieving water resilience for the year 2050 in the Netherlands (Delta Program, 2018). In order to achieve this, the central government, provinces, municipal councils and water boards have agreed to conduct stress tests in order to map out the vulnerabilities in their areas by no later than 2019. A majority of the governments have initiated such stress tests; however, many have not yet addressed all four issues (pluvial flooding, drought, heat, and floods) or covered their entire territory (Delta Program, 2018). The stress test pluvial flooding is standardised by Dekker et al. (2018) to identify vulnerabilities in a consequent way that forms the basis for risk-dialogues. A standardisation enlarges the comparability between the Dutch regions and eventually elucidates the problem nationwide. The ambition of the Delta Decision on Spatial Adaptation is to provide insights in the negative consequences of climate change and subsequently make a substantiated decision if this consequence is accepted or has to be dealt with. So, the ambition of this standardisation is not to be normative, although climate-ambitious regions may strive to accomplish these standards.

Table 2.1: Standardised rain events for the stress test pluvial flooding in urban areas Dekker et al. (2018)

Duration	Return Period current climate [year]	Rainfall current climate [mm]	Rainfall 2050 [mm]	Climate change factor (Van den Hurk et al., 2014)
1 hour	100	60	70	21 %
1 hour	250	75	90	21 %
2 hour	1000	130	160	21 %

The standardised stress-test pluvial flooding assesses the future expected impact of climate change on pluvial flooding and prescribes rain scenarios that are implemented in the simulations for pluvial flooding. For these scenarios a step-wise approach that simulates rain events with a return period of 100, 250 and 1000 year is prescribed (Dekker et al., 2018). The scenarios are divided between short (1 and 2 hours) and long (48 hours) rain events. Since urban areas are particularly sensitive to short high-intensive rain events, only short rain events are used as a scenario in Rotterdam. The Delta Decision on Spatial Adaptation aims at securing a climate-proof and water resilient spatial design in the Netherlands by 2050 (Delta Program, 2018). Therefore, the standardisation considers the expected climate in 2050 in the prescribed rain scenario's. The intensities of the 1 and 2 hour rain events are based on return periods in the current climate combined with a 21 % climate factor based on Van den Hurk et al. (2014) to estimate the 2050 climate, as shown in table 2.1. A major assumption in the standardised stress test is the assumption that the rain events are spatially and temporally uniform and constant. This assumption however, makes a direct step-wise approach possible and simplifies the execution calculation-wise (Dekker et al., 2018).

The stress test pluvial flooding in Rotterdam is conducted by executing 14 sub-model 3Di simulations based on the DEM of 2016 (Nelen & Schuurmans, 2018). Maps of resulting water depths for the city of Rotterdam are shown in figure B.1, figure B.2 and figure B.3 in appendix B. Besides water depths throughout the city, two ways of expressing the impact of pluvial flooding are used: the passability of roads and the risk of water nuisance per building. Per 3Di rain event simulation, the resulting passability of roads and the resulting risk of water nuisance per building are presented in figure 2.1. Figure 2.1 shows that more rain generally results in more impact, displayed by less passable roads and more buildings at risk of water nuisance. The impact-increase between a 70 mm in one hour and a 90 mm in one hour rain event is comparable to the increase between a 90 mm in one hour and a 160 mm in two hours rain event.

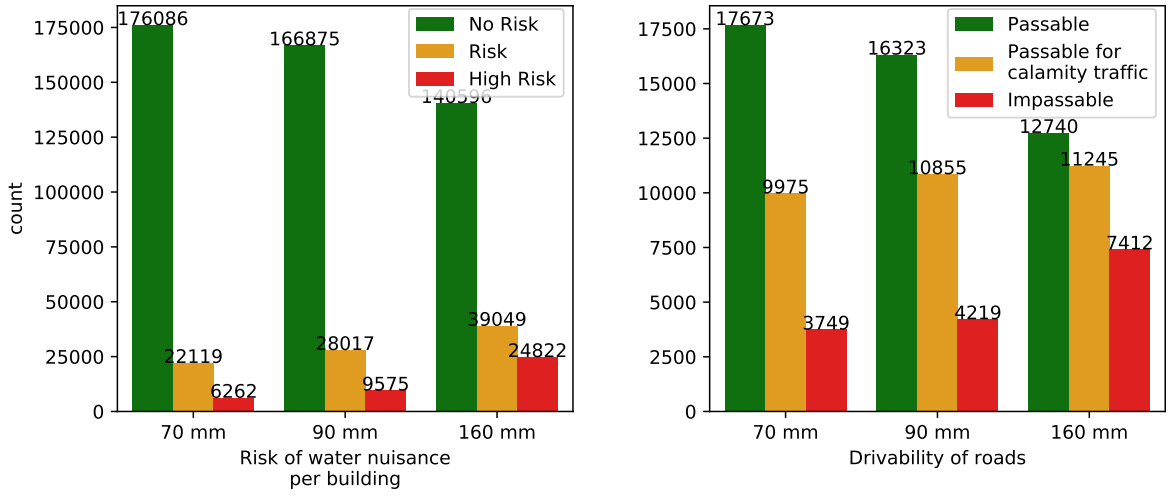

Figure 2.1: Resulting impact of pluvial flooding based on based on the conducted stress test pluvial flooding in Rotterdam (Nelen & Schuurmans, 2018). Left: Count-plot of the risk of water nuisance per building and right: the passability of roads

2.2. Land Subsidence

2.2.1. Processes

Subsidence is the downward movement of the ground surface and includes the processes compression/compaction, consolidation and oxidation (Glopper and Ritzema, 2006). In addition, landfill subsidence is an important process causing land subsidence in Rotterdam (van Leeuwen, 2019).

- Compression is the change in soil volume produced by the application of a static external load. Compaction is produced artificially by momentary load application such as rolling, tamping, or vibration (USDI, 1974).
- Consolidation is the gradual, slow compression of a cohesive soil due to weight acting on it, which occurs as water, or water and air, are driven out of the voids in the soil. Secondary consolidation is called creep and is a phenomenon, mostly observed in clay, that can last for ages (Haan, 1994; Verruijt, 2009).
- Oxidation is the process by which organic carbon is converted to carbon dioxide and lost to the atmosphere (Beckett and Young, 2006).
- Landfill subsidence is a process that occurs principally because of creep and decomposition of solid organic particles (O'kelly, 2005).

2.2.2. Causes

Compression/compaction and consolidation occur both naturally and anthropogenic (Allen, 1984). The natural causes include tectonics, loading by ice sheets, by sediments or by the ocean/sea and natural sediment compaction (Erkens et al., 2015). Consolidation only occurs in clay or other soils of low permeability like peat (Glopper and Ritzema, 2006). Alluvial or coastal sediments consisting of alternating layers of sand, clay, and peat are specifically compressible and vulnerable for oxidation. This is related to the physical characteristics of these sediments and makes low-lying coastal and delta areas specifically prone to subsidence (Erkens et al., 2015). Using this alluvial sediment or river dredge to fill land in preparation of construction can lead to landfill subsidence. Landfill subsidence can be significant and continues indefinitely but at progressively slow rates (O'kelly, 2005). In deeper layers, subsidence is caused by extraction of resources such as oil, gas, coal, salt, and groundwater. In most of the large delta cities where land subsidence is severe (Jakarta, Ho Chi Minh City, Bangkok, Dhaka, Shanghai, and Tokyo), the main cause is extraction of deep aquifer groundwater (Erkens et al., 2015). Contrary to most large delta cities, deep aquifer extraction is not the primary cause of subsidence in Rotterdam. Although gas extraction causes subsidence in the Pernis neighbourhood (Streng and Platteleeuw, 2008), the mere part of the subsidence in Rotterdam is due to the lowering of phreatic ground water and therefore consolidation and oxidation occurs in the Holocene peat layer (Koster et al., 2018). In the Netherlands about 6 million inhabitants live on 'soft soils', peat and clay (Lambert et al., 2014) and approximately 9 % of Dutch territory is composed of peat soils. The major part of these soils is subsiding (van den Born et al., 2016). In rural areas, subsidence is closely related to dewatering for the benefit of agriculture and dairy farming. As a reaction to dewatering, the peatland above the water table subsides as the weak soil settles and organic matter oxidises (van den Born et al., 2016). Consequently, these lands are further dewatered to maintain its agricultural function (level indexation) and the process of oxidation repeats itself. In urban areas, human induced land subsidence dominates the total subsidence process (Erkens et al., 2015). Anthropogenic compression and compaction of shallow soft layers is caused by loading. Anthropogenic subsidence can also occur as a result of drainage and subsequent consolidation and oxidation of the Holocene peat and clay layer (Erkens et al., 2015; Koster et al., 2018). The urban areas of Rotterdam and Amsterdam are less subjected to oxidation because of the protection of anthropogenic brought-up soil and oxidation is restricted to soil above the phreatic groundwater level. On the other hand this thick anthropogenic applied soil covering peat has caused it to compress in the past (Koster et al., 2018). These anthropogenic layers in Rotterdam are often the result of land fillings and can contain dredging spoil from the river Nieuwe Maas (van Leeuwen, 2019). This alluvial sediment is vulnerable to landfill subsidence.

2.2.3. Damage

The total damage worldwide induced by land subsidence is estimated at billions of dollars annually (Erkens et al., 2015). Land subsidence causes two different types of damage. Firstly, land subsidence causes damage to buildings, foundations, infrastructure, and subsurface structures. Secondly, land subsidence increases

flood risk because flood water depths and inundation time increases and the drainage systems become less effective (Chen and Tfwala, 2018; Erkens et al., 2015; Higgins, 2016; Koster et al., 2018). Municipalities that are located on weak soil spend about 40 % more per year on the reconstruction of roads and sewers (Cebeon, 2015; Lambert et al., 2014). A secondary, indirect, type of damage is the release of greenhouse gasses, particularly CO_2, that has consequences for the climate (Hoogland et al., 2012; van den Born et al., 2016). Currently CO_2 emissions from the agricultural peat soils amounts about 4 million ton per year which represents 2 % of the total yearly Dutch greenhouse gas emission.

Besides damage to (water management) infrastructure, the Netherlands cope with foundation problems, particularly buildings founded on wooden piles and buildings founded on shallow foundations. Subsiding peat and clay soils can pull wooden and concrete foundation piles down, which is called a 'negative adhesive'-force. This reduces the loading capacity of the foundation (van Workum et al., 2016). Furthermore, wooden piles can rot when the groundwater level becomes too low and buildings founded on wooden piles can experience the same problems as buildings on shallow foundations (KCAF, 2019). Buildings on shallow foundation subside with the topsoil. Buildings are damaged in two ways by land subsidence. Firstly, when subsidence is not evenly, tilt and cracking of the houses may occur. Secondly, sinking of the buildings increases the vulnerability to inflow of (ground)water. In the Netherlands, it is estimated that 400.000 buildings face foundation problems and the potential maximum amount of damage can amount up to 40 billion euros (Hoogvliet and van de Ven, 2012). Subsidence-induced damage on buildings with insufficient foundation is a big issue in the city of Rotterdam. It is estimated that the total amount of buildings where foundation restoration is needed in the municipality of Rotterdam amounts several thousand of buildings within the next 15 years (Dieters and Groenendijk, 2010; van Workum et al., 2016).

Subsidence and its resulting damage is likely to increase under the influence of ongoing urbanisation and population growth in delta areas (Erkens et al., 2015). Additionally, global warming will further accelerate land subsidence due to oxidation, leading to elevated risks of flooding and increasing upward seepage of brackish and nutrient rich ground water (Hoogland et al., 2012). Today, over 15 km^3 of Holocene peat remains embedded in the Dutch subsurface. Consequently, the subsidence potential of the coastal deltaic plain of the Netherlands remains high (Hoogland et al., 2012; Koster et al., 2018; van den Born et al., 2016). Estimations are that in the Dutch urban area, the potential extra costs and damage to infrastructure caused by consolidation in the period up to 2050 will amount to between 1.7 and 5.2 billion euros, and the extra costs related to the restoration of inadequate foundations in weak soils will add up to at least 16 billion euros (Delta Program, 2018; van den Born et al., 2016). The extent of expected damage, the secondary effect on climate change via CO_2 emissions and the complexity of the processes and solutions regarding land subsidence attracted national attention and setting up a national soil subsidence program is one of the three general recommendations that is presented by the Delta Program (2018). The Dutch government decided in 2018 to factor in soil subsidence within the framework of the Delta Plan on Spatial Adaptation.

2.2.4. Counter-action

Subsidence can be slowed down and even stopped, although this requires expensive measures (van den Born et al., 2016). Policy strategies for subsiding cities can be divided in mitigation and adaptation. Mitigation only works for human-induced subsidence. Mitigation measures typically include restrictions of groundwater extraction, artificial recharging aquifers or raising phreatic water levels in areas with organic rich soils. Next to that, building with lighter materials decreases the load on soft soils, thereby decreasing consolidation and compression. Adaptation measures focus on reducing the impact of subsidence, for instance by decreasing the vulnerability of a certain asset to the negative impacts of subsidence (Erkens et al., 2015). In Rotterdam, the prioritising of sewer maintenance is based on age, possible system adaptations, complaints, foundation risks and maintenance status although land subsidence is normative in general. A sewer is often replaced due to land subsidence before alarming technical conditions are reached (Bunt and Essing, 2015). A threshold indicator for sewer and road maintenance used by the city of Rotterdam is 30 cm subsidence regarding the issuance level (van der Meer and van Herck, 2016). The issuance level is a theoretic ground level that secures spatial developments to have no negative influences on water bodies, sewer and groundwater and shown in figure D.1 in appendix D. If road and sewage maintenance is performed integrally, the ground level is restored to issuance level. In practice however, streets cannot be constructed at issuance level if the doorstep height of the adjacent buildings is lower than issuance level, because this will cause water nuisance per definition. For the coming 10 years regions are selected where integral or separate maintenance work will be performed and presented in figure D.2 in appendix D.

2.2.5. Measurement

Interferometric synthetic aperture radar (InSAR) is used to estimate land subsidence rates in Rotterdam by Maccabiani (2014). InSAR is a powerful technique to measure motion of the Earth's surface (Gabriel et al., 1989). Labour-intensive spirit levelling and costly GPS stations have been used less over recent years to measure land subsidence, since SAR processing-chains can provide millions of data points over a large area and are often less expensive than sparse point measurements. Moreover, SAR results have shown that land displacements due to groundwater withdrawal and injection are characterised by a spatial variability almost impossible to detect by other surveying techniques (Gambolati and Teatini, 2015). Once the surface topography contribution is removed and the atmospheric disturbance mitigated, SAR-based methodologies allow for the detection and measurement of subcentimeter-scale ground movement with high spatial detail and high measurement resolution (Bürgmann et al., 2000; Gambolati and Teatini, 2015). Maccabiani (2014) used the Persistent Scatterer Interferometry(PSI)-technique (Ferretti et al., 2000) as radar interferometric time series analysis technique to measure subsidence rates in Rotterdam. The PSI focuses on the coherent phase history of a subset of points which show relatively constant scattering properties in time, so-called Persistent Scatterers (PS). Persistent Scatterers are located on sharp-edged objects like buildings and stone covered dikes, more than smooth surfaces like roads or grassland. This makes the use of InSAR more applicable in densely built areas (SkyGEO, 2018). Because of the reflection dominance of these persistent scatterers within an image resolution cell, the effect of geometric decorrelation is also strongly reduced. PSI uses these isolated persistent scatterers to derive displacement time series per scatterer. The benefit of a radar interferometric time series analysis is to circumvent the influence of the phase contribution of the atmospheric signal, together with temporal and geometric decorrelation (van Leijen, 2014). Due to the use of the stack of radar acquisitions, the temporally uncorrelated atmospheric phase component in the observations can be estimated and removed (van Leijen, 2014). The theory behind InSAR is further explained in appendix C.

The precision of PS deformation measurements is in the millimeter range, for linear deformation even better than 1 mm/yr (Hanssen, 2003; SkyGEO, 2018). This precision mainly depends on the number of available acquisitions and the temporal and spatial baselines. Hanssen (2003) shows that PSI can lead to linear deformation accuracies with standard deviations better than 0.4 mm/yr for deformations and better than 2 m for topography. Additionally, in the context of the Terrafirma Validation Project, Crosetto et al. (2008) compared a large set of measurement points in Alkmaar and Amsterdam and estimated the standard deviation of the deformation velocity of 0.4-0.5 mm/yr. Furthermore, Crosetto et al. (2008) states that these values are representative for PSI studies with similar characteristics to those of the test sites. Although InSAR can measure deformation with high precision, the challenge in urban areas is knowing what deformation you measure. An important characteristic of the method is that it is an opportunistic technique: the exact location of persistent scatterers in an interferometric stack cannot be predicted (Hanssen, 2003). This makes it difficult to determine beforehand whether a specific deformation phenomenon, say, the deformation of a specific house, may be monitored. SkyGEO (2018) indicates a precision of 1-2 m for the X,Y-location and a precision of 1-1.5 m for the Z-location for high quality measurements. In addition, Maccabiani (2014) only measures Line of Sight deformation. The radar's Line of Sight is sensitive to both horizontal and vertical deformation due to the skewed incidence angle of the signal. It is a three-dimensional vector denoted by components in for example East, North and Up direction. It is not possible to determine the three deformation components from a single inferogram (van Leijen, 2014). When investigating land subsidence, often an assumption is made regarding the deformation's direction and only vertical and horizontal deformation is examined. This is why Maccabiani (2014) detects tilting of buildings as sinking of buildings in Rotterdam. Combining data-sets with different incidence angles, for example ascending and descending direction, can improve this determination because two observations are available to determine two unknown deformation values, the system has a unique solution. However, because of the insensitivity of the deformation vector in North-South direction, the full three-dimensional vector can still not be resolved and an assumption regarding the direction of the horizontal deformation remains required (van Leijen, 2014).

3

Data

This chapter introduces the data used in this research. Gathered data for the land subsidence analysis is presented and discussed in 3.1. Limits in time and computational capacity compelled this research to scope down to a case study. The reasoning behind this selection is explained in 3.2. Before used as model-input, the gathered data is processed, as explained in 3.3. This processing derives relevant values from the raw data input and rejects data based on accuracy and the case study selection.

3.1. Gathering

3.1.1. InSAR

Subsidence rate per point

As presented in table 3.1, one ascending (133 images) and one descending (162 images) TerraSAR X orbit is used to estimate subsidence rates in Rotterdam between 05/02/2009 and 20/09/2014. In total, Maccabiani (2014) expresses the subsidence rate for about 1,5 million ascending Persistent Scatterers (PS) and 1,9 million descending PS. The PS points are divided into low and high points to distinguish points located on buildings(high) and open space(low). To make this division, Maccabiani (2014) combined the z-coordinate of every point with the Rotterdam DEM of 2014. If the z-coordinate is over 2 m higher than the Rotterdam DEM of 2014, a point is classified as high. The subsidence rates divided on high and low and ascending and descending are presented in appendix E, as shown in table 3.1. The maps in appendix E show that low points generally subside faster than high points, as expected since most buildings in Rotterdam are sufficiently founded. Figure 3.1 show the translation from 162 images to one linear fitted subsidence rate for one PS. In addition to this rate, Maccabiani (2014) expresses a Root Mean Square Error (rmse) in mm/yr and a point quality value for all 1.7 million low points and for all the 1.6 million high points (table 3.1). Table 3.2 presents the precision estimation by Maccabiani (2014). The rmse deviations are used as an estimation of the noise per point. The median value of the rmse-value of all the ascending points is 2.2 mm and from the descending points 2.1 mm. The rmse expresses the precision of the applied fit as shown in figure 3.1, but a high rmse-value does not necessarily mean that the estimated linear fit is blurred by noise. Physically, high rmse can be caused by high seasonal variations, for example soil moisture and temperature that causes soils or buildings to swell/shrink (Weissgerber et al., 2017). The point quality value is based on the local coherence estimator. Coherence is determined with respect to the closest point of the primary network (Maccabiani, 2014). Table 3.2 indicates a precision of 1 m for the X,Y-location and a precision of 0.3-0.5 m for the Z-location for high quality measurements.

Table 3.1: InSAR data-set characteristics (Maccabiani, 2014)

Satellite	Orbit	Period	Images	Resolution	PS high	PS low	Presented:
TerraSAR-X	Ascending	05/02/2009- 06/06/2014	133	3.0 m x 2.8 m	758 329	712 019	E.1, E.2
TerraSAR-X	Descending	08/04/2009- 20/09/2014	162	3.0 m x 3.1 m	846 936	1 011 609	E.3,E.4

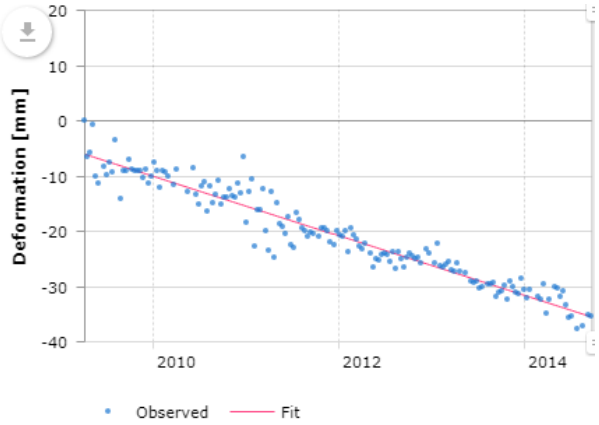

Figure 3.1: Translation from 162 InSAR images from a descending TerraSAR-X orbit to a linear subsidence rate for a low point.

Table 3.2: Precision estimates of the subsidence rates expressed per point by Maccabiani (2014)

	Descending orbit	Ascending orbit
Median value of rms deviations from model	2.1 mm	2.2 mm
Percentiles (5,95) of rms deviations from model	1.28 - 2.60 mm	1.54 - 2.62 mm
Expected leakage of seasonal signal into linear rates	neglegible	neglegible
Estimated relative horizontal positioning accuracy	1 m	1 m

Subsidence rate per polygon

To reduce the influence of point-specific measurement-errors and improve the areal coverage, the 3.5 million subsidence rates per point are translated to polygons. The subsidence rates per low point are translated to neighbourhoods, sub-neighbourhoods, blocks and streets and per high point to buildings or building blocks. Per polygon, Maccabiani (2014) expresses this translation in several values:

- Mean subsidence rate of the points per polygon (mm/yr)
- Several percentile values of subsidence rate of the points per polygon (mm/yr)
- Standard deviation of the subsidence rates of the points per polygon (mm/yr)
- Number of points (PS) per polygon

Figure 3.2(top) shows the measured subsidence rate per low point measured by a descending and ascending satellite orbit between 2009-2014 (Maccabiani, 2014). Additionally, sub-neighbourhoods in Rotterdam are presented. Note that a negative subsidence rate represents a downward movement. Figure 3.2(bottom) demonstrates the translation from individual InSAR low points to subsidence rates per sub-neighbourhood. It presents the mean of all the subsidence rates per low point inside one sub-neighbourhood. In stead of the mean, it is also common to present InSAR data with a percentile value of all the points per polygon. A percentile value is useful to identify areas at risk. If there is no division between high and low points the mean subsidence rate will include PS on founded areas, which causes a distorted estimation of the subsidence rate. The city of Rotterdam uses the 25^{th} percentile value to identify areas at risk (City of Rotterdam, 2019), detect buildings with the risk of foundation problems (Funderingsloket, 2019) or predict the maintenance need of roads (van der Meer and van Herck, 2016).

Land subsidence analysis

To analyse the process of land subsidence in Rotterdam, a distinction is made between land subsidence of open space and buildings. To acquire a high level of detail of subsidence behaviour, the land subsidence-analysis of open space is based on individual low points. The land subsidence-analysis of buildings is based on building-polygons that contain statistical data of all the subsidence rates per high point inside the polygon. The InSAR data per building in Rotterdam delivered by Maccabiani (2014) is created by combining the subsidence rate of 1.6 million high points (table 3.1) with 168 246 BAG (Basisregistratie Adressen en Gebouwen)-buildings from the Netherlands' Cadaster, Land Registry and Mapping Agency. The subsidence

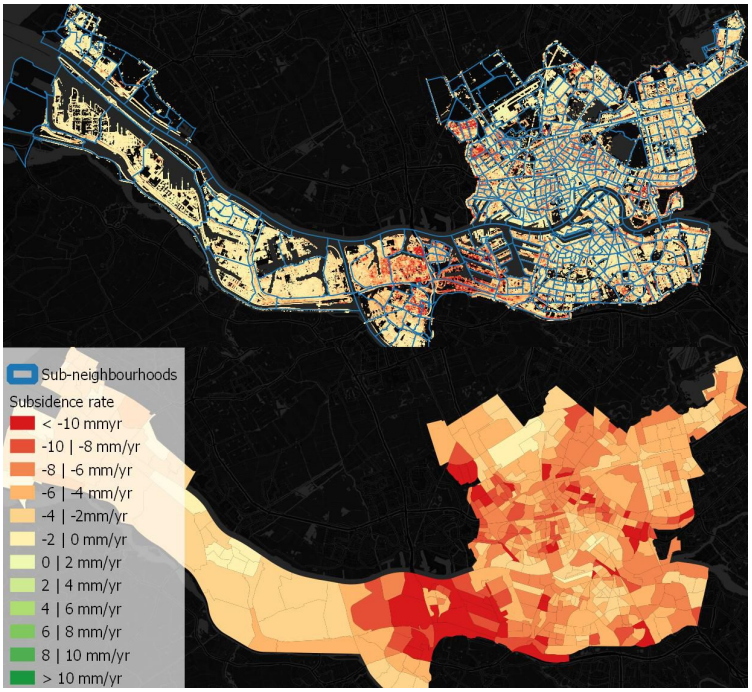

Figure 3.2: Top: Subsidence rate per low point measured by a descending and ascending satellite orbit and sub-neighbourhoods in Rotterdam. Bottom: Mean of all the land subsidence rates in mm/year per low point inside one sub-neighbourhood in the period April 2009 until September 2014, (Maccabiani, 2014). Note that a negative subsidence rate represents a downward movement.

rates expressed per BAG-building is preferred over building block or individual high point in this research because the information about foundation type in the Funderingsloket (2019) and the stress test results in Nelen & Schuurmans (2018) are also based on BAG-buildings. The mean and the standard deviation of all the subsidence rates per high point located on a BAG-building is compared to the number of high points located on a BAG-building and presented in figure 3.3. Uneven sinking causes subsidence-related damage, as stated in 2.2.1. To assess this disparity per building the standard deviation is examined per building. High differences between the subsidence rates measured by a descending and an ascending orbit per building can be detected by high standard deviation per building. This difference is an indicator of tilting buildings. A high standard deviation per building can also indicate a high influence of measurement noise, especially when the number of points per building is low. Buildings with low numbers of InSAR points show a wider spread of mean subsidence rates and standard deviations in figure 3.3 compared to buildings that are based on more points. Buildings based on only one InSAR point will, by definition, have standard deviation of 0.

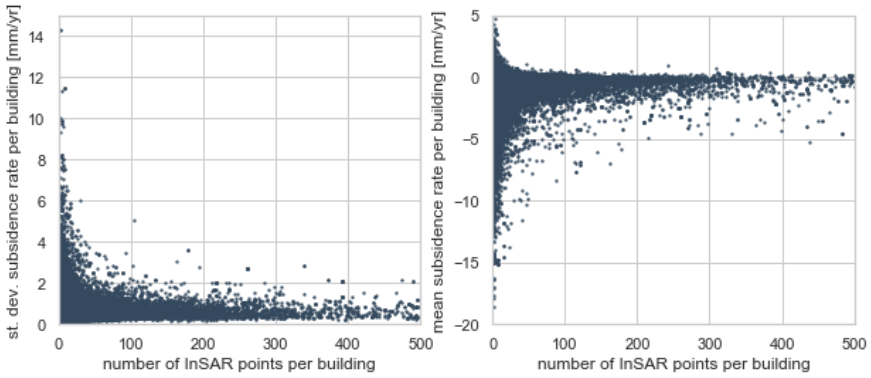

Figure 3.3: Standard deviation(left) and mean(right) of the subsidence rate of the high points per building versus the number of high points per building

3.1.2. Foundation types

Several foundation types are present in Rotterdam, but knowledge of the exact applied type of foundation per building is scarce. From 45 000 buildings, roughly 25 % of the buildings in Rotterdam, foundation types are identified in the so-called 'Funderingsloket'. Within the Funderingsloket (2019), the city is actively continuing the gathering of more foundation information. From the examined buildings, most rest on wooden or concrete piles or on shallow foundations (Funderingsloket, 2019). More data about foundation type variation on neighbourhood- and sub-model-scale is presented in appendix G.

3.1.3. Subsurface

Subsurface data used in this research is based on GeoTOP, retrieved via Dinoloket (2019) and presented in appendix H. GeoTOP describes the geometry and properties of the shallow subsurface to a maximum depth of NAP - 50 m and schematises the subsurface in a regular grid of rectangular blocks, called voxels, each measuring 100m × 100m × 0.5m. Each voxel contains estimates of the lithostratigraphic unit and the representative lithological class. These classification estimations are calculated using stochastic techniques (Kruiver et al., 2017; Stafleu et al., 2012). In appendix H it can be seen that almost whole of Rotterdam's top layer is classified as anthropogenic applied soil. In Rotterdam, some of these anthropogenic applied layers contain river dredge. The suspected location of this anthropogenic applied river dredge is shown in figure 3.4. This suspicion is based on historical data and soil samples containing alluvial soils (van Leeuwen, 2019).

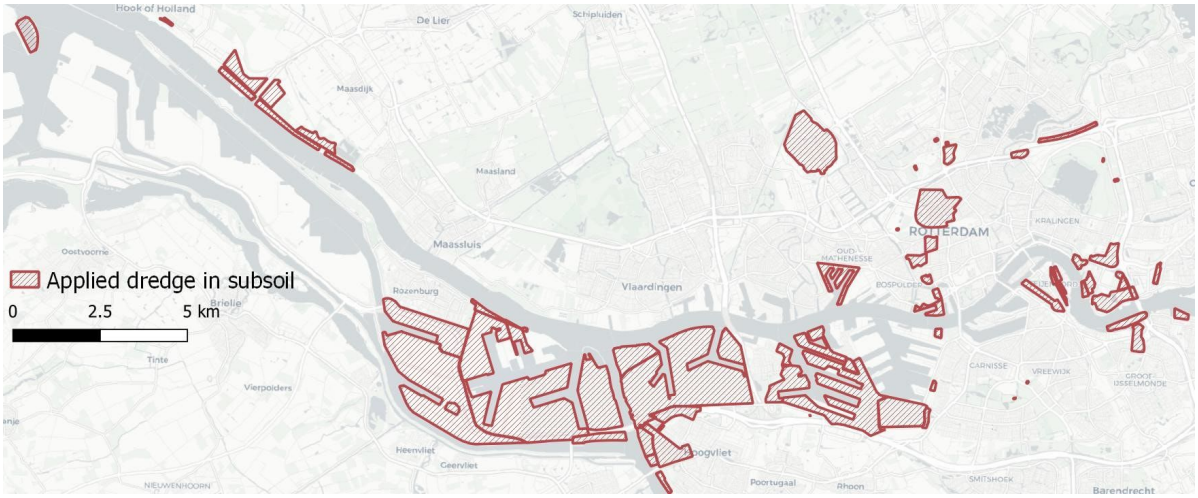

Figure 3.4: Locations where river dredge is presumably used as landfill material (van Leeuwen, 2019)

3.1.4. Drainage depth

To monitor drainage depths depth, the city of Rotterdam uses 1834 monitoring wells that express the ground water level compared to surface level roughly once per month for a period between 1-1-2005 and 3-9-2015. Per monitoring well, the average and the 5^{th} and 95^{th} percentile value of the drainage depths per well between 1-1-2005 and 3-9-2015 are expressed, where the 5^{th} percentile value is considered as the lowest groundwater level and the 95^{th} percentile as the highest groundwater table (Bunt and Zondag, 2015).

3.1.5. Land use classification

Based on a BGT-land use classification map (Basisregistratie Grootschalig Topografie, Cadastre) 3 mainland use classifications are identified in Rotterdam: roads, vegetated terrain and unvegetated terrain. Vegetated terrain contains forests, grasslands, bushes, agricultural and arable lands and landscaping, while unvegetated terrain contains property lands, paved area and sandy areas (van den Brink et al., 2013). In Rotterdam, public parks and gardens are generally classified as vegetated terrain, while private gardens are classified as unvegetated terrain.

3.2. Case study

Limits in time and computational capacity compelled this research to scope down to a case study. To gain results that supplement the results of the performed stress test and to limit the influence of hydrological

modelling errors, the existing 3Di sub-models, that are presented in appendix B, are used as a starting point in the case study selection. The location of these 14 3Di-sub-models is based on hydraulic and geological boundaries and watermark zones (Nelen & Schuurmans, 2018). The case study selection is based on several factors:

- Results of the stress test (Nelen & Schuurmans, 2018)
- The applicability of existing 3Di-models
- Data availability of foundation types (Funderingsloket, 2019)
- Expertise of the city of Rotterdam
- Land subsidence rates Maccabiani (2014)
- 'Rotterdams Weerwoord Urgentiedocument' (City of Rotterdam, 2019)

Based on these factors, the 3Di sub-model of IJsselmonde is selected as a case study.

3.2.1. IJsselmonde

The IJsselmonde sub-model contains four neighbourhoods, namely Oud IJsselmonde, Groot IJsselmonde, Lombardijen and Beverwaard. There are several differences between these neighbourhoods in terms of land subsidence and urban flooding. Based on the performed stress tests, Beverwaard is least vulnerable to future extreme rain events. The fact that this neighbourhood is accommodated with a stormwater sewer system, as shown in figure K.1, may explain its higher stormwater capacity. In figure 3.6, it is also demonstrated that generally the open space and buildings in Beverwaard subside slower than in the other neighbourhoods and figure 3.5 shows that there are, in contrary to Groot IJsselmonde and Lombardijen, no known buildings founded on shallow or wooden pile foundations. The northern neighbourhood Oud IJsselmonde contains dredge in its subsoil as shown in figure 3.4. The subsoil characteristics of the sub-model are presented in appendix I. In the coming 10 years, road and sewer maintenance is planned for several sub-neighbourhoods within Groot IJsselmonde and Lombardijen as shown in 3.5. The IJsselmonde sub-model will be used to perform 3Di calculations based on the DEM of 2016 (the results of the stress test) and the theoretical DEM of 2030 in- and excluding maintenance and comparing its results will assess the influence of land subsidence on urban flooding in the future.

3.2.2. Tuinenhoven

Within the IJsselmonde sub-model, one of the 30 sub-neighbourhoods, called Tuinenhoven (figure 3.5, is selected as case study to simulate a DEM at design level. The creation of Tuinenhoven at design level required a level of detail that is too time-consuming to conduct for the whole IJsselmonde sub-model. In addition, clipping an existing 3Di and calibrate it to show similar output as the stress test results is challenging. In Tuinenhoven, a road called 'Koninginneweg' is located. At this road urban flooding is a known problem based on experience and supported by the 3Di-results. The mere part of the buildings in the Konninginnenweg rest on shallow foundation and experience subsidence-related problems. In addition to known and expected flooding and subsidence problems, the sub-neighbourhood Tuinenhoven is a suitable case-study because the water system is relatively isolated from the IJsselmonde 3Di model. As presented in figure K.2, about 70 % of Tuinenhoven's water system is surrounded by water bodies and the A16 highway in the north. The interaction between the rest of the model is limited to two closed orifices, two weirs, two sewer connections and a constant pump inflow from the north that flows directly into the water body. The surface area of Tuinenhoven is roughly 50 hectares.

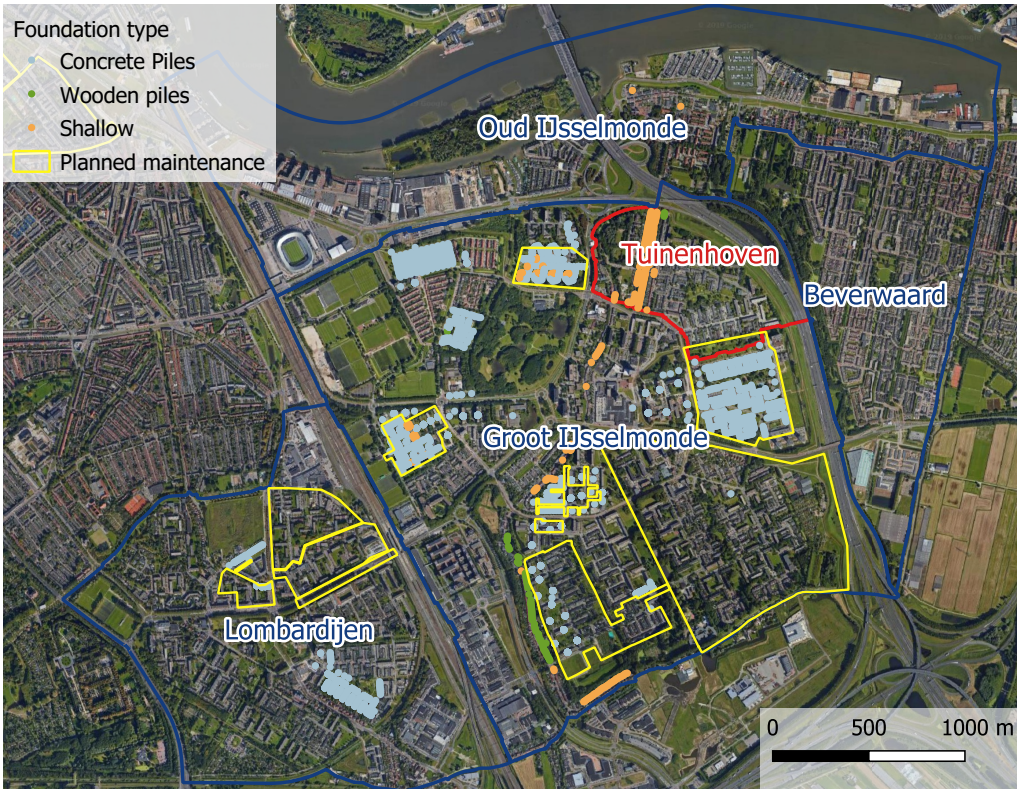

Figure 3.5: Foundation types per sub neighbourhood inside IJsselmonde sub model, (Funderingsloket, 2019) and the planned maintenance (van der Meer and van Herck, 2016)

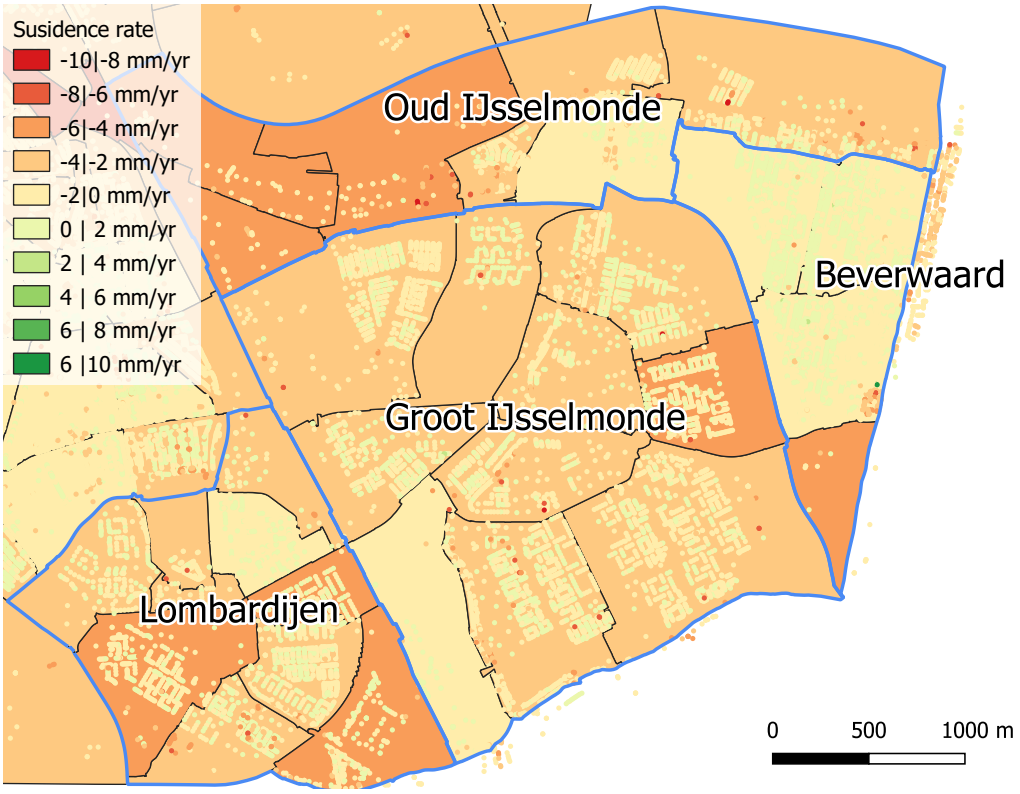

Figure 3.6: Mean subsidence rates per building compared to mean subsidence rates per sub neighbourhood within the IJsselmonde sub-model

3.3. Processing

3.3.1. Buildings

As discussed in 2.2.5, InSAR is able to measure subsidence rates with an error standard deviation of 0.4-0.5 mm/yr per individual point. To check whether this precision corresponds with the precision of Maccabiani (2014), several presumably stable buildings are selected. Buildings that are founded on concrete piles are presumed to show stable subsidence behaviour. In addition, the minimal number of points per building is set on 50. Figure 3.7 show standard deviations per building between 0.3 and 1 mm/yr. Corresponding to Crosetto et al. (2008), most presumably stable buildings show a standard deviation around 0.5 mm/yr. As stated in 2.2.5, a major factor that influences the precision of InSAR data is the determination of the exact location of persistent scatterers in an interferometric stack. This means that the points that are assigned to a building can actually be located on the nearby street or garden. The fact that Maccabiani (2014) distinguishes low and high points, reduces this influence, but it is still present.

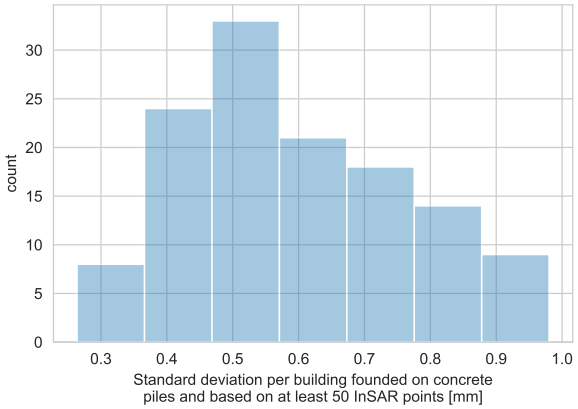

Figure 3.7: Standard deviation of presumably stable buildings in Rotterdam. Presumption is based on a minimum number of 50 points and foundation type of concrete piles per building .

Figure 3.3 shows that buildings based on a low number of points show a higher variation of mean subsidence rates and standard deviation. As explained in 2, this is expectantly due to signal noise or incorrect localisation of points, but it can also indicate uneven subsidence. Small buildings (with a low number of points) in Rotterdam are generally terrace houses and from these houses it is known that subsidence is difficult to measure because sinking houses can partly lean on neighbouring houses. This phenomenon can cause fast subsidence measurements on one side of the house and slow subsidence rates on the other. This difference results in an underestimation of the actual mean subsidence rate but also a higher standard deviation per building. In addition, deformation not predominantly in y-direction, for example tilting of buildings, is inversely detected by the ascending and descending orbit. This inversion is detected by a high standard deviation per building. So, on one hand a high standard deviation can be caused by measurement noise but on the other hand a high standard deviation indicates unequal subsidence. To minimise the influence of InSAR-noise but still examine the useful standard deviation per building to examine uneven subsidence, a threshold for the minimum points per buildings is set. The trade-off in the determination of this threshold is to find an acceptable signal-noise ratio and still retain enough buildings to analyse the land subsidence processes in Rotterdam. In appendix F, a threshold of at least 11 points per building is determined. Figure F.4 shows that setting this threshold affects the distribution of the standard deviation and decreases the number of samples from 168.246 to 40.424 buildings in total. Due to the exclusion of buildings only based on one point, the median of the standard deviation per building increases from 0.4 mm/yr to 0.55 mm/yr. The shape of the distribution of the mean subsidence per building is not strongly affected by setting this threshold in figure F.4, although the median of the mean subsidence rate per building shifts from -0.39 to -0.31 mm/yr.

Foundation type

As described in 2.2.1, foundation problems are expected to form a problem in the city of Rotterdam and form the primary influence on the subsidence behaviour of buildings. The foundation type per building, based via the Funderingsloket (2019), and the mean and standard deviation of the subsidence rate between 2009-2014, based on Maccabiani (2014) are compared. After buildings based on less than 11 points are filtered out

buildings are divided on their foundation types:

- Concrete piles (1080 buildings)
- Shallow foundation (396 buildings)
- Wooden piles (8831 buildings

3.3.2. Open Space

Within the IJsselmonde sub-model, the subsidence rates of 51.786 ascending and 67.210 descending Low Points are expressed by Maccabiani (2014). Figure F.3 in appendix F shows the standard deviation of the rmse and subsidence rate per low point with a certain quality indicator. To continue the analysis in this research a minimum threshold of 0.6 point quality is maintained, particularly to exclude the outliers show in figure F.3 in appendix F. This threshold eliminates 3449 points but does not influence the distribution's shape drastically.

Land Use
Inside the IJsselmonde sub-model, the low points are divided on the land use classification based on the BGT:

- Vegetated terrain (5231 points)
- Unvegetated terrain (24738 points)
- Road (63202 points)

As explained in chapter 2.2.5, InSAR technique is less applicable on grasslands and plants. This explains why the least points are located on vegetated area. Per land classification the subsidence rate will be examined.

3.3.3. Subsurface

Based on the Dinoloket (2019) subsurface maps presented in H and I several subsurface characteristics are determined determined per building in Rotterdam and per InSAR low point in IJsselmonde:

- The depth of the anthropogenic layer
- The depth of the first sand layer, the first sand layer is defined as the first 1.5 m of soil classified as sand (fine, fine-coarse and coarse) or gravel.
- The distance between the first sand layer and the anthropogenic depth
- The dominant soil type, this is the most occurring soil classification between the anthropogenic layer and the first sand layer.
- The top soil type, defined as the first soil type under the anthropogenic soil.

Table 3.3 confirms the observation in H and I that the dominant soil type between surface level and first sand layer is clay, followed by sand and clay in the Rotterdam subsurface. The top soil type under the anthropogenic layer contains relatively more peat. Within the IJsselmonde sub-model the number of low points located on a peat top soil type exceeds the number of low points located on top of sand top soils.Furthermore, buildings and low points are split into in-side dredged areas or outside dredged area. The number of buildings and the number of low point per subsurface characteristic are presented in table 3.3.

Table 3.3: Number of Buildings in Rotterdam and Low Points in IJsselmonde per subsurface characteristic

	Dominant soil type			Top Soil type			Dredge	
	Clay	Peat	Sand	Clay	Peat	Sand	Inside	Outside
Total buildings Rotterdam	30450	1941	6969	21304	5791	11240	3556	32255
Concrete piles	866	22	39	717	55	116	49	1031
Wooden piles	6919	478	638	4392	643	3157	372	8459
Shallow foundation	347	25	18	215	13	93	0	396
Low Points in Ijsselmonde	75399	3993	16519	66735	10729	8559	3456	112091

3.3.4. Drainage depth

149 wells are located within the IJsselmonde sub-model. Comparing drainage levels with the subsidence behaviour of buildings and open space based on Maccabiani (2014) is difficult because the InSAR data expresses one subsidence rate over a period of 5 years, while the ground water fluctuates monthly. To assess this fluctuation the range between highest and lowest monitored depth is compared with the subsidence behaviour. The levels in between these wells are interpolated, based on Thiessen's method (Rhynsburger, 1973), as shown in figure J.1. The Thiessen method is a robust method of interpolation that excludes the influence of for example intermediate water bodies between a monitoring well and a building or low point. To exclude InSAR points too far away from a monitoring well to be represented by its ground water level, only points within a buffer of 50 m are taken into account per monitoring well.

4

Method

This chapter describes how the presented data in 3 is used to answer the research questions in 1.2. To understand the process of land subsidence in Rotterdam, an analysis is performed. The method and assumptions behind this analysis is described in 4.1. For the Tuinenhoven case-study, a DEM is created that approximates design level. Furthermore, two DEM's are created for the IJsselmonde sub-model that prognose land subsidence untill 2030 and include Rotterdam's maintenance policy. The calculation-method and -steps behind these created DEM's are described in 4.2. Finally, the theory behind 3Di is assessed in 4.3. Next to calculation-wise characteristics, the method of interpreting resulting water depths as impact of urban flooding is described.

4.1. Land subsidence analysis

4.1.1. Influences

As described in 2.2.1, several characteristics influence the land subsidence process and can cause differences in subsidence behaviour per building and open space in Rotterdam. Using these process-based influences as a starting point, land subsidence in Rotterdam is examined. Per possible influence, data is gathered and processed, as presented in 3.1. Python-scripting is used for the the comparison with the InSAR data delivered by Maccabiani (2014). The land subsidence is divided based on the different influences and its distribution is plotted in histograms with bin-sizes based on the Freedman-Diaconis rule (Freedman and Diaconis, 1981). The following influences are examined:

- Foundation type (only per building)
- Land use classification (only per low point)
- Presence of dredge in the subsoil
- Top soil type
- Dominant soil type
- Depth anthropogenic layer
- Drainage depth

4.1.2. Statistical significance

To test whether these influences on subsidence rate are significant, an unequal t-test, also called Welch' t-test, is performed. In case of samples with a different sample variance the unequal t-test should be preferred over the Student's t-test or Mann-Whitney U test (Ruxton, 2006; Zimmerman and Zumbo, 2007). In the analysis, an influence is assumed significant if the calculated two-tailed p-value is less than 0.01. To express the strength of the linear relationship of the influences on the subsidence behaviour, Spearman's rank correlation coefficient is calculated. Spearman's coefficient assesses how well an arbitrary monotonic function can describe a relationship between two variables, without making any assumptions about the frequency distribution of the variables (Hauke and Kossowski, 2011). When Spearman's coefficient is lower than 0.5, the relation between two variables is assumed to be neglectible.

4.2. Fictional DEM's

4.2.1. Raster Caster

To create fictional ground level maps, RasterCaster is used (van Wolfswinkel, 2019). RasterCaster creates digital elevation models from vector data (points, lines and polygons) in GEOtiff-format. Its application is not for elevation only, but can be used for all continuous variables that are better represented in a raster- than vector-format. RasterCaster interpolates points close to the polygon's border to create a raster inside the polygon based on Triangulated Irregular Network (tin). Another benefit of RasterCaster is that its outcome matches the 3Di-input demands for GeoTiff-formats like projection and nodata values.

4.2.2. Design level

As presented in figure D.1 in appendix D, issuance levels are prescribed by the city of Rotterdam. Newly constructed buildings and maintenance works are based on these levels. Because figure D.1 lacks the level of detail to be used in hydrological modelling, it is scaled-down for the Tuinenhoven case study by several adaptions:

1. The northern dike under the A16 highway is absent in the bathymetry of figure D.1. It is assumed that this dike is currently at design level. Because this dike is higher than issuance level and sloped, the precise height is not necessary as long as the runoff direction is correct and rain flows downward. Most of the runoff at this dike ends up in the water body at the dike's toe.

2. Per parcel and public space, based on BGT-polygons, the average issuance level is assumed for the whole parcel. So gardens will be flat as is likely in Rotterdam.

3. Buildings and waterways are filtered out, because flow on these polygons is impossible or represented by 1D channels.

4. Roads, parking lots and cycling paths are assumed to be 10 cm under issuance level. This 10 cm is based on the curb design-height in the city of Rotterdam. To realise a smooth course of the roads the tin method is applied, as explained in 4.2.1. Per BGT-polygon circumventing points and their corresponding issuance level are determined and the values within these polygons are interpolated.

4.2.3. Future ground level

To predict the future ground level the current land subsidence expressed as point-vectors is converted to an area covering map in GeoTiff-format. In figure 3.2, the subsidence rates are expressed as the mean value of all the low points per sub neighbourhood. However, individual low points can address a much higher level of detail of the subsidence behaviour within a sub-neighbourhood. It's challenging to interpolate between these low points because the subsidence rate per low point can be caused by totally different processes. Additionally, more than 100.000 low points are heterogeneously spread through the IJsselmonde sub-model, causing calculation-wise limitations. To prevent interpolation between points that are subject to different subsidence-causing processes, the low points are split based on the results of the land subsidence analysis. BAsed on the land subsidence analysis in 5.1 shows that land use classification is the strongest factor influencing land subsidence behaviour of open space. In addition to roads, vegetated terrain and unvegetated terrain, a category named 'other' is specified. Next to the splitting of low points, the polygons defined by this BGT are used as RasterCaster input. Interpolated subsidence rates per road are only influenced by low points located on roads. The BGT-polygons and their circumventing points form the basis for the tin-RasterCaster application. After the conversion from low point-vectors to an interpolated land-subsidence map in GeoTiff-format this map times 14 years is extracted from the 2016 DEM to create the prognosed 'DEM 2030 excluding road and sewer maintenance'. In figure 3.5, the planned maintenance work on roads and sewer is presented for the coming 10-15 years inside the sub-model IJsselmonde. To simulate this maintenance, all the BGT-polygons classified as pedestrian path are restored to issuance level. Roads and cyclist paths are restored to issuance level minus 10 cm (design height of curbs). Open terrain like gardens and parks are maintained at the current elevation height. After simulating, these adaptions with RasterCaster, a DEM is created that equals the 2016 DEM but the pedestrian paths and roads inside the planned maintenance regions are at design level. If the interpolated land subsidence map times 14 years is extracted from this map, the prognosed 'DEM 2030 including road and sewer maintenance' is created. Summarising, 5 DEM's are used as input for the 3Di simulations of a 70 mm in one-hour rain event in this research:

1. Tuinenhoven sub-model based on a DEM of 2016, equal to the stress test (Nelen & Schuurmans, 2018)
2. Tuinenhoven sub-model based on a fictional DEM that approximates design level
3. IJsselmonde sub-model based on a DEM of 2016, equal to the stress test (Nelen & Schuurmans, 2018)
4. IJsselmonde sub-model based on a prognosed DEM of 2030 excluding road and sewer maintenance
5. IJsselmonde sub-model based on a prognosed DEM of 2030 including road and sewer maintenance

4.3. 3Di model

4.3.1. Calculation background

3Di is a process-based, hydrodynamic model for flooding, drainage and other water management studies. It can be used for the computation of water flow in 1D and 2D (Nelen & Schuurmans, 2019). The computations of flow in both domains are based on Conservation of mass and Conservation of momentum. The 2D surface flow is based on the 2D depth-averaged shallow water equations. In the finite volume approach, used in 3Di, a volume domain equals a computational cell. Sources and sink terms are generally terms like rainfall or infiltration that are added or extracted in a domain.

The interaction between 2D surface flow and 1D flow in 3Di can be defined by three types of 1D flow sections: isolated, embedded, or connected. In the 'isolated' sections, there is no interaction between 1D and 2D. For embedded sections, the 1D cross-sectional profile is included in the 2D sub grid elevation and resistance grid. For connected sections, a relationship is defined between the 2D water level and the 1D water level. Computation time is generally a limiting factor for the use of high resolution bathymetry data in hydrological modelling (Volp et al., 2013). 3Di uses a so-called structured, staggered sub-grid introduced by Casulli (2009) to discretise space and time. It is based on the principle that the bed level can vary strongly over short distances, while water levels vary over larger scales. The sub-grid method deals with two grids, a coarse computation grid and an underlying sub-grid with a higher resolution. The bed level is defined on the sub-grid and the water level is assumed to be uniform within a coarse grid cell. The computation of cell volumes and cross-sections are performed using the high resolution bathymetry data (Volp et al., 2013). To automatically make the grid less coarse 3Di uses a method called quad-tree refinement, where the grid is defined by dividing a cell in 4, still structured, cells (Stelling, 2012).

4.3.2. Model scenario's

The 3Di-models of Tuinenhoven and IJsselmonde are presented in figure K.1 and K.2 in appendix K. To answer the research questions, several scenarios are composed. The starting point of this composition are the scenarios used in the Rotterdam stress tests as described in 2.1.2, because the results of these tests are currently consulted and critically inserted in the Rotterdam management policy. As stated in table 2.1, the current 3Di-simulations are based on a rain event of 70 mm in one hour, 90 mm in one hour and 160 mm in two hours. Because the results of the stress test show almost a linear increase of the impact of urban flooding with the rainfall depth in figure 2.1, this research focuses on the 70 mm in one-hour rain event. This rain event corresponds with an expected return period of 100 year in the year 2050 based on Dekker et al. (2018). As explained in 3.2, two sub-models are used in this research. The Tuinenhoven sub-model is used to compare 3Di results based on the 2016 DEM, representing the stress test, with 3Di results based on a DEM that approaches Tuinenhoven at design level. The IJsselmonde sub-model is used to compare the results of the stress test with 3Di simulations based two prognosed DEM's for the year 2030, one DEM including maintenance and one DEM excluding maintenance.

4.3.3. Output

The resulting water depths from the 3Di simulations are translated to the passability of roads and the risk of water nuisance per building to express the impact of urban flooding.

Passability of roads

The passability of a road is classified as 'Passable', 'Impassable' or 'Passable for calamity traffic'. This classification identifies the possible discomfort for civilians and it supports decisions in the prioritising of road maintenance or it can be used to optimise the emergency protocol by identifying possible unreachable areas of crisis during the same extreme weather event. The classification is based on the maximum water depth

and the inundated surface per road based on the 2D water depths produced by a 3Di model simulation. The intervals of the classification are shown in table 4.1. Roads are divided in road segments based on TOP10NL. TOP10NL is the basic land use database of the The Netherlands' Cadastre, Land Registry and Mapping Agency. The lowest classified road segment is normative for the classification of the road. Per road segment a buffer of 0,5 m around the centre line is analysed. Within this buffer the 90^{th} percentile-value of the maximum water depth and the percentage wet surface is calculated. Only the centre line per road segment is considered since roads are designed sloping towards the gullies that are located at the roadsides. In hydraulic modelling these gullies are often neglected and schematised at the manholes. Adding gully pots to a hydraulic model can lead to a significant decrease in water depths, as is investigated by van Haaren et al. (2018) for Lombardijen neighbourhood, however this difference decreases with more intense rain events since sewer overload will be the dominant failure mechanism. The passability of roads is calculated for all 5 scenario's as shown in table 4.2.

Table 4.1: Classification boundaries of the passability per road

Classification	90th percentile value water depth [cm]		Inundated surface [%]
Passable	Smaller than/equal to 10 cm	OR	Smaller than/equal to 5 %
Passable for calamity traffic	Higher than 10 cm AND smaller than 30 cm	AND	Higher than 5 %
Unpassable	Higher than 30 cm	AND	Higher than 5 %

Risk of water nuisance per building

The risk of water nuisance per building is used to identify risks per building or at neighbourhood-scale. The results are interesting for insurances, preventive measures or sewer reconstruction. One official college target for the city of Rotterdam is increasing the amount of buildings that are not at risk of water nuisance from 88 % to 90 % (City of Rotterdam, 2019). These percentages are based on so-called BlueLabels, that are based on the risk per building calculations in the stress tests (Zweers, 2019). In the stress tests, buildings are classified as 'No risk of nuisance', 'Risk of nuisance' and 'High risk of nuisance' per scenario. The maximum water depths calculated with the 3Di model are used as input. Pixels with a water depth less than 2 cm are filtered out. In principle all the adjacent water on the streets that is higher than the doorstep level can flow in the building and cause nuisance. Within a buffer of 0,5 m per building the highest water level is examined and used to determine the risk per building. Sometimes a building has a very high adjacent maximum water depth, although the adjacent volume is very low. To quantify this volume, all the water within a 5 m buffer per building higher than the doorstep level is calculated. If this volume divided by the surface area of the building is smaller than 0.005, the building is classified as 'No risk of nuisance'. Crucial in the determination of risk per building, is the doorstep level threshold per building (Wezenberg et al., 2016), but data about these levels is scarce. To approach this threshold level in hydrological modelling, the adjacent DEM pixels per building are examined and the 75^{th} percentile-value of these pixels plus 15 cm is calculated (Wezenberg et al., 2016). This 15 cm represents the actual doorstep height compared to surface level. Because buildings in Rotterdam are influenced by land subsidence, a 15 cm doorstep height is absent in some buildings. Therefor, the threshold values per building in Rotterdam are approached by calculating the 75^{th} percentile-value of the adjacent DEM pixels per building without additional doorstep heights. To include the doorstep height however, buildings are classified at 'Risk' and 'High Risk', as is shown in table 5.2. 'High Risk' means that the adjacent water level is at least 15 cm higher than the threshold value. This means that even buildings with a sufficient doorstep height are at risk.

For the Tuinenhoven scenario the risks per building are not calculated because it is assumed that buildings have a sufficient threshold when the design situation is approximated, as is shown in 4.2. When the design situation is considered, all buildings have a doorstep height of at least 15 cm. So, buildings classified at 'Risk' are because of there sufficient threshold value, not at risk. Due to the very flat created design DEM, it is not likely that waterdepths bigger than 15 cm will be calculated. In the simulation of a 2030 simulation, two methods of calculating a threshold value per building are possible. One way is the 'traditional' method based on the 75^{th} percentile-value of the adjacent DEM-pixels. This method is also used in the stress test. Basing the 2030 threshold value on the adjacent DEM-pixels means that the future threshold depends on the open space subsidence. Another method to determine the threshold value per building is extracting the building-specific mean subsidence rate based on Maccabiani (2014) from the 2016 determined thresholds. Both methods are applied for the 2030 scenario's as shown in 4.2. Comparing the results of both methods will elucidate the effect of the difference between open space- and building-subsidence.

Table 4.2: The calculated impacts of urban flooding per calculated 3Di simulation

Sub Model	DEM	Passability of roads	Risk of water nuisance per building
Tuinenhoven	2016	Yes	No
Tuinenhoven	Design	Yes	No
IJsselmonde	2016	Yes	Yes, threshold only based on adjacent DEM
IJsselmonde	2030 inc. maintenance	Yes	Yes, threshold based on 75th percentile value adjacent 2030 DEM and threshold based on building-specific subsidence rate
IJsselmonde	2030 exc. maintenance	Yes	Yes, threshold based on 75th percentile value adjacent 2030 DEM and threshold based on building-specific subsidence rate

5

Results

This chapter presents and briefly discusses the results acquired in this research. Firstly, the results of the land subsidence analysis are presented. Whether these results correspond to the expectations is discussed and thereafter the most important factors influencing land subsidence are selected. The selected factor are used in the second part of this chapter, namely the creation of the fictional and prognosed DEM's. In addition to the 2016 DEM of Tuinenhoven and IJsselmonde, three created DEM's are presented, as enumerated in 4.3.2. A DEM that approximates Tuinenhoven sub-neighbourhood at design level is created, mainly based on the prescribed issuance levels in Rotterdam. Furthermore, two DEM's are created that prognose subsidence until 2030, one including planned road maintenance and one excluding road maintenance. Thirdly, the created DEM's are used as 3Di-input, the resulting water depths are translated to impact of pluvial flooding and the results are presented and discussed.

5.1. Land subsidence analysis

5.1.1. Foundation type

The distribution of the mean subsidence rates per building categorised by foundation types is presented in figure 5.1(left). Buildings on shallow foundations show fastest subsidence rates (-1.46 mm/ yr median) in general, followed by buildings founded on wood (-0.47 mm/ yr median) and concrete (-0.14 mm/ yr median), respectively. The standard deviation per building categorised by foundation type is shown in figure 5.1(right). Based on Welch' T-test, only the differences between the standard deviation of buildings founded on shallow foundation and buildings on wooden piles are statistically significant. Buildings founded on wooden piles show a median standard deviation of 0.58 mm/year compared to buildings on shallow foundations with a standard deviation of 0.49 mm/yr. As expected in 2.2.2, buildings on shallow foundations generally subside faster than buildings founded on concrete or wooden piles. However, buildings founded on wooden piles show a higher standard deviation per building compared to buildings on shallow foundation. This indicates the occurrence of uneven subsidence, which causes structure-damage, as explained in chapter 2.2.3. As explained in chapter 2.2.2, pole rot is a known problem in Rotterdam that affects the bearing capacity of wooden piles. This chemical process develops differently per pole and causes uneven subsidence of buildings founded on wooden piles.

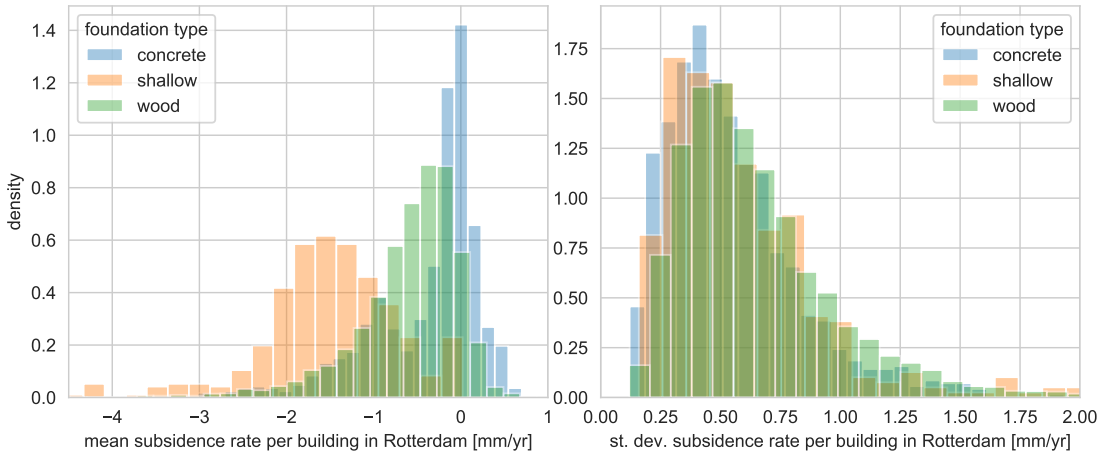

Figure 5.1: Mean(left) and standard deviation(right) of the subsidence rates of the high points per building in Rotterdam categorised by foundation type

5.1.2. Land use

Subsidence rates per low point categorised by land use classification within the IJsselmonde sub-model are compared and presented in figure 5.2(left). Low points on roads show a higher subsidence rate in general than vegetated and unvegetated terrains (respective medians of -3.2, -2.4 and -1.6 mm/yr). So, low points located on roads show roughly twice as fast subsidence rates as low points located on unvegetated area in IJsselmonde. Vegetated areas represent vegetated public parks and public garden in general. Unvegetated areas are generally represented by gardens that can contain either pavement or vegetation. As discussed in 2.2.2, Koster et al. (2018) stated that anthropogenic compression caused by loading is an important cause of urban land subsidence. So, differences in subsidence behaviour between land use classifications can be explained by the fact that roads experience dynamic loads from traffic and static loads from pavement or contain artificially applied sub soil.

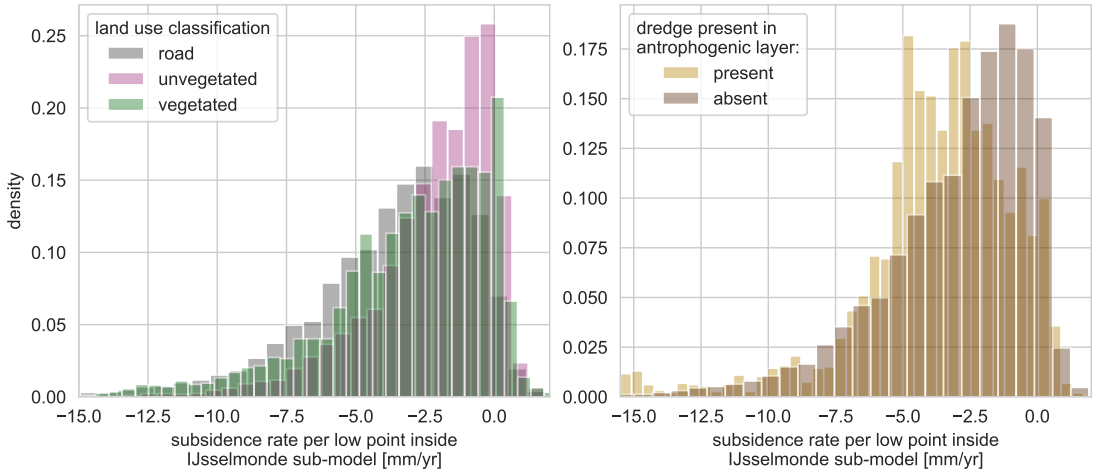

Figure 5.2: Left: Subsidence rates per low point inside IJsselmonde sub-model categorised by land use classification. Right: subsidence rates per low point inside IJsselmonde sub-model divided in points that are located on top of dredge-containing soils and low points that are not located on dredge-containing soils.

5.1.3. Presence of dredge in the subsoil

Figure 5.3 shows the distribution of the mean and the standard deviation of the subsidence rate per building located on top and outside dredge-containing soils. The median mean subsidence rate of buildings within dredged areas is -0.49 mm/yr and -0.30 mm/yr for buildings outside dredged areas. The standard deviation of the subsidence rate per building of buildings within dredged areas is 0.62 mm/yr and outside dredged

areas 0.54 mm/yr. Additionally, in the IJsselmonde sub-model, figure 5.2(right) shows that low points located on top of dredge-containing soils show higher subsidence rates than points outside dredge-containing soils (median of -3.4 compared to -2.3 mm/yr). The fact that buildings in Rotterdam and low points inside the IJsselmonde sub-model on top of dredge-containing soils show faster subsidence rates and higher standard deviations than buildings and low points outside these dredge-containing soils supports the occurrence of landfill subsidence in Rotterdam. As illustrated in appendix H, the major part of Rotterdam's cover layer is classified as anthropogenic applied soil (Dinoloket, 2019). Exact properties of these applied layers are not addressed by GeoTop. The observation that the likely presence of dredge in this applied soil influences the subsidence behaviour, shows that better knowledge of the exact composition and origin of these layers is important to understand the occurring processes behind land-subsidence in Rotterdam.

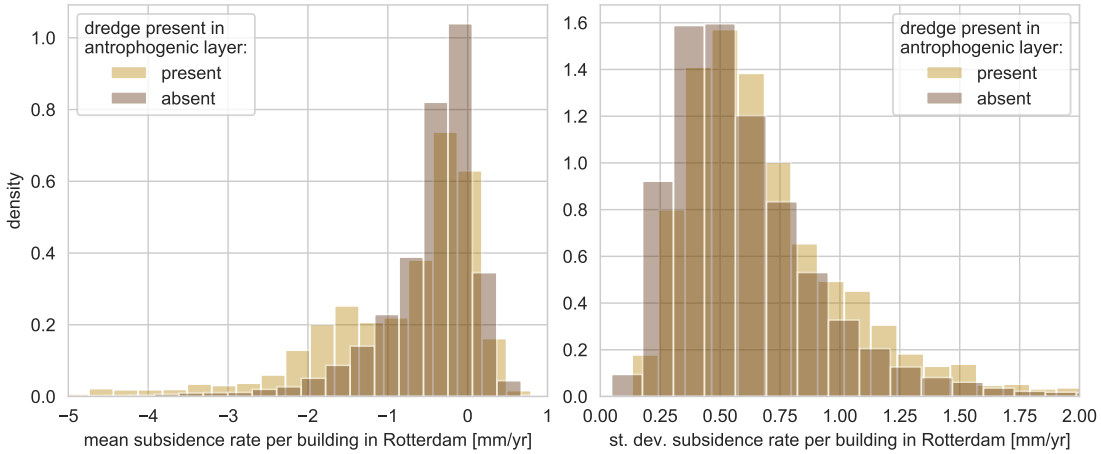

Figure 5.3: Mean(left) and standard deviation(right) of the subsidence rates of the high points per building in Rotterdam located on top of dredge-containing soils versus buildings that are not located on dredge-containing soils.

5.1.4. Underlying soil types

The distribution of the mean and standard deviation of the subsidence rate per building in Rotterdam categorised by the underlying predominantly sand and peat soils are presented in figure 5.4. Based on Welch' T-test, no significant difference between the mean and standard deviation per buildings on a predominantly clay soil and buildings on other predominantly soil types was found. So, buildings that are located on top of predominantly clay soils are excluded in figure 5.4. Furthermore, buildings on top of predominantly sand soils seem to subside equally fast (median of -0.27 mm/yr compared to a median of -0.29 mm/yr) and show an equally standard deviation per building (0.52 mm/yr compared to 0.49 mm/yr). So, no strong influence of the dominant soil type on the land subsidence behaviour of buildings in Rotterdam is detected. In addition, the distribution of the subsidence rate per low point in the IJsselmonde sub-model categorised by the dominant soil type is presented in in figure 5.6(left). It illustrates that low points on top of dominant clay soils slightly subside faster than dominant sand and peat soils (medians of -2.3, -2.0 and -1.9 mm/yr). In addition to the fact that the difference between the median subsidence rate of low points on predominantly sand- and peat soils is only 0.1 mm/yr, the difference is insignificant based on Welch' T-test. The distribution of the mean and standard deviation per building in Rotterdam categorised by the underlying top soil type is presented in figure 5.5. Contrary to the analysis of the mean subsidence rate of buildings categorised by dominant soil types, the differences categorised by top soil types are statistically significant for all soil types based on Welch' T-test. In addition, the subsidence rates of low points categorised by top soil type differ statistically significant for all three types, as presented in figure 5.6(right). Figure 5.5 shows that buildings located on sandy top soil generally subside fastest, followed by respectively clay and peat (medians of -0.35, -0.31 and -0.23 mm/yr respectively). So, buildings located on top of peat soils show about 1.5 times slower subsidence rates than buildings located on top of sand or clay in general. The comparison between the standard deviation per buildings on different top soil types is only significant for top soil types peat and sand, as presented in figure 5.5(left). However, buildings founded on a top soil type of sand have an relatively equal standard deviation to buildings founded on peat (median standard deviation of 0.58 mm/yr compared to 0.54 mm/yr). So, the influence of the top soil type on the standard deviation per building inside the IJsselmonde sub-model is

small. In addition to buildings in Rotterdam, low points in the IJsselmonde sub-model located on sand top soils subside faster than points on clay and peat top soils (respective medians of -3.0, -2.2 and -1.8 mm/yr) as is presented in figure 5.6(right). The fact that top soil type influences the subsidence behaviour of buildings and open space more significantly that the dominant soil, supports that land subsidence in Rotterdam is caused in the Holocene peat and clay layers influenced by phreatic groundwater as stated by Erkens et al. (2015), instead of the deeper layers. The fact that both buildings and low points located on top soils of peat show slower subsidence rates than buildings and low points on top of sand and clay top soils, supports the absence of significant peat oxidation in Rotterdam as stated by van den Born et al. (2016). To explain the fact that buildings on top soils of sand subside faster than buildings on top of peat and clay, a suspected correlation between top soil type and the presence of dredge in the anthropogenic layer is suggested in IJsselmonde. Figure 3.4 and appendix I show that the top soils of sand are primarily located in the northern part (Eiland van Brienenoord) of the IJsselmonde sub-model, where also dredge is present in the anthropogenic layer.

5.1.5. Anthropogenic depth and drainage depth

As described in 4.1.2, Spearman's correlation coefficient is used to asses how well an arbitrary monotonic function can describe a relationship between two variables. Based on this coefficient, no significant influence of anthropogenic depth or the drainage depth on either the mean subsidence rate or standard deviation per building or low point is identified. Despite it is shown that land subsidence behaviour is more influenced by the top soil type that is sensitive to phreatic groundwater compared to the more deep dominant soil type, the occurrence of landfill subsidence is supported and the fact that the influence of groundwater on land subsidence in Rotterdam is theoretically inevitable, there is no significant correlation found between the drainage depth and subsidence rates based on Maccabiani (2014). Comparing drainage levels with the subsidence behaviour of buildings and open space based on Maccabiani (2014) is difficult because the InSAR data expresses one subsidence rate over a period of 5 years, while the ground water fluctuates monthly. Splitting the subsidence rate shorter interval measurements can improve the assessment of the influence of drainage depth per monitoring well on subsidence behaviour. However, the benefit of a radar interferometric time series analysis is to circumvent the influence of the phase contribution of the atmospheric signal, together with temporal and geometric decorrelation (van Leijen, 2014). Looking at shorter periods affects these benefits. A second cause for the difficulty of detecting a relationship between drainage depth and subsidence behaviour is the heterogeneous shallow sub-surface soil types and structure that strongly influence the subsurface' permeability that is characteristic for urban areas. More detailed subsurface data than GeoTop is needed to asses the influence of this heterogeneous urban subsurface. In addition, the fact that no relation is detected between the thickness of the anthropogenic applied layer and subsidence rates is detected suggests that the composition of this layer differs. Better knowledge of the exact composition and origin of these layers is important to understand the occurring processes behind land-subsidence in Rotterdam.

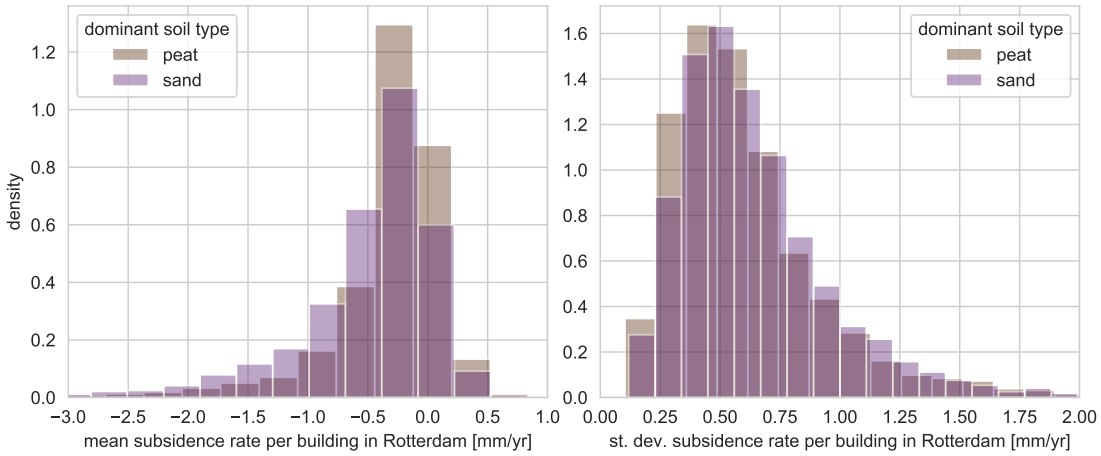

Figure 5.4: Mean(left) and standard deviation(right) of the subsidence rates of the high points per building in Rotterdam categorised by underlying dominant soil type

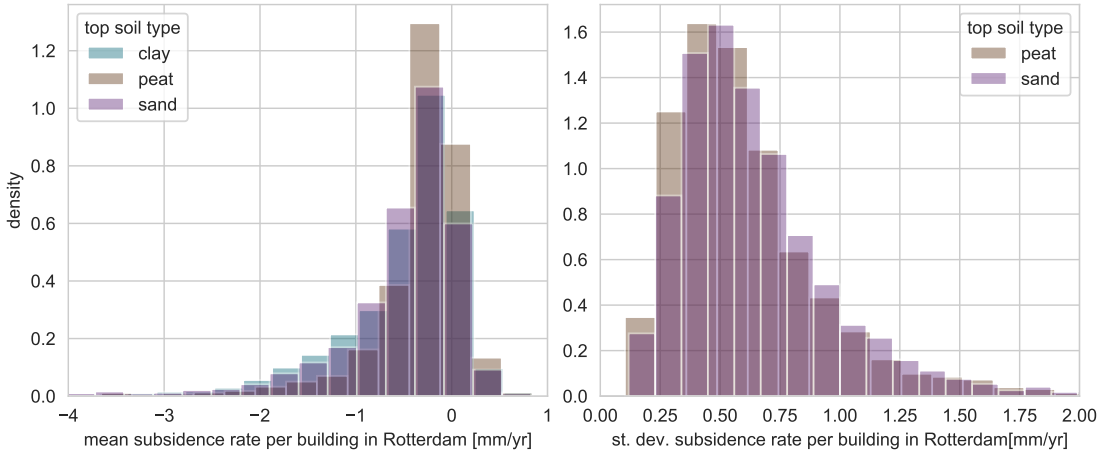

Figure 5.5: Mean(left) and standard deviation(right) of the subsidence rates of the high points per building in Rotterdam categorised by underlying top soil type

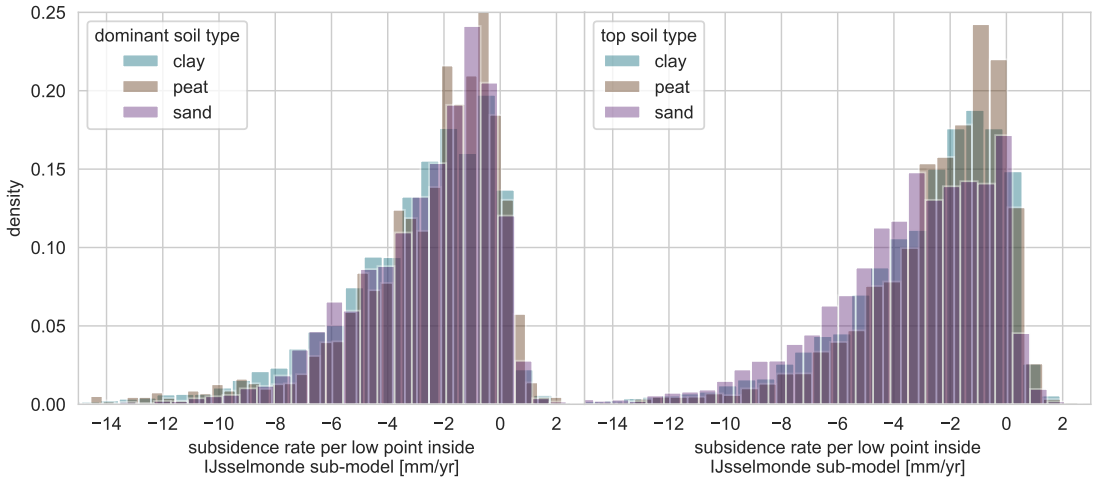

Figure 5.6: Subsidence rates per low point inside IJsselmonde sub-model categorised by underlying dominant (left) and top (right soil type.

5.1.6. Summary

The land subsidence indicated the presence of several land subsidence processes and influences in Rotterdam. As expected, foundation type is found to be the most important factor influencing mean subsidence rates of buildings. Buildings on shallow foundation subside faster than buildings founded on piles. Buildings founded on wooden piles subside more uneven than buildings on shallow foundation, presumably caused by the process of pole rot. In addition, the buildings located on top of dredge-containing anthropogenic applied soil show faster subsidence rates than other buildings in Rotterdam, which supports the occurrence of landfill subsidence in Rotterdam. Contrary to the dominant soil type, the subsidence behaviour of buildings is influenced by the top soil type. Buildings located on top peat soils subside slower than buildings located on sand and clay top soils. This supports the absence of peat oxidation in Rotterdam. Land use classification is found to be the most important factor influencing the subsidence behaviour of low points. Low points located on top of roads subside faster than low points on top of vegetated and unvegetated areas, as expected due to the higher dynamic traffic loads and static loads from pavement or artificially applied sub soil. Alike buildings, the presence of dredge in the anthropogenic applied soil and the top soil type classification influences the subsidence behaviour of low points. Open space where the anthropogenic soil contains dredge subsides generally faster than than open space outside these areas in IJsselmonde, which supports the occurrence of landfill subsidence in Rotterdam. Alike buildings, open space located on top of peat top soils show the slowest subsidence rates, which supports the absence of oxidation in Rotterdam. Open space located on sandy top soils subside fastest, which is likely to be caused by the presence of dredge in the subsoil. The influence of the dominant soil type on the subsidence behaviour is lower than the influence of top soil type. This supports that subsidence in the Netherlands is due to phreatic groundwater level lowering and the consequent consolidation in the Holocene clay layers (Koster et al., 2018). No strong influence between the depth of the anthropogenic layer or drainage depth and the subsidence behaviour of Rotterdam is detected. Time-scale difficulties in the drainage depth and the lack of more detailed properties of the anthropogenic soil were the primary limitation in this detection. In addition, Geotop-voxels of 100m x 100m are not likely to represent the heterogeneous urban shallow sub-surface.

5.2. Created DEM's

The created DEM's that are used as input for the 3Di simulations are compared to the DEM 2016 and presented in in figure 5.7, 5.8 and 5.9. For the Tuinenhoven case-study a DEM is created that approximates the design level. For the IJsselmonde case-study, two DEM's are created that prognoses subsidence until 2030, one in- and one excluding road maintenance.

5.2.1. Tuinenhoven

When the created DEM that approximates Tuinenhoven at design level is compared to the 2016 DEM in figure 5.7, it becomes clear that almost the whole sub-neighbourhood is under design level. The highest level difference of almost 50 cm is located in the Koninginnenweg. The created DEM for Tuinenhoven at design level is fictional and is used to demonstrate a case-study not influenced by subsidence. The probability that this design level DEM has at one point represented the Tuinenhoven surface level is low, because buildings and roads are constructed in different periods. As described in 4.2.2, the created design level is majorly based on the prescribed issuance level map, presented in figure D.1. To improve the level of detail of this map a curb height of 10 cm is implemented in the design DEM. Design prescriptions, like slopes in the roads and pedestrian paths towards the gully pots, from the city of Rotterdam that are not included in the creation of the fictional design DEM. Because this research focuses on extreme rain events, the absence of this slope is expected to not influence the results drastically, as supported by van Haaren et al. (2018). The red zones in figure 5.7 represent locations where the DEM 2016 is higher than the design DEM. These zones are generally located in public parks, close to water bodies and in gardens. Contrary to public roads, the issuance level is not strictly followed in these zones in reality. Public parks and zones close to water bodies can deviate from the issuance level because of aesthetic reasons or because the surface is naturally formed. Private gardens are not maintained by the municipality and can deviate from issuance level influenced by the owner.

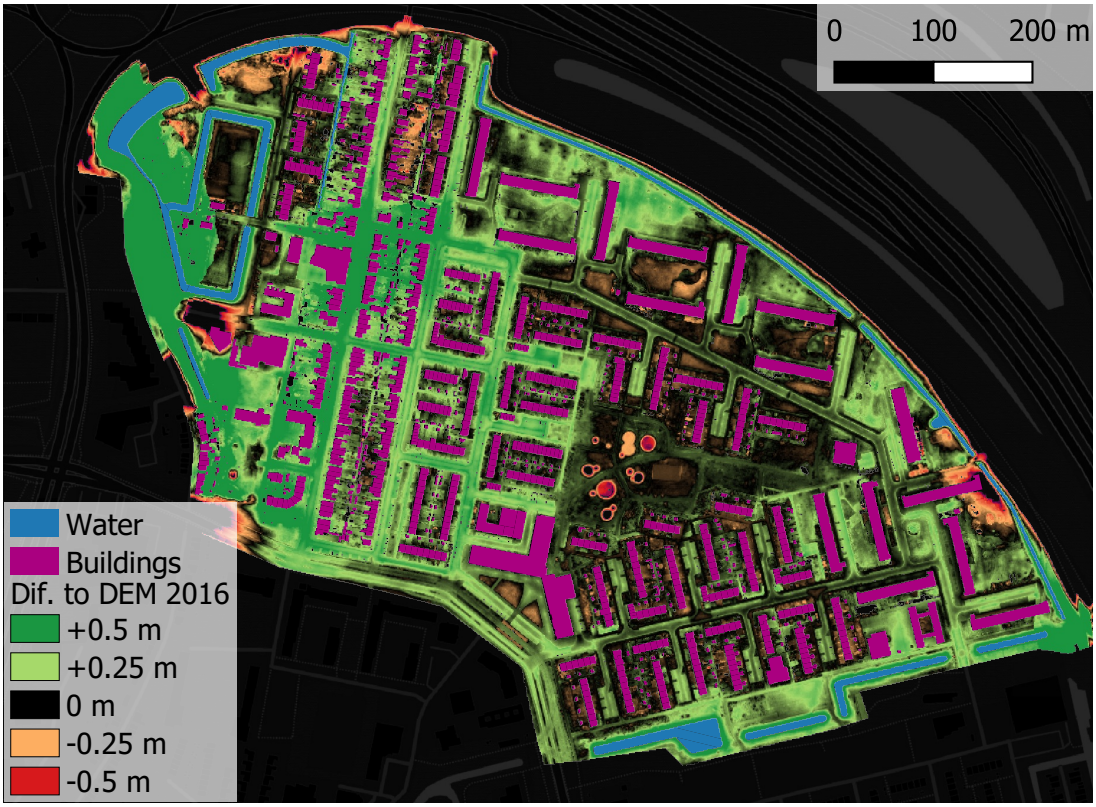

Figure 5.7: Created DEM of Tuinenhoven at design level compared to the DEM 2016. Note that green represents locations where the design DEM is higher than the 2016 DEM

5.2.2. IJsselmonde

Figure 5.8 and 5.9 show the comparison between the 2016 DEM of IJsselmonde and the prognosed DEM of 2030 excluding (5.8) and including (5.9) maintenance. Note that this is a prognosis of the subsidence of open space and subsidence of buildings is not included. The highest expected subsidence is 18 cm in 14 years, which corresponds with a subsidence rate of roughly 13 mm/yr. Subsidence rates are noted to be higher around main infrastructure works like the A16 highway, the Rotterdam Lombardijen train station, the Stadionweg and the Oostdijk in the North. This indicates the influence of dynamic traffic or passive infrastructure loads on the subsidence behaviour within IJsselmonde. As illustrated in the land subsidence analysis, figure 5.2L shows that low points located on top of roads subside faster than low points located in gardens and public parks too. This suggests the occurrence of consolidation due to the weight of infrastructure and its foundation. In agreement with figure 3.6, high sub-neighbourhood subsidence is noted in Lombardijen, eastern Groot IJsselmonde and in the sub-neighbourhoods close to the Meuse-river. In improvement of figure 3.6, figure 5.8 elucidates inner-sub-neighbourhoods variation. The mean subsidence rates of sub-neighbourhoods, expressed in figure 3.6, close to main infrastructure are influenced by the subsidence rates of this infrastructure, whilst the causing subsidence-process and severity can be totally different inside the sub-neighbourhood. This causes overestimation of the subsidence-severity per sub-neighbourhood, especially when the 25^{th} percentile value is used to express the land subsidence per sub-neighbourhood. More detailed inner-sub-neighbourhood subsidence behaviour is needed to match the building-specific results from 3Di in this research.

Figure 5.8: Prognosed DEM of IJsselmonde in 2030 excluding maintenance compared to the DEM 2016. Note that green represents locations where the prognosed 2030 DEM is higher than the 2016 DEM

Figure 5.9: Prognosed DEM of IJsselmonde in 2030 including maintenance compared to the DEM 2016. Note that green represents locations where the prognosed 2030 DEM is higher than the 2016 DEM

5.3. Urban flooding

5.3.1. Tuinenhoven sub-model

Figure L.1 and L.2 in appendix L show the results of the 3Di-simulations of a 70 mm in one hour rain event based on the 2016 DEM (stress test scenario) and the design DEM for the Tuinenhoven case-study. The 3Di results of Tuinenhoven at design level show water depths between 0 and 5 cm throughout the major part of the sub-neighbourhood. Compared to the 2016 DEM, water depths are less deep and more evenly distributed, but the total area covered in water is larger. Because variations in the bathymetry of the design DEM are minimal, water depths variations are too. As stated, this scenario is fictional to test whether water nuisance occurs if subsidence has never occurred. Figure 5.10 shows the cumulative 2D flow for the 3Di simulation based on the 2016 DEM, representing the stress test, and the design DEM. Positive '2D flow to 1D' represents sewer/water body inflow and negative '2D flow to 1D' represents sewer/water body outflow. Constant infiltration is a small part of the water balance and depends on inundated permeable surface. During the 70 m in one hour simulation based on the 2016 DEM, the maximum amount of water stored on the surface is roughly 25000 m^3, which corresponds with roughly 50 mm. Based on the design DEM, the amount of water stored on the surface is 25000 m^3 too. After one hour, when also the peak water storage on the surface occurs, roughly 14000 m^3 water has flown in and 12000 m^3 water has flown out the 1D system based on the 2016 DEM scenario. The 1D interaction is less for the scenario based on design level, 8000 m^3 water has flown in and 6000 m^3 water has flown out of the 1D system. This demonstrates that rain does not reach the sewer inflow points or water bodies during the simulation based on the design DEM, but also that less water flows out from the sewer. Overloading of urban water structures is a primary cause of urban flooding (Delta Program, 2017; ten Veldhuis, 2011) and the sewer capacity in Tuinenhoven is insufficient to cope with 70 mm in one hour. The Tuinenhoven case study showed that the total amount of water stored on the street is not affected by the DEM. The DEM affects the distribution of the water. As expected, the water depths at the Koninginnenweg in the design simulation are less deep compared to the stress test results. Figure L.3 and L.4 presents the 2D flow pattern during the 3Di-simulation and show that during a simulation based on the 2016 DEM, sewer outflow occurs at the Koninginnenweg. A simulation based on the design DEM generally shows sewer inflow at the Koninginnenweg. This explains the decrease of water nuisance at the Koninginnenweg.

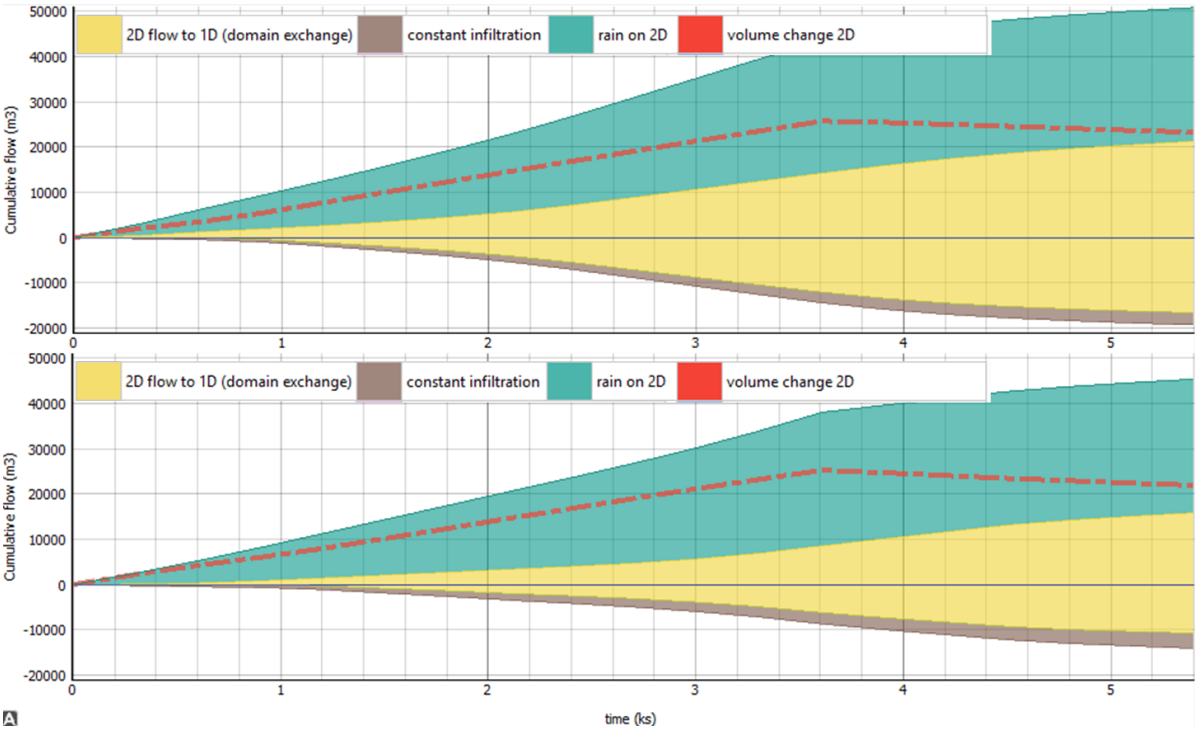

Figure 5.10: Cumulative discharge in the 2D-domain for 3Di simulation of a 70 mm in one hour rain event for the Tuinenhoven case-study based on the 2016 DEM (top) and design DEM(bottom). Positive '2D flow to 1D' represents sewer/water body inflow and negative '2D flow to 1D' represents sewer/water body outflow. The 'volume change 2D' expresses the amount of water stored on the surface.

Table 5.1: Passability-classification of roads based on 3Di simulation of a 70 mm in one hour rain event based on 5 different scenario's.

Scenario	Passable		Passable for calamity traffic		Unpassable	
Tuinenhoven DEM 2016 (stress test)	4065 m	55 %	2999 m	41 %	295 m	4 %
Tuinenhoven DEM design	3935 m	53 %	3423 m	47 %	0 m	0 %
IJsselmonde DEM 2016 (stress test)	126669 m	59 %	76326 m	35 %	12516 m	6 %
IJsselmonde DEM 2030 excluding maintenance	121784 m	57 %	77996 m	36 %	15730 m	7 %
IJsselmonde DEM 2030 including maintenance	135115 m	63 %	68123 m	32 %	12273 m	6 %

The resulting water depths are translated to passability per roads and summarised in table 5.1. Elevating Tuinenhoven results in a decrease from 4 % to 0 % 'Unpassable' roads but an increase from 41 % to 47 % roads that are only 'Passable for calamity traffic' compared to the stress test. Figure L.2 shows that raising the ground level solves the roads classified as 'Unpassable' at the Koninginnenweg. However, the water that is located at the Koninginnenweg in the 2016 scenario, is spread throughout the neighbourhood in the design level scenario and decreases the number of roads that are 'Passable'. The results of the passability of roads demonstrate that land subsidence makes the impact of urban flooding more severe, but raising the vulnerable surfaces does not solve the overloading of the sewer system and can increase the total impact of urban flooding.

5.3.2. IJsselmonde sub-model

The results of the 70 mm in one hour rain event 3Di simulation on the IJsselmonde sub-model based on the DEM of 2016, the prognosed 2030 DEM excluding maintenance and the prognosed 2030 DEM including maintenance are presented in figure M.1, M.2 and M.3 in appendix M. Table 5.1 shows the resulting passability of roads in the IJsselmonde sub-model. By comparing the 2016 DEM-scenario and the 2030 DEM excluding maintenance, it becomes clear that the prognosed subsidence decreases the passability of roads from 59 % to 57 %. In addition, figure M.5 presents the expected passability per neighbourhood and shows that the passability of roads decreases in all neighbourhood for 2030. When maintenance is included in the prognosis, the passability of roads in the total sub-model increases from 59 % to 63 % compared to the stress test. Figure M.5 shows that the differences in passability between the DEM 2030 in- and excluding maintenance are caused in Groot IJsselmonde and Lombardijen, because in these neighbourhoods maintenance is planned (figure 3.5) and simulated (figure 5.9). The neighbourhoods Oud IJsselmonde and Beverwaard show a comparable decrease in passability between 2016 and 2030 for the scenario in- and excluding maintenance. So, the current maintenance regime is effective in terms of increasing the passability of roads during extreme rainfall.

The threshold per building is based on two methods. The first method assumes that the 75^{th} percentile value of the adjacent DEM pixels corresponds with the threshold value per building. The second method subtracts the building-specific measured subsidence rate per building between 2009 and 2014, based on Maccabiani (2014), and subtracts this rate 14 years from the 2016 threshold used in the stress test. The method of threshold calculation per building strongly influences the resulting risk of water depths in the whole sub-model of IJsselmonde. The method using building-specific subsidence rates to determine the threshold value per building is considered most realistic. Using both methods as calculation-input however, will asses the effect on buildings that subside at a different rate than their surroundings compared to buildings that have a similar subsidence rate compared to their surroundings. Table 5.2 shows the resulting risk per building for the IJsselmonde sub-model based on all the scenarios and the different methods of threshold determination per building, categorised per neighbourhood. Figure 5.11 supplements table 5.2 by showing bar charts including the number of buildings at risk per neighbourhood and divides buildings classified at 'Risk' and at 'High Risk'.

Table 5.2 shows that the prognosed 2030 DEM-scenario excluding maintenance results in less buildings at risk of water nuisance compared to the DEM 2030 including maintenance. Depending on the threshold value this difference ranges between 0.4 % and 1.6 %, which corresponds with 126 - 504 buildings. Figure 5.11 shows that these differences occur in the neighbourhoods where maintenance is planned, namely Groot IJsselmonde and Lombardijen. Contrary to a decrease of roads classified as 'Unpassable' or 'Only passable for calamity traffic', the 3DI-simulation of prognosed 2030 DEM-scenario including maintenance results in an increase of buildings at risks compared to the prognosed 2030 DEM-scenario excluding maintenance. As demonstrated for the Tuinenhoven case-study in figure 5.10, insufficient capacity of the sewer system is the principal cause of urban flooding in the IJsselmonde sub-model. Raising the streets increases its passability but decreases its storage capacity, which is an important characteristic of streets (Delta Program, 2017). Water previously stored on these streets finds its way to gardens and puts buildings at an increasing risk.

Table 5.2: Resulting Risk per building from 3Di simulation of a 70 mm in one hour rain event based on a 2016 DEM, a prognosed 2030 DEM excluding maintenance and a prognosed 2030 DEM including maintenance. Buildings at risk include buildings classified at 'Risk' and at 'High Risk'. The threshold-value per building for the prognosed scenario's are based on two methods. The first assumes that the 75th percentile value of the **adjacent DEM** pixels corresponds with the threshold value per building. The second method subtracts the **building-specific** measured subsidence rate per building between 2009 and 2016, based on Maccabiani (2014), and subtracts this rate 14 years from the 2016 threshold per building. The 2016 threshold per building is based on the adjacent DEM.

		DEM2016	DEM 2030 exc.		DEM 2030 inc.	
	Buildings	Adjacent DEM	Adjacent DEM	Building-specific	Adjacent DEM	Building-specific
Beverwaard	7182	2.9 %	2.5 %	2.4 %	2.5 %	2.4 %
Groot IJsselmonde	11205	11.1 %	12.1 %	9.7 %	13.1 %	13.5 %
Lombardijen	8814	12.8 %	12.6 %	10.1 %	13.0 %	10.9 %
Oud IJsselmonde	4337	21.5 %	28.1 %	11.0 %	28.1 %	11.0 %
Total	31538	11.1 %	12.3 %	8.3 %	12.7 %	9.9 %

Table 5.2 shows that generally, the risk per building is expected to decrease. When the threshold value is based on the building-specific subsidence rate expressed by Maccabiani (2014), the number of buildings at 'Risk' and at 'High Risk' decreases with from 11.1 % (DEM 2016) to 8.3 % (DEM 2030 excluding maintenance). However, more buildings are at 'Risk' in 2030 compared to the 2016 scenario when the threshold is based on the 75^{th} percentile value of the adjacent DEM values per building (increase from 11.1 % to 12.3 %). Whether the 75^{th} results in an in- or decrease of risks per building differs per neighbourhood, as shown in figure 5.11. Which indicates that the threshold method is a strong influence of the risk classification per building. The risk of water nuisance per building can increase in two ways, either the adjacent water level increases or the threshold value decreases. Figure 5.12 and 5.13 present the comparison between the increase of water level and the decrease of the threshold value per building for all 4 calculations compared to the stress test, for respectively Beverwaard, Groot IJsslmonde, Lombardijen and Oud IJsselmonde. All scatter located above the bottom left to top right diagonal represent buildings where the risk of water nuisance increases compared to the stress test result. All scatters located below the bottom left to top right diagonal represent buildings where the risk of water nuisance decreases compared to the stress test result. The distribution plots above and on the right-hand-side of the scatter plots illustrate the scatter density. Per neighbourhood and per threshold method, different phenomena concerning the risk of water nuisance per building are noted. Next, the observations per neighbourhood are discussed. Most scatter is located at the double negative part of the bottom left to top right diagonal, especially for the DEM 2030 excluding maintenance scenario with thresholds based on the adjacent DEM-pixels. This indicates that the thresholds and their surroundings show a similar subsidence rate and that this subsidence directly influences the lowering of the adjacent water level. This shows that the 2D flow is not drastically influenced by subsidence, because then larger water level deviations compared to the stress test would be detected.

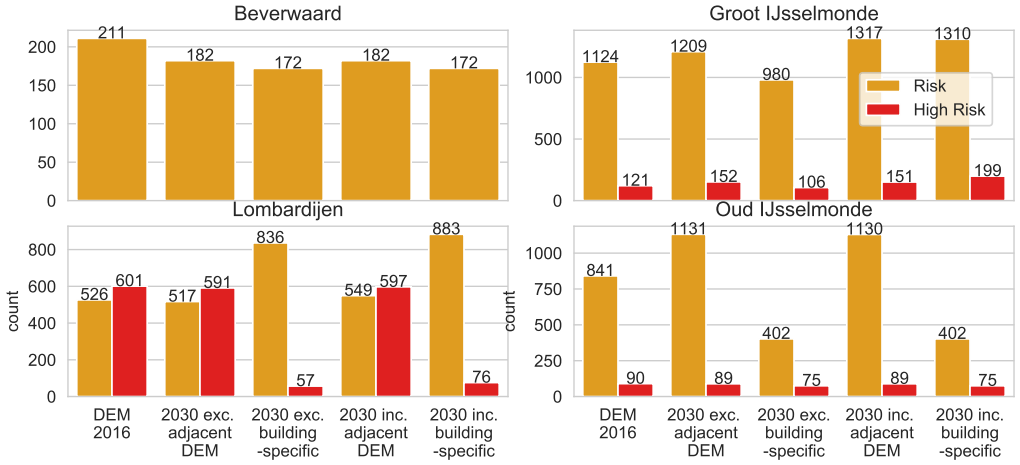

Figure 5.11: Risk of water nuisance per building resulting from a 70 mm in one hour 3Di simulation based on three DEM-scenario's for the IJsselmonde sub-model categorised by neighbourhood

Beverwaard
Figure 5.11 shows that no buildings are classified at 'High Risk' in all the scenario's for thresholds based on both methods. Because no maintenance is planned in the coming 14 years, there are no differences between the buildings at risk an passability of roads for the simulation based on the 2030 DEM in- and excluding maintenance. When the scatterplots are compared horizontally in figure 5.12(top) the absent influence of including maintenance in the calculation is illustrated, because horizontally the scatter plots do not differ. Table 5.2 shows that, compared to the stress test, the amount of buildings at risk is expected to decrease for both threshold methods. So water is increasingly stored at locations not-adjacent to buildings. Because figure M.5 shows a decrease of the passability of roads, this water presumably stored at the relatively fast subsiding streets. The distribution charts on top of the scatter plots in figure 5.12(top) show that the threshold decrease determined with the building-specific method is slightly lower than the threshold decrease determined with the adjacent 2030 DEM-pixels. So, buildings subside slightly slower than their surroundings. This explains that when the threshold value is based on the building-specific subsidence rate, less buildings are at risk compared to thresholds based on the adjacent DEM-values in figure 5.11.

Groot IJsselmonde
Compared to figure 5.12(top), figure 5.12(bottom) shows a larger spread of the scatterers (roughly 0-5cm compared to -15 - 15 cm) for both threshold values and water levels increase. This indicates that Groot IJsselmonde subsides faster than Beverwaard, both buildings and open space. If maintenance is excluded in the scenario, less buildings are at risk compared to the stress test when the thresholds are based on building-specific subsidence rates in table 5.2. The amount of buildings at risk increases compared to the stress test result when the thresholds are based on building-specific subsidence rates. In other words, buildings subside generally slower than their surroundings. In Groot IJsselmonde, maintenance will increase the number of buildings at risk based for both threshold methods, based on figure 5.11, but increases the passability of roads, based on figure M.5. When the horizontal scatter plots are compared, it is clear that the including of maintenance results in higher water levels compared to the simulations excluding maintenance. This shows that water formerly stored on roads is in the 2030 scenario stored against a building possibly via the garden. Figure 5.12(bottom) also illustrates that including of maintenance leads to an elevation of the threshold values when based on the adjacent DEM-values. This is unrealistic because buildings, and doorstep heights, in Rotterdam generally subside. This unrealistic raise of the threshold value explains why less buildings in the DEM 2030 including maintenance scenario are at risk in table 5.2 than when the threshold value is based on adjacent DEM values compared to when the threshold is based on the building-specific subsidence rate.

Lombardijen
The observations in Lombardijen are similar to Groot IJsselmonde. Compared to figure 5.12(bottom), figure 5.13(top) shows a smaller spread of the scatterers for both threshold values and water levels increase. Buildings subside slower than their surroundings as shown by the bar charts on top of the scatter plots in figure 5.13top for the scenario excluding maintenance. Furthermore, maintenance generally result in a lower amount if buildings at risk in table 5.2 in both neighbourhoods. Additionally, this reduction is even more illustrated in 5.11 by a transition from building at 'High Risk' to 'Risk'. Furthermore, the including of maintenance results in more buildings at risk and more passable roads in both neighbourhoods. Contrary to the observations in Groot IJsselmonde, the scenario excluding maintenance shows a decrease of buildings at risk for both threshold methods. In other words, if the current subsidence rate continues and no maintenance is performed, water nuisance for buildings is expected to decrease in the Lombardijen neighbourhood.

Oud IJsselmonde
Including maintenance does not influence the resulting buildings at risk (table 5.2) or the passability of roads (figure M.5), because no maintenance is planned in Oud IJsselmonde in the coming 11 years (figure 3.5). The differences in resulting buildings at risk between the threshold values in table 5.2 are large in Oud IJsselmonde (28.1.% compared to 11.0 %) Compared to the stress test results, basing the thresholds on adjacent DEM pixels per buildings results in a strong increase of buildings at risk and basing the thresholds on the building-specific subsidence rate shows a strong decrease of buildings at risk. Figure 5.13 shows this difference because the thresholds based on the building-specific subsidence rate are concentrated closer to 0. This shows that the difference of the subsidence rate between open space and buildings is high in Groot IJsselmonde. Figure 5.2 showed that the presence of dredge in IJsselmonde could be the cause of the fast subsiding behaviour.

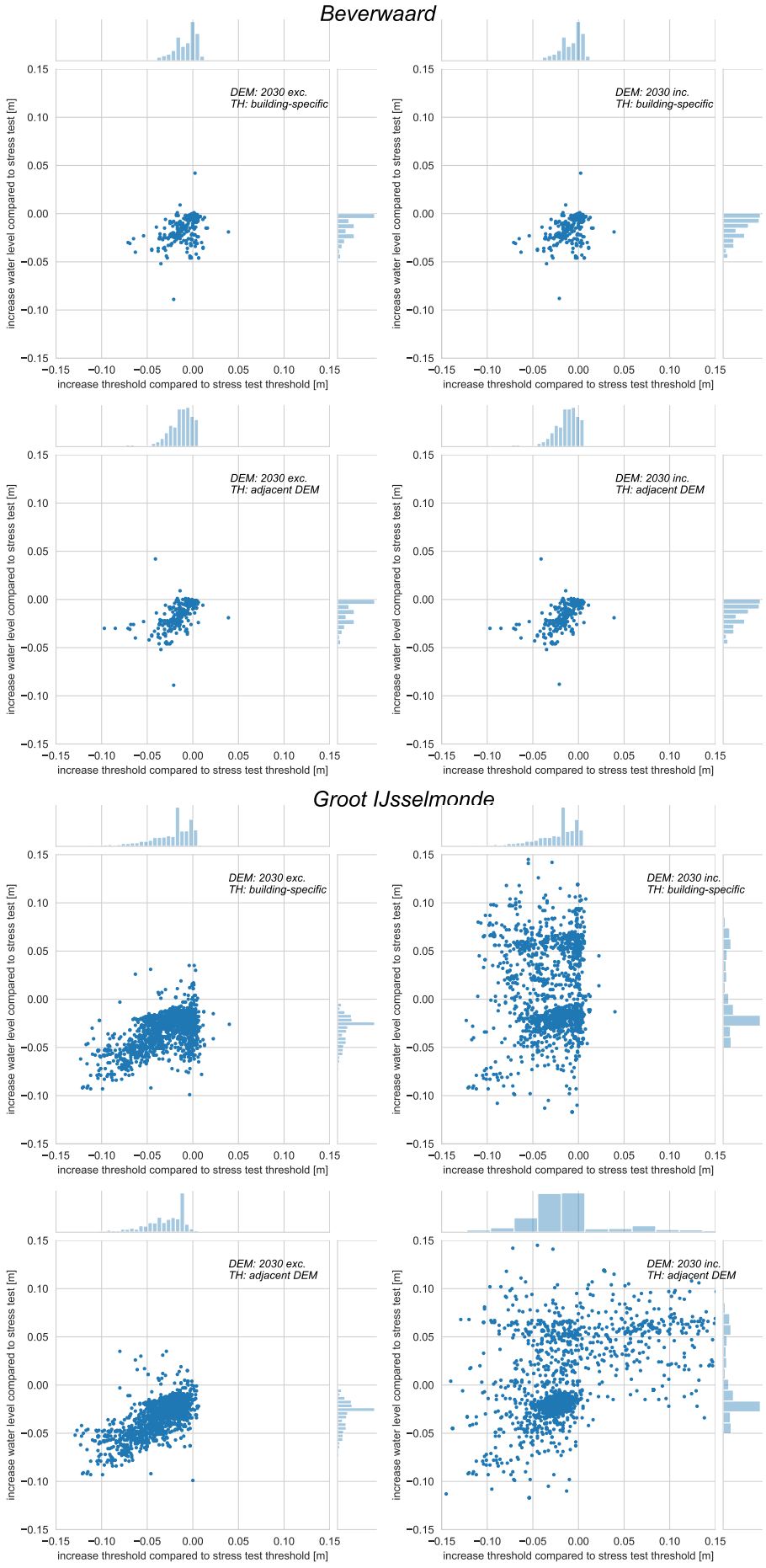

Figure 5.12: Increase/decrease of adjacent waterlevel (y) versus the increase/decrease of the threshold value per building (x) in the neighbourhood Beverwaard (top) and Groot IJsselmonde (bottom) compared to the stress test scenario. Two DEM-scenario's are simulated: one prognosed 2030 DEM excluding maintenance and one 2030 DEM including maintenance. The threshold value per building is determined by calculating the 75^{th} percentile value of the adjacent DEM pixels per building and by subtracting 14 years times the building-specific subsidence from the 2016 threshold per building.

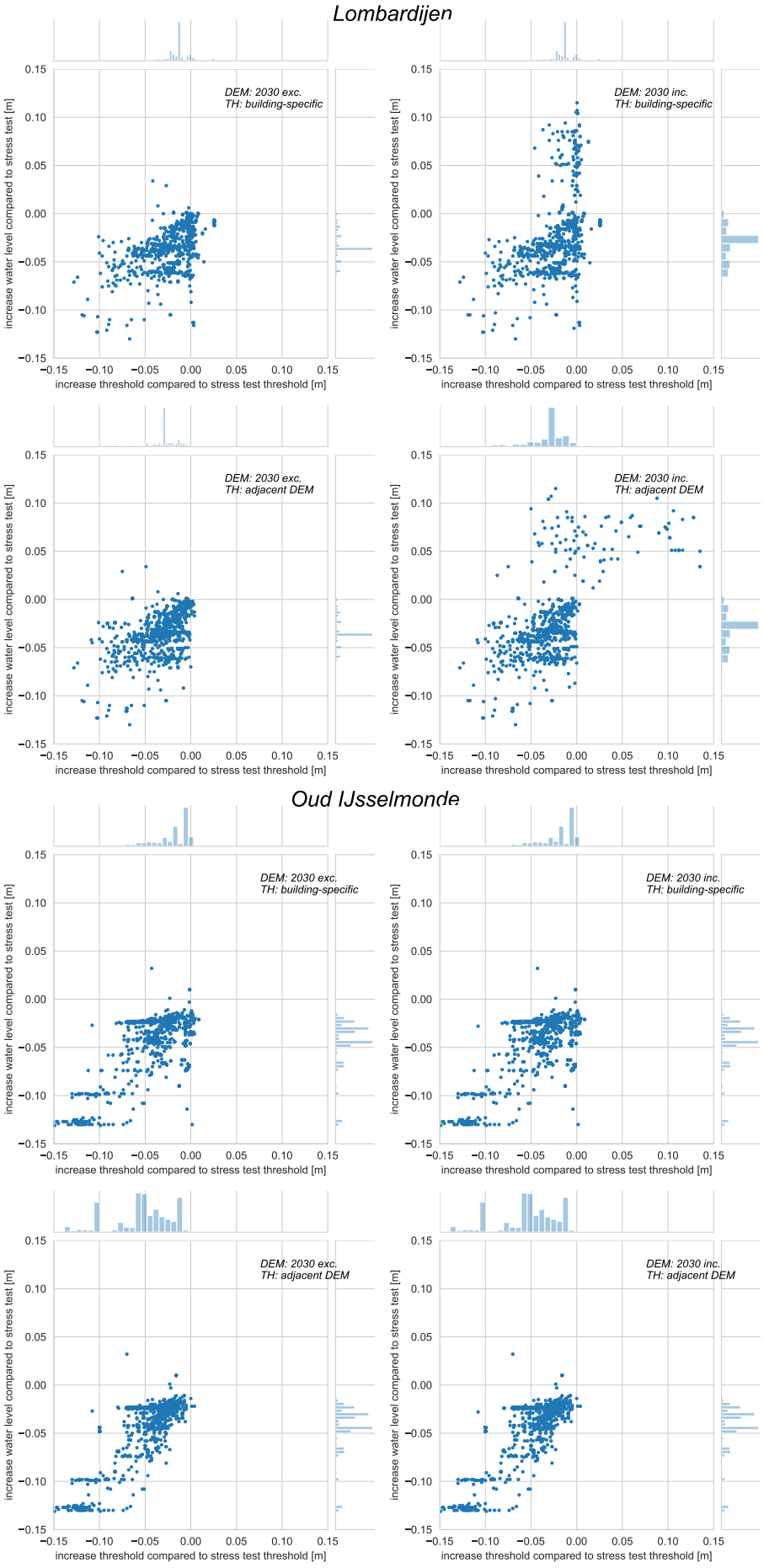

Figure 5.13: Increase/decrease of adjacent waterlevel (y) versus the increase/decrease of the threshold value per building (x) in the neighbourhood Lombardijen (top) and Oud IJsselmonde (bottom) compared to the stress test scenario. Two DEM-scenario's are simulated: one prognosed 2030 DEM excluding maintenance and one 2030 DEM including maintenance. The threshold value per building is determined by calculating the 75^{th} percentile value of the adjacent DEM pixels per building and by subtracting 14 years times the building-specific subsidence from the 2016 threshold per building.

6

Discussion

The results of this research demonstrate several complexities concerning land subsidence and its influence on pluvial flooding. However, this research‘ method is based on several assumptions that strongly influence the location-specific certainty of its outcome. These assumption are necessary to overcome data-insufficiency and -accuracy, calculation-wise limitations and to maintain political affiliation. Critical assumptions and other factors that constrain direct applicability of this research‘ results are discussed in this chapter. Firstly, the land subsidence analysis and its underlying data are critically reviewed in 6.1. Secondly, the method and results of the created DEM's are discussed in 6.1.2. Thirdly, the use of the hydrological model 3Di to translate land subsidence to pluvial flooding is discussed in 6.3.

6.1. Land subsidence analysis

The goal of the land subsidence analysis is identifying different land subsidence processes in Rotterdam. This identification is used in the prognosis of land subsidence to the future.

6.1.1. InSAR inaccuracy and limitations

To asses land subsidence in Rotterdam, this research uses a InSAR data-set 2009-2014, processed and supplied by Maccabiani (2014). When presumably stable buildings are assessed, a precision of 0.5 mm/yr is confirmed, which agrees with Crosetto et al. (2008) and Hanssen (2003). However, the complexity of InSAR data is not precisely knowing what is measured, because the exact location of persistent scatterers in an interferometric stack cannot be predicted (Hanssen, 2003). Maccabiani (2014) states a X-Y accuracy of 1 m per PS, which can be the difference between road and garden or between two neighbouring buildings. To divide buildings from open space, the Z-coordinate is included to split points between high and low points. TerraSAR-X has a Z-accuracy of 1 m (SkyGEO, 2018). Still, points located on low-lying parts of a building can be identified as low points incorrectly. In addition to the X-Y-Z inaccuracy, subsidence rates can differ pointwise, even when a comparable rate is expected. Points located within one building are expected to show similar subsidence rates for example. However, a rooftop of a fast subsiding building that partially leans on its neighbouring, slow subsiding building can contain different subsidence rates per point located on the same rooftop. Another example can be a fast subsiding chimney compared to a steady rooftop. These phenomena can cause a standard deviation larger than 0.5 mm/yr per building, even when the point-measurements are very precise. In addition, Maccabiani (2014) only measures Line of Sight deformation and assumes that the direction of this deformation is predominantly vertical. This assumption detects tilting of buildings as sinking of buildings. The fact that Maccabiani (2014) uses two orbits, decreases the influence of this assumption. If a building tilts, it is detected by a positive subsidence rate based on one orbit and a negative subsidence rate based on the other orbit. This ratio depends on the direction of the tilt. The accuracy of detecting tilting in North-South direction is low (van Leijen, 2014). Maccabiani (2014) does not split the ascending and descending points when the mean subsidence rate is expressed per building. If differences between ascending and descending orbits are large or opposite, it will be expressed by a high standard deviation per building. The trade-off between deleting measurement errors and using variation of subsidence rates is challenging. In addition to this challenge, it is crucial to remain enough data for the land subsidence analysis. Setting a threshold of at least 11 points per building eliminates roughly 3/4 of the buildings.

Furthermore, Maccabiani (2014) expresses only one subsidence rate in mm/yr between 2009 and 2014. The circumstances within and just before this period are crucial for this rate and are likely to differ from the current or future circumstances. Applying additional loads right before this period or a dry spell within this period are examples that influences the location-specific land subsidence behaviour. The limitation to one subsidence rate is a major influence on the land subsidence analysis. The land subsidence development trough time is very useful in distinguishing different land subsidence processes. This could for example identify compression right after maintenance work, or increasing consolidation when the ground water table is low due to droughts.

6.1.2. Input data limitations

Whether different land subsidence processes can be distinguished depends on the quality of the compared data. Soil type data is based on GeoTOP, retrieved via Dinoloket (2019). GeoTOP expresses soil types in so-called voxels of 100 m x 100 m x 0.5 m depth. Top layers in urban areas generally contain sewers, underground infrastructures and artificially applied soil. These contents are generally smaller than 100 m x 100 m. As supported by the land subsidence analysis, land subsidence processes generally take place in the top layer. Artificially applied soil is classified in GeoTOP as anthropogenic layer. Precise properties of these layers are unclear. The land subsidence analysis showed that anthropogenic layers containing dredge, subside faster than layers not containing dredge. This indicates that the composition of the anthropogenic layer influences subsidence behaviour. In addition, no relation was detected between the thickness of the anthropogenic layer and subsidence rates. If the anthropogenic layer was a uniform soil type sensitive to subsidence, a relation would be expected. Furthermore, data on foundation types is scarce in Rotterdam, although the city is actively gathering more data on foundation types. Roughly 25 % of the foundation types are identified or confidently estimated by Funderingsloket (2019). The availability of foundation types influences the selection of buildings used in the land subsidence analysis based on InSAR data. When knowledge on foundation types increase, this selection can be improved.

6.2. DEM creation

The stress test scenario is based on the 2016 DEM of Rotterdam. Land subsidence directly influences a DEM. To simulate or prognose subsidence, adaptions are implemented in the DEM. To answer this research' questions, two case studies are selected. The Tuinenhoven case-study and the IJsselmonde case-study. For Tuinenhoven a DEM is created that approximates Rotterdam at design level, which is discussed in 6.2.1. Using the design DEM as 3Di-input and comparing its results with the stress test results, assesses the influence of land subsidence on the current expected pluvial flooding. For IJsselmonde, land subsidence is prognosed until the year 2030 and based on this prognosis, two 2030 DEM's are created, one including and one excluding maintenance.

6.2.1. Design DEM

The created design DEM in the Tuinenhoven case-study represents a situation where land subsidence has never occurred in Rotterdam. The design DEM is based on Rotterdam issuance level in combination with design guidelines. It is unlikely that this design DEM has ever represented the actual surface level of Rotterdam, because streets, buildings and parks are constructed at different times. The design DEM should therefore be considered purely fictional. The created design DEM is mainly based on the issuance levels, but the current issuance level map misses a high level of detail. The A16 highway is not specified by issuance levels for example. Detecting absences of detail in the issuance level is very time-consuming and compelled the case study to be limited to Tuinenhoven. The results based on the Tuinenhoven case-study are deemed sufficient to answer sub-question 1. In addition, whether raising streets to design level solves the problems concerning pluvial flooding is also addressed in the DEM 2030 including maintenance scenario for whole IJsselmonde. In addition to manually solving the lack of detail, the issuance level map is adjusted by lowering roads by 10 cm to simulate prescribed curb height. The remaining surface of the neighbourhood is raised to issuance level. In reality, this raising is impossible because the doorstep heights of buildings at the Koninginnenweg are below issuance level. Elevating adjacent pedestrian paths or gardens to issuance level would cause water nuisance per definition in reality. Again, this shows that the design DEM is fictional. Other design guidelines, like slopes and bulges for the dewatering effect in roads were not simulated. This means that water is not naturally flowing towards gullies. Due to the fact that gullies are absent in the 3Di model and that the dewatering towards gullies is not significant during extreme rainfall (van Haaren et al., 2018), implementing these

design guidelines is deemed unnecessary. Another imperfection in the creation of the design DEM is that the sewer in the 2016 3Di model is simulated in the design 3Di model as well. In reality, it is expected that sewer experienced a similar subsidence as its covering road. Redesigning a sewer is deemed too time-consuming to include in this research and its inclusion would make the result-analysis too complex. Moreover, the sewer is expected to be fully saturated during extreme rainfall, as is also demonstrated by the Tuinenhoven results. This expectation makes the inclusion of the influence of land subsidence on sewer levels unnecessary.

6.2.2. Land subsidence prognosis

Following the land subsidence analysis, subsidence is prognosed until 2030 for the IJsselmonde case study. The land subsidence analysis categorises low points per land use classification, because that is found to be the most influencing factor of land subsidence in IJsselmonde. The categorised points are interpolated with RasterCaster through TIN-interpolation. Interpolating 120.000 points requires a lot of calculation-power. The use of this RasterCaster is primarily motivated by calculation-technical problems. The land-use categorisation of low points is influenced by a 1 m inaccuracy in X-Z plane (Maccabiani, 2014) and will be less accurate close to the borders between roads and gardens. In addition some points are incorrectly classified as low point, while it actually represents a building. The purpose of including the categorisation in the subsidence prognosis is to demonstrate how findings in a land subsidence analysis can be combined with InSAR data. The land subsidence prognosis assumes that the linear rates measured by Maccabiani (2014) continue until 2030. This is a major assumption in the subsidence prognosis because theoretically the expected prognosis differs per process. Consolidation and compression are expected to muffle out during time. Oxidation can continue gradually, but stops once the groundwater table is reached. Landfill subsidence and secondary consolidation can continue at a stable rate for a long period. Furthermore, these expectations assume stable conditions for the coming 14 years. It is unlikely that the conditions between 2009-2014 will be stable until 2030. Compression will increase if roads are elevated by using sand and droughts can lower the groundwater table which stimulates consolidation and oxidation for example. As shown in the land subsidence analysis, multiple factors play part in the subsidence behaviour of Rotterdam. Before choosing an alternative for the linear prognosis, a clear understanding of the occurring processes is crucial. The results of the land subsidence were to diverse to choose an alternative prognosis method. Furthermore, even when one specific subsidence process is identified and the conditions are expected to remain relatively stable in the coming 14 years, it is almost impossible to prognose subsidence in a non-linear way based on only one subsidence rate in time. Additional information like total subsidence duration, a subsidence rate measured at a different time, more detailed soil specifications or final setting is essential. The inclusion of maintenance in the 2030 prognosis is very similar to the creation of the design DEM in Tuinenhoven and contain similar inaccuracies. Alike the design DEM, the doorstep height per building is not considered in this raising and the sewer remains equal to 2016. In the neighbourhoods where maintenance is planned for the coming 11 years, all pedestrian paths are raised to issuance level and all roads and cycling lanes are raised to issuance level minus 10 cm. Gardens and public parks are unaffected.

6.3. 3Di

The use of the hydraulic model 3Di to translate DEM influenced by subsidence to pluvial flooding and its impact is in follow-up of the conducted stress test on pluvial flooding by Nelen & Schuurmans (2018). The accuracy of a hydraulic models is strongly affected by the quality of input data and the model description and implementation by the modeller (Heckens and Engel, 2017).

6.3.1. Stress test scenario

To maintain political affiliation, the stress test scenario's and the existing 3Di model of IJsselmonde are used in this research. Although the stress test is deemed to be the most realistic approach available, it is still an attempt to simulate reality. Dekker et al. (2018) standardised the stress test scenario nationally to facilitate national comparison between different conducted stress tests. The standardised stress test scenario prescribes a rain event of 70 mm in one hour, 90 mm in one hour and 160 mm in two hours, temporally and spatially constant. This constancy is not likely to occur in real life, but eases the practicability calculation-wise (Dekker et al., 2018). The intensities of the standardised rain events are based on rain events with a return period of 100, 250 and 1000 year, multiplied by a factor 21 % based on the worst climate change scenario in van den Born et al. (2016). Because these standardised scenario's are extreme and to limit the amount of calculations, this research only focused on the mildest rain event, 70 mm in one hour. When working with a model as

complicated and extensive as the IJsselmonde 3Di-model, errors appear along the way. Because the stress test is followed as close as possible, small optimisation adjustments were left aside in this research, because influence of the adjustments would blur the influence of subsidence on the 3Di-outcome. In addition, the model verification can always be improved.

6.3.2. Translation to impact of pluvial flooding

Next to 3Di-inputs, the stress test method is followed in translating 3Di-output to impact of pluvial flooding. The impact of pluvial flooding is expressed in the passability of roads and the risk of water nuisance per building. These expressions are useful in risk-identification or policy-making, but the assumptions behind it are essential. The doorstep threshold value per building is a major influence of the risk classification per building, but data on doorstep heights is absent in Rotterdam. To overcome this absence, the stress test assumed that the threshold value per building is equal to the 75^{th} percentile value of the adjacent DEM pixels. In follow-up of this method, threshold values per building in the 2030 simulation are also based on the 75^{th} percentile value of the adjacent 2030 DEM pixels. When maintenance is included in this DEM, the threshold value of some building raises with more than 10 cm compared to the stress test thresholds. This shows that the 75^{th} percentile is devious. To improve threshold determination, building-specific subsidence rates are used, via Maccabiani (2014). The building-specific subsidence rate subtracted 14 years from the 2016 threshold, approaches a 2030 threshold unaffected by the subsidence of the adjacent open space. This method gives a more realistic 2030 threshold value, although it can be sensible to measurement inaccuracies as discussed in 6.1.1.

The method of threshold determination strongly influences the risk per building. The building-specific threshold prognosis is deemed to be more realistic and in addition it is more likely to identify fast-subsiding buildings. Generally, the 75^{th} percentile threshold prognosis method resulted in an increase of buildings at risk and the building-specific threshold prognosis to a decrease of buildings at risk. This makes sense, because the locations where open space relatively subsides fast, experiences more water. If the threshold-value is also based on this fast subsiding open space, a double increase of risk per building is simulated.

7

Conclusion

As stated in 6, a lot of assumptions and inaccuracies are present in the method and results of this research. These inaccuracies impede results to be interpreted location-specific. However, the findings in this research illustrate the complexity of investigating the influence of land subsidence on pluvial flooding. This complexity is particularly noted when the land subsidence processes and its prognosis to the future are assessed. In the Netherlands, Delta Program (2018) dictates that investigating the expected impact of land subsidence is a matter of national concern. This dictation imposes a new political assignment to municipalities and water boards. The method and results demonstrated in this research explore this assignment and identify potential challenges for future investigations. The research presented in 1.2, are subsequently addressed in sub-chapters 7.1, 7.2 and 7.3

7.1. Current influence land subsidence on pluvial flooding

This research considers the conducted stress test on pluvial flooding by Nelen & Schuurmans (2018) as most detailed approximation of the expected impact of pluvial flooding in Rotterdam. In addition, its political relevance is high and future policy is based on its results (City of Rotterdam, 2019). To supplement the stress test on pluvial flooding, this research follows its methodology and results. This supplementation means that an existing 3Di-model if IJsselmonde is used as case-study and that the rain event scenario is a 70 mm in one hour rain event, based on Dekker et al. (2018). Results are generally presented in comparison to the stress test result.

The Tuinenhoven case-study demonstrates that land subsidence increases the current severity of the impact of pluvial flooding but that the main cause of pluvial flooding during extreme rainfall is the limited capacity of the drainage system. The 3Di-simulation of Tuinenhoven illustrates that raising the whole subneighbourhood to design level decreases the number of roads classified as 'Unpassable' but increases the number of roads classified as only 'Passable for calamity traffic' compared to the stress test results. In total, the number of roads classified as 'Passable' decreases. So, the severity of the impact decreases, but the total amount of impact increases. For both 3Di-simulations, one simulation based on a design DEM and one simulation based on the 2016 DEM, the same amount of water is stored on the 2D surface. This observation confirms that the primary cause of floods are storm events that lead to overloading of rivers and urban water infrastructures (Delta Program, 2017; ten Veldhuis, 2011). During extreme rainfall, the drainage system is filled and the surplus of rain is stored on the surface. The bathymetry of the DEM's distributes the overloaded water. The bathymetry of a DEM is directly influenced by land subsidence.

7.2. Land subsidence in Rotterdam

InSAR-data is a useful method to asses land subsidence on a larger scale and high accuracy compared to other available sources. The InSAR measurements used in this research can achieve a precision of 0.5 mm/yr standard deviation. When used with sufficient competency, the possibilities with InSAR are promising. However, its application requires full understanding of the technique and assumptions behind the method. The (political) impact of land subsidence will be substantial in the coming years (Delta Program, 2018) and (incorrectly) identifying regions as problematic due to land subsidence can have consequences. For the land subsidence analysis, this research omitted the mere part of the InSAR data per building by setting a threshold of at least

11 points per building. This threshold was set to delete measurements that were too blurred by noise and still remain enough data to use in the analysis. The challenge in this trade-off is determining if the noise is due to measurements error and abnormal measurements or that it represents uneven subsidence of buildings. The available InSAR data in this research was limited to one expressed subsidence rate between 2009 and 2014. Detecting and distinguishing different land subsidence processes and prognosing this rate to the future is impossible with only one subsidence rate. In addition, it is unlikely that the circumstances between 2009-2014 are representative for the years outside this period.

Identifying location-specific dominant land subsidence processes based on the land subsidence analysis turns out to be impossible because of the limitations of the InSAR-data, GeoTOP-soil data, foundation type knowledge and land use classification as discussed in 6. In addition, a combination of processes and influences can play a role in location-specific subsidence, which makes the identification even more complex. However, the land subsidence analysis resulted in several findings concerning land subsidence in Rotterdam:

- Foundation type was found to be the most influencing factor on the subsidence behaviour of buildings. Buildings on shallow foundation subside faster than buildings founded on piles. Buildings founded on wooden piles subside more uneven than buildings on shallow foundation, presumably caused by the process of pole rot.
- Buildings and open space located on dredge-containing soils subside faster than buildings and open-space not on top of these soils, which supports the occurrence of landfill subsidence in Rotterdam.
- Peat top soil types generally subside slower than top soil types of sand and clay, which supports the absence of significant peat oxidation in Rotterdam, as stated by Koster et al. (2018).
- The top soil type is found to be a more influencing factor than the dominant soil type. This supports that subsidence in the Netherlands is due to phreatic groundwater level lowering and the consequent consolidation in the Holocene clay layers (Erkens et al., 2015; Koster et al., 2018).
- Land use classification is the most influencing factor of land subsidence behaviour of open space in IJsselmonde. Roads subside faster than gardens and parks, most likely due to the weight of roads and gardens are higher compared to public parks that causes clay consolidation (Erkens et al., 2015; Koster et al., 2018). In addition dynamic traffic loads can cause compaction.
- Although the influence of phreatic groundwater is theoretically inevitable on the subsidence behaviour in Rotterdam and the land subsidence analysis supports the occurrence of consolidation and landfill subsidence , no relation between drainage depth and subsidence behaviour is detected.

In conclusion, land subsidence in Rotterdam is complex. Although the results are not directly implementable in a land subsidence prognosis, it demonstrates how a land-subsidence analysis based on a InSAR data-set can be performed by using different processes as a starting-point. In the coming years, the city of Rotterdam will have to counteract land subsidence also for scopes further than reducing the pluvial flooding-impact. This counteraction requires understanding of the ongoing land subsidence processes. This research demonstrates how InSAR data can be interpolated and prognosed to the future. For this prognosis, the land-use classification is assumed to be the dominant influencing-factor on subsidence in Rotterdam. This prognosis assumed linear progress from the rates measured between 2009-2014, which is a major assumption. Consolidation, compression and oxidation are typically processes that are not expected to develop linearly. In addition, it is highly unlikely that subsidence-influencing circumstances remain constant for the coming 14 years. Compression and consolidation will increase if roads are elevated and droughts can lower the groundwater table which stimulates consolidation and oxidation for example. Results of the land subsidence analysis are however too versatile to use alter prognosis-methods.

7.3. Future influence land subsidence on pluvial flooding

Based on the demonstrated simulations in this research, land subsidence is generally expected to slightly decrease the passability of roads and decrease the risk of water nuisance per building. Crucial influence in these decreases is the relative subsidence. As discovered in the land subsidence analysis and as subsequently simulated in the land subsidence prognosis, roads subside faster than gardens and public parks. This explains why the passability of roads generally decreases. As demonstrated in the Tuinenhoven case-study, the

bathymetry of a DEM determines the water distribution on top of the surface during extreme rainfall. Subsidence influences this bathymetry and can make the impact of pluvial flooding more severe. The fact that the risk per building is expected to generally decreases can be explained by the fact that buildings subside slower than open space. This means that the threshold per building elevates compared to the adjacent DEM. The dominant influence of the relative threshold subsidence on the risk classification becomes particularly clear when the two methods of threshold determination are compared. Basing the threshold value on adjacent DEM pixels per building generally results in more buildings at risk compared to basing the threshold value on building-specific prognosed subsidence rates. In Groot IJsselmonde and Oud IJsselmonde, the adjacent DEM threshold method leads to an increase of buildings at risks compared to the stress test scenario, while the building-specific threshold method decreases the amount of buildings at risk. Furthermore, the decreased adjacent water level per building is generally a direct result of the adjacent open space subsidence. Only when including maintenance in the simulation, increases of the water level were noticed. When maintenance is increased in the simulations, it becomes clear that raising streets is an effective way to increase the passability of roads, but increases the risk of water nuisance per building. As demonstrated in the Tuinenhoven case-study, main cause of urban flooding is the limited capacity of pluvial flooding. Water formerly stored on the streets, flows to gardens when the streets are raised and increases the risk of water nuisance per building. In conclusion, simply raising the surface to counteract the land subsidence is an ineffective method concerning the impact of pluvial flooding.

8

Recommendations

In the Netherlands, Delta Program (2018) dictates that investigating the expected impact of land subsidence is a matter of national concern. Although the results of the IJsselmonde case-study are not to be interpreted location-specific due to simulation-inaccuracies, potential risks and future recommendations for the mitigation of and adaptation to land subsidence are identified. These identifications are useful when the scope of the research is enlarged to the whole city of Rotterdam. This research explores how the expected influence of land subsidence on pluvial flooding can be investigated and several potential challenges are identified. Firstly, several findings and recommendations are elaborated concerning land subsidence, its measurement and its analysis. Secondly, limitations and potential improvements in the translation between land subsidence and the expected (future) pluvial flooding are discussed. Thirdly, the effect of the current land-subsidence maintenance-regime on the future pluvial flooding are demonstrated by the results of this research.

8.1. Land subsidence analysis

The most obstructing component of the research was analysing and prognosing land subsidence in Rotterdam. Because this is a key point of the research, it drastically influenced the applicability of the outcome. The land subsidence analysis uses different land subsidence processes as a starting point and tries to identify and distinguish different processes throughout Rotterdam. Identifying different processes is crucial when a land subsidence prognosis is aspired. Outside the scope of this research, comprehension of the occurring land subsidence processes is important when mitigating measures are considered. If the static/dynamic load of a road is identified to cause compaction of soil for example, active ground water management is an ineffective measure. Using light filling material in the road's foundation layer would be more effective. In addition, to asses the influence of land subsidence on the other stress test themes drought, heat and floods, a proper land subsidence analysis is required. If the consolidation of the Holocene clay layer, influenced by the ground water table, is identified as the dominant subsidence process for example, the influence of droughts will be high. The influence of the groundwater table on land subsidence is inevitable and the expected increase of droughts due to climate change is expected to directly influence land subsidence via future groundwater abnormalities (Delta Program, 2018). So, when future land subsidence is assessed in a climate-adaptive perspective, the relation with ground water is essential.

The method used in the land subsidence analysis in this research is recommended in future research, although the InSAR-data delivered by Maccabiani (2014) on land subsidence needs to be extended and segregated. Firstly, shorter interval-periods of InSAR data improve the possibilities of identifying different land subsidence processes in Rotterdam. Land subsidence rate trends are very process-specific. A shorter interval-period of InSAR data is also very useful to indicate the influence of sudden or temporal changes of subsidence-influencing subsidence. For example, the subsidence behaviour of a road right after it is elevated, or the subsidence behaviour of a peat-containing park during a drought are very useful subsidence-influencing factors to measure and analyse. The land-subsidence analysis in this research failed to detect a relation between drainage depth and subsidence behaviour. It is believed that increasing the temporal resolution of subsidence rates can improve this detection.

An important benefit of using satellite-based data is that you can look back in time. Increasing the time span of InSAR data enables to analyse the influence of specific droughts, construction works or road elevations on subsidence behaviour in Rotterdam. Investigating the influence of raising streets as an adaptive maintenance-operation on the subsidence behaviour of that same street is interesting when the efficiency of the maintenance regime is assessed. Rotterdam has been raising its streets as reaction to land subsidence for years and experienced that the additional load of the applied raising material continued the subsidence process. This provokes a call for applying lighter building material, but its application and consequences are not yet fully understood.

When the InSAR data is extended, it is important to realise what the goal of this extension is. A goal can deviate from this research' goal when the field of interests is enlarge beyond the scope of this research. With this goal in mind, the extensive possibilities of InSAR data should be considered. One of the challenges in this research was the trade-off between deleting subsidence rates of buildings that were considered incorrect and using buildings that actually show deviating subsidence rates. One major influence on these incorrectly measured subsidence rates is that Maccabiani (2014) only measures Line-Of-Sight deformation. This means that tilting of buildings is measured as sinking of a building. This measurement can be improved when the differences between ascending and descending measurements are assessed in the pre-processing of InSAR images. Eliminating the influence of this factor on the standard deviation per building, improves the detection of unevenly subsiding building and increases the possibilities for a land subsidence analysis. So, the goal of analysing building-specific subsidence behaviour should be stated before processing InSAR data. That way, a more consequent distinction between ascending and descending points can be maintained throughout the InSAR-processing. Furthermore, extending InSAR data and using different satellites for this extension, measures the subsidence behaviour of objects for a longer period and with different angles of incidence. This improves the possibility of object monitoring. When the standard deviation of a building is high based on multiple data sets and over a long period, it is likely to subside unevenly. In addition, the quality the soil type data should be improved. The soil type data in this research was based on GeoTOP. This approximates the subsurface structure of Rotterdam in voxels of 100 m x 100 m x 0,5 m depth. It is recommended to improve the resolution and specifications of this data. Particularly the anthropogenic influences in the Rotterdam subsurface should be improved. The land subsidence analysis dredge-containing androgenic layers generally subside faster than soils that do not contain dredge. During the execution of this research, the city of Rotterdam started a project to improve the mapping of subsidence-sensitive soil layers in Rotterdam.

8.2. Translation to pluvial flooding

The assumptions behind the land subsidence prognosis and the hydrological modelling are too influential to interpret the result of this research location-specific. The land subsidence prognosis will improve once the land subsidence analysis is improved. In (hydrological) modelling, the input data and scenario majorly influences the model-output (Heckens and Engel, 2017). Because this research strictly follows the model used in the conducted stress test on pluvial flooding, inaccuracies in that model are repeated in both results. The decreased adjacent water level per building is generally a direct result of the relative adjacent open space subsidence. In addition, the results of this research showed that the doorstep-height approximation is the largest influence on the risk classification per building. This threshold value is influenced by the relative subsidence per building. Again, to asses this relative subsidence, an improved land subsidence analysis is required. When the prognosis of the relative threshold value per building compared to its surroundings is improved, a first estimation can be made whether buildings classified at 'Risk' in the stress test result will have a higher or lower risk in the future. This estimation does not require 3Di and would bypass the uncertainties and requirements of time and competency concerning hydrological modelling. Additionally, the simulations conducted in this research does not require all functionalities of 3Di. Subsidence of sewer is not simulated for example, because it was deemed unnecessary because the Tuinenhoven case study shows that the sewer is fully saturated during extreme rainfall. Furthermore, following the standardised stress-test scenarios underused 3Di capabilities. In low-lying countries like the Netherlands urban pluvial floods are currently characterised by small depths and consequently small direct flood damage and the cumulative damage of less-severe successive flood events can have a comparable impact to extreme rainfall (ten Veldhuis, 2011). When the influence of land subsidence on pluvial flooding during non-extreme, non-uniform or non-constant rainfall events is investigated, hydrological models should be assessed however. Because saturated sewer systems are also less plausible during non-extreme rainfall-events, this model should also include the subsidence-induced developments of sewers.

8.3. Land subsidence policy

Raising streets to design level as an adaptive subsidence-measure generally increases or displaces impact of pluvial flooding based on the results of this research. Water formerly stored on streets, flows to other locations, like gardens, and puts buildings at risk. This shows that raising streets to counteract subsidence is ineffective concerning pluvial flooding. When streets are maintained, its water-storing function should be considered. In addition, this research showed that the risks per building are generally expected to decrease. This decrease is caused by the fact that most buildings subside slower than their surroundings and the doorstep-height relatively raises. According to the stress-test scenario, Lombardijen contains a lot of buildings classified at 'High Risk'. When the prognosed subsidence is simulated and maintenance is excluded, this amount of buildings buildings strongly decreases. Again, the results should not be interpreted location-specific, but it demonstrates that sometimes 'doing nothing' solves expected subsidence-induced water nuisance. However, singular buildings that subside faster than their surrounding should always be considered. Instead of applying mitigated measures for a whole neighbourhood, adaptive measures for specific buildings can be more effective.

A

Climate change in the Netherlands

Observed climate change

The global climate system is changing. Since the 1950s, warming of the atmosphere and ocean, shrinking of the amount of snow and ice, rising of the sea level and increasing of the concentrations of greenhouse gasses have been observed (Stocker et al., 2013). According to the Intergovernmental Panel on Climate change the frequency of heat waves as well as heavy precipitation events has increased in Europe. Evidently based on the increasing greenhouse gas concentrations in the atmosphere, positive radiation forcing, observed warming and understanding of the climate change, human influence on the climate system is clear (Stocker et al., 2013). Based on the Fifth Assessment Report of IPCC, the Royal Netherlands Meteorological Institute (KNMI) has published 'Climate Scenarios for the Netherlands'. In this report it is stated that average temperatures in the Netherlands increased by 1.8 °C between 1901 and 2013. Most of this increase, 1.4 °C, occurred between 1951 and 2013 as can be seen in figure A.1L. The increase since 1951 is about twice the global increase averaged over all land and oceans (Van den Hurk et al., 2014). Annual precipitation in the Netherlands increased 26% between 1910 and 2013, as can be seen in figure A.1R. All seasons except summer have become wetter. Next to that the number of days per year with at least 10 mm precipitation in winter and the number of days with at least 20 mm precipitation in summer increased (Van den Hurk et al., 2014).

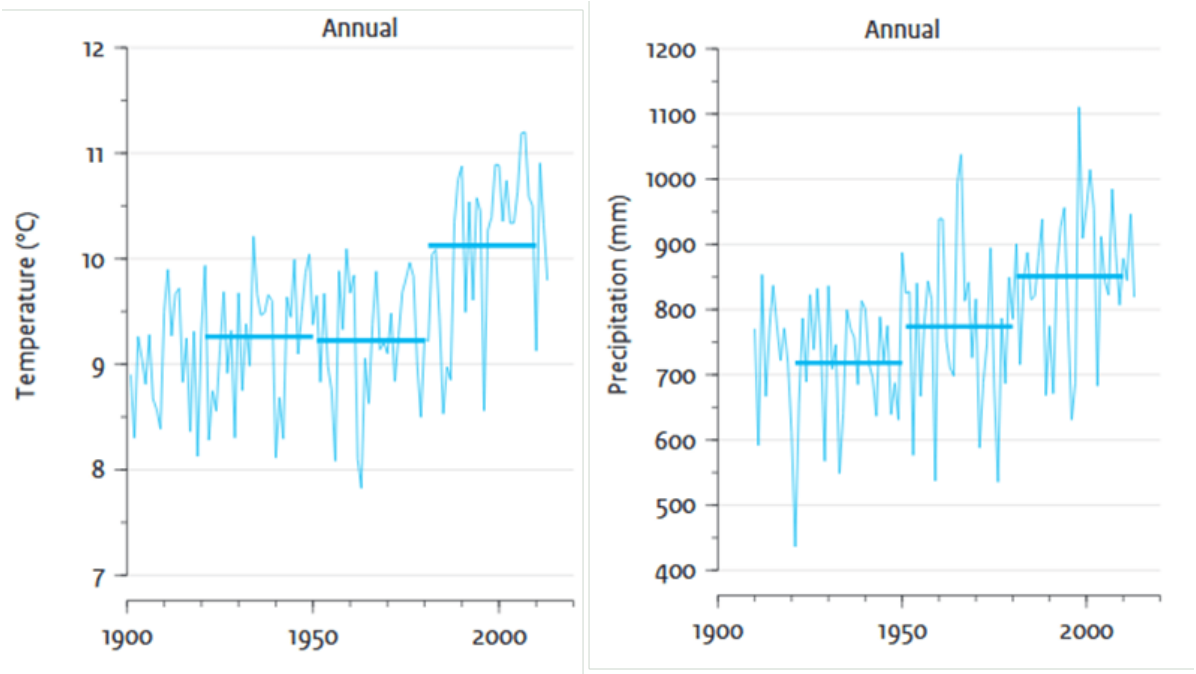

Figure A.1: Observed annual mean temperature at the Bilt (Netherlands), horizontal bars represent the 30-year averages. R: Observed annual precipitation for the Netherlands, horizontal bars represent the 30-year averages (Van den Hurk et al., 2014)

Expected climate change

Further warming and changes in all components of the climate system will be caused if emissions of greenhouse gasses are continued. One of the expected changes in the global water cycle is the increase of the contrast between wet and dry regions and between wet and dry season, although regional exceptions may occur. In the Netherlands, the future temperatures will continue to rise, mild winters and hot summers will become more common, precipitation in general and extreme precipitation in winter will increase, intensity of extreme rain showers in summer will increase and hail and thunderstorms will become more severe (Van den Hurk et al., 2014).

B

Water depths as a stress test result in Rotterdam

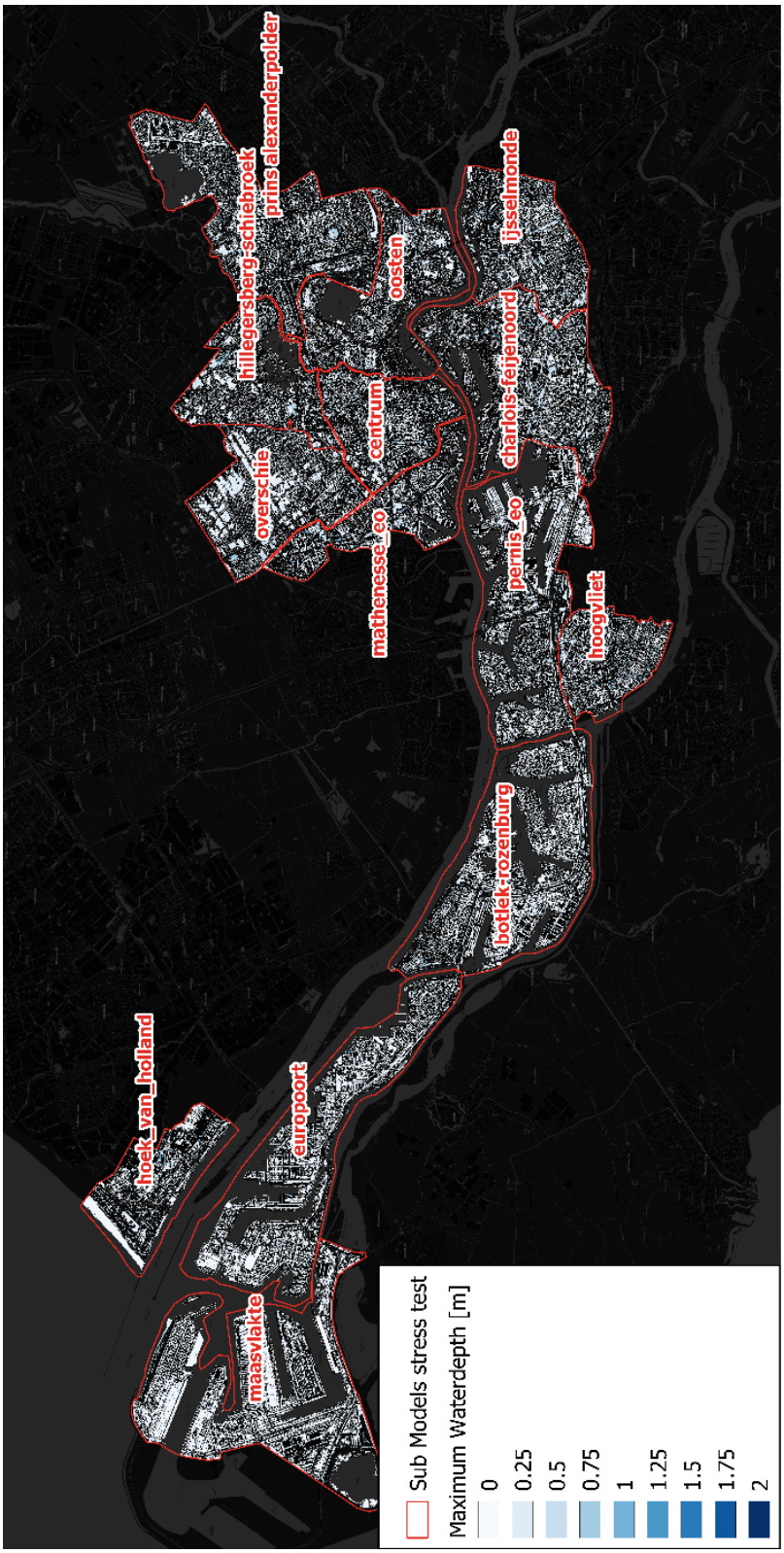

Figure B.1: Resulting water depths based on a 70 mm in one hour rain event 3Di simulation in Rotterdam(Nelen & Schuurmans, 2018)

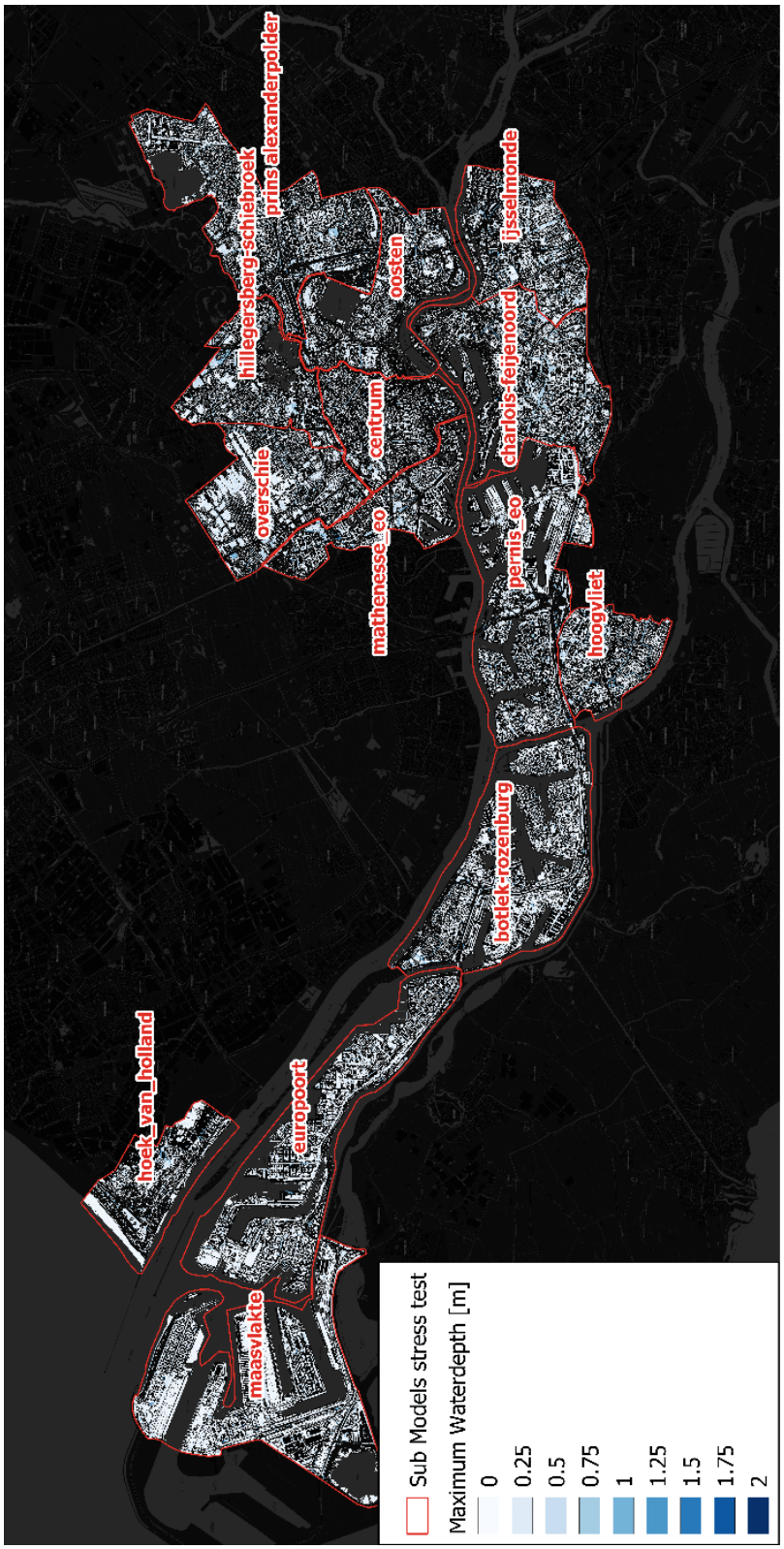

Figure B.2: Resulting water depths based on a 90 mm in one hour rain event 3Di simulation in Rotterdam, based on a 2016 DEM (Nelen & Schuurmans, 2018)

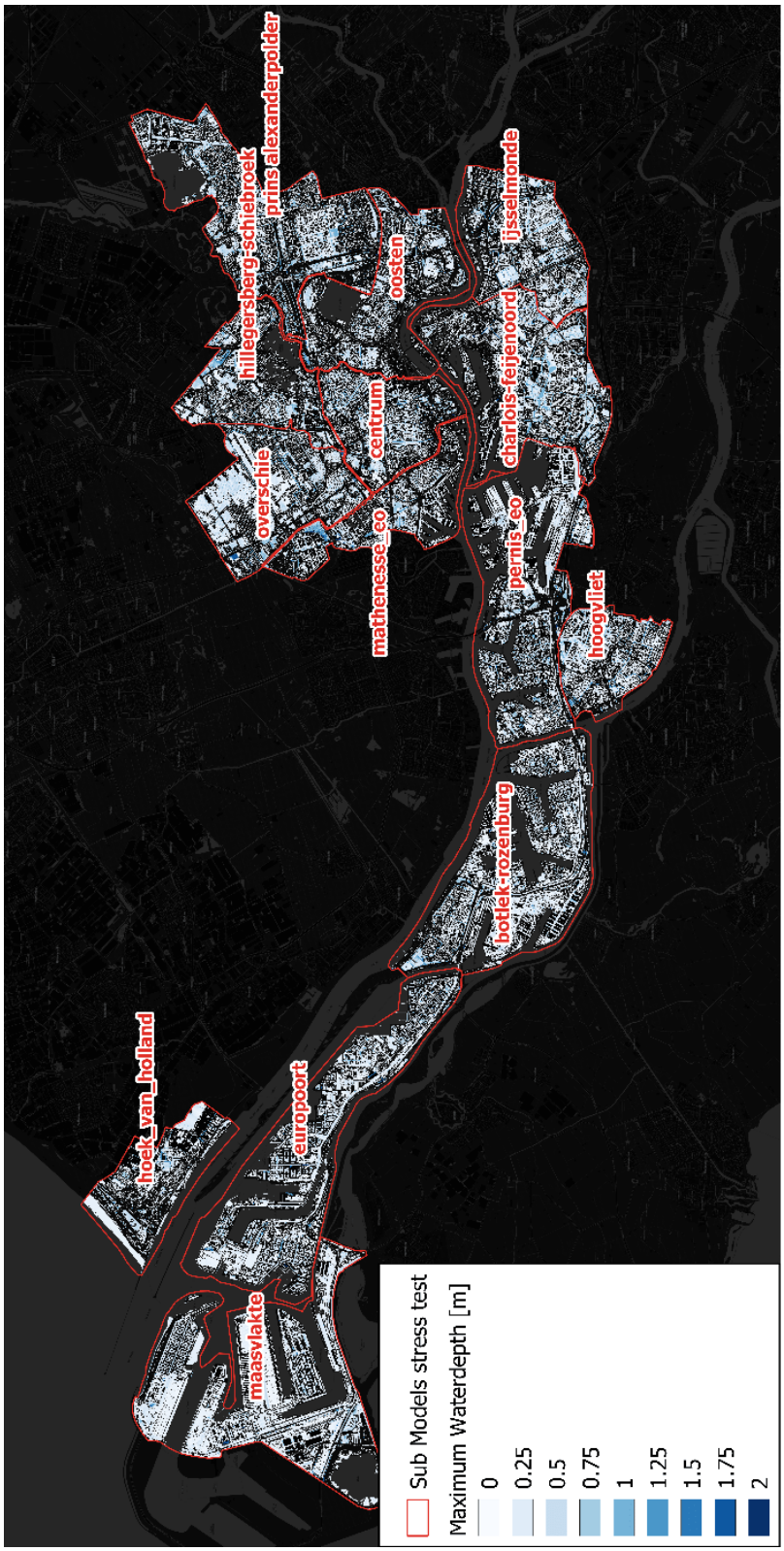

Figure B.3: Resulting water depths based on a 160 mm in two hours rain event 3Di simulation in Rotterdam, based on a 2016 DEM (Nelen & Schuurmans, 2018)

C

Extensive theory InSAR

Synthetic Aperture Radar (SAR)

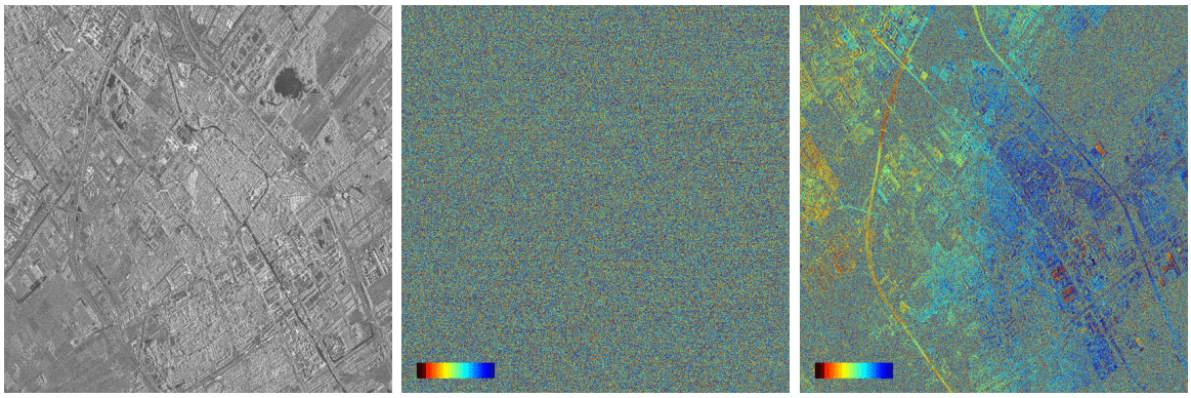

Figure C.1: Left) Amplitude of an SLC image (Delft, The Netherlands, acquired by the TerraSAR-X satellite). Middle) Phase of an SLC image. Right) Phase of an interferogram. After combination of two SLC images, interpretable phase information is obtained (van Leijen, 2014)

Gabriel et al. (1989) showed that synthetic aperture radar (SAR) images can be used to measure very small(1 cm) surface motions with good resolution(10 m). SAR images stored in Single-Look Complex (SLC) format are acquired by active radars on-board airborne or spaceborne platforms like the TerraSAR-X satellite. These SLC-images contain information about both the intensity of the reflection from, and the travel time to, the earth's surface. The intensity of the reflection is expressed by the magnitude or amplitude and the amplitude of an SLC image is shown in Figure C.1, where strong reflections are visualized in white and areas with limited reflection towards the satellite (such as water bodies) are represented in black. The travel time between sensor, surface and sensor determines the measured fractional phase ψ of the received radar signal. The total radar measurement per pixel is denoted by the complex phasor P and can be divided in a Real and Complex value (Hanssen, 2001):

$$\begin{aligned} P &= Ae^{i\psi} \\ ReP &= Acos(\psi) \\ ImP &= Asin(\psi) \end{aligned} \tag{C.1}$$

Inside a pixel multiple reflecting objects may be present, scatterers. The complex value of a resolution cell within the radar image is formed by the summation of all reflections. As presented in figure C.2, scatterers are divided in two main types. Persistent scatterers (PS) are reflections within a pixel that contain objects that have high reflectance properties. These objects reflect most of the signal received by the satellite from a certain pixel, whereas the surrounding is only adding noise or clutter. Distributed scatterers (DS) are pixels where multiple objects show a weaker reflection within one pixel, at a relatively similar strength. The strength of this reflection is dependent on the physical (e.g., slope, morphology, roughness, inhomogeneities) and electrical (i.e., dielectric constant) properties of the surface (Elachi, 1988). Sharp-edged objects like buildings and stone covered dikes reflect better than smooth surfaces like roads or grassland. This makes the use of InSAR more applicable in densely built areas (SkyGEO, 2018).

The phase ψ of an SLC image is shown in figure C.2. Middle) Phase of an SLC image. Right) Phase of an interferogram. After combination of two SLC images, interpretable phase information is obtained (van Leijen, 2014). Per pixel this phase is influenced by several signals (van Leijen, 2014):

$$\psi = -2\pi a + \psi_{range} + \psi_{atmo} + \psi_{scat} + \psi_{noise} \tag{C.2}$$

Where a is the phase ambiguity (the number of full phase cycles), ψ_{range} the range dependent phase, ψ_{atmo} the atmospheric signal delay, ψ_{scat} is the scattering phase and ψ_{noise} is the noise. Only the fractional phase of the received signal is recorded, resulting in phase values between $[-\pi, +\pi]$. This small radar wavelength (31 mm for TerraSAR-X) in comparison with the pixel spacing, atmospheric delays and scattering objects distribution, cause that the SLC phase observations cannot be interpreted directly. Combining two SLC-images by creating an interferogram increases the interpretation possibilities.

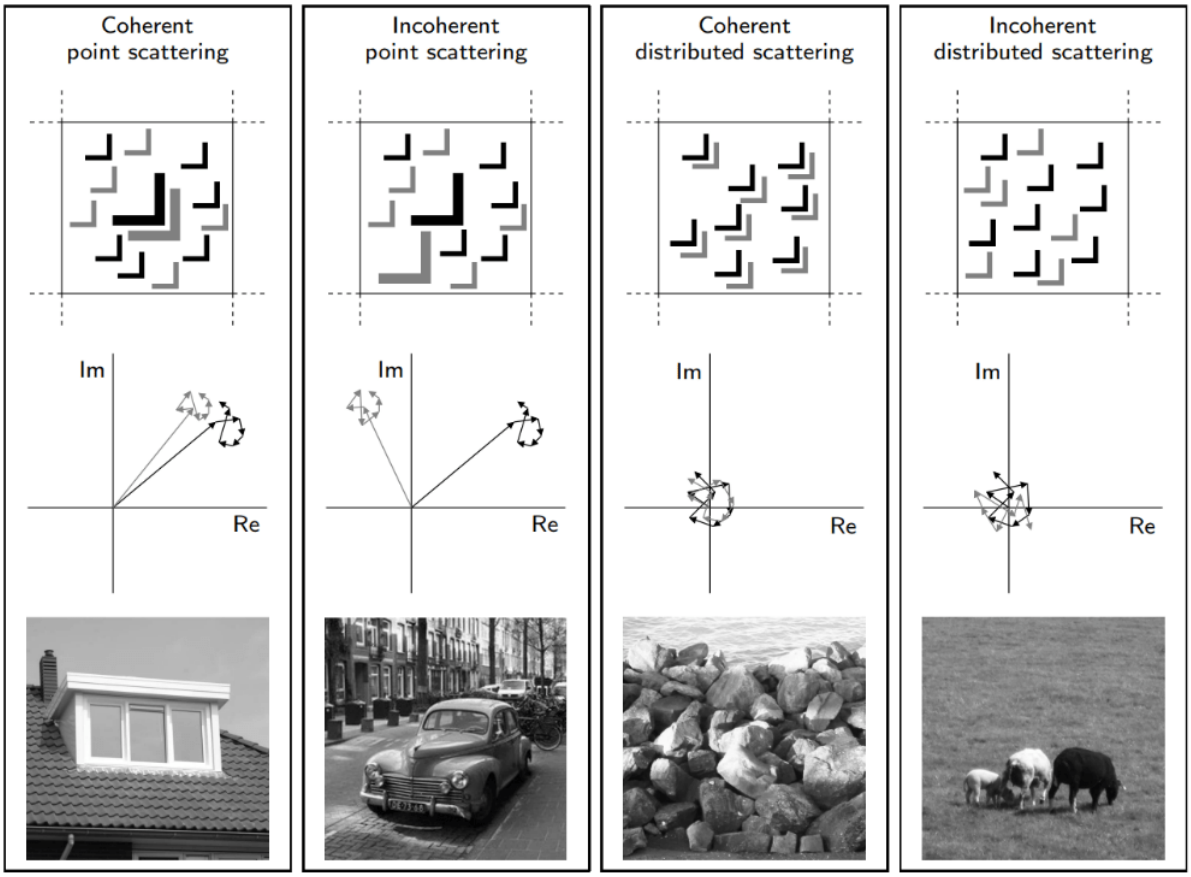

Figure C.2: Left) Point scattering versus distributed scattering in case of coherence or incoherence. Top) Scattering objects within a resolution cell at two acquisitions (indicated by black and gray reflecting objects). Middle) Phasors for the two acquisitions (again in black and gray). Bottom) Examples of scattering objects (van Leijen, 2014)

Interferometric Synthetic Aperture Radar InSAR

The objective of each radar interferometric analysis is the retrieval of information from the pixels showing sufficiently coherent scattering behaviour. The coherence is a measure for the amount of correspondence between two complex observations. Both scattering mechanisms can, over time, either be coherent or incoherent as is shown in figure C.2. Moving objects and vegetation are typically incoherent and not useful. Usai and Hanssen (1997) showed that a considerable number of particularly man-made objects remain coherent over long periods of half a year. The coherence stability of these structures can be used for long time-scale monitoring of slow deformation processes. A complex interferogram expresses the interferometric phase $\phi^{m,s}$ created by combining two aligned or co-registered SLC images, one slave(s) and one master(m) image (van Leijen, 2014):

$$\psi^{m,s} = \psi^{m} - \psi^{s} = -2\pi a + \phi_{flat} + \phi_{topo} + \phi_{defo+}\phi_{atmo} + \phi_{orb} + \phi_{scat} + \phi_{noise} \tag{C.3}$$

Here, the range depended phase is split in a flat Earth φ_{flat}, topographic φ_{topo} and a deformation φ_{defo} term. Errors in the orbit parameters of the master and slave acquisitions introduce an additional error term φ_{orb} and typically cause a (small) trend in the interferogram (Hanssen, 2001). The flat earth phase describes the contribution due to a reference surface. The topographic phase φ_{topo} describes the influence of topography above the reference surface. The deformation phase is the result of a displacement of the surface.

$$\phi_{defo} = -\frac{4\pi}{\lambda} D_{LOS} \tag{C.4}$$

DLOS is the deformation in the radar's Line of Sight and is sensitive to both horizontal and vertical deformation due to the skewed incidence angle of the signal. It's a three-dimensional vector denoted by components in for example East, North and Up direction. It is not possible to determine the three deformation components from a single inferogram. Therefore, often an assumption is made regarding the deformation's

direction under investigation and only vertical and horizontal deformation is examined. Combining datasets with different incidence angles, for example ascending and descending direction, can improve this determination because two observations are available to determine two unknown deformation values, the system has a unique solution. However, because of the insensitivity of the deformation vector in North-South direction, the full three-dimensional vector can still not be resolved and an assumption regarding the direction of the horizontal deformation remains required.

The atmospheric phase φ_{atmo}, also called atmospheric delay, is caused by the difference between the atmospheric states during the two images. The interferometric scattering phase $\varphi_{scat}$is effectively an additional noise term. It describes the difference between the scatter characteristics of the observed area within a resolution cell during the two acquisitions and is expressed in different decorrelations (van Leijen, 2014):

- Temporal decorrelation, caused by physical changes of the Earth's surface within the resolution cell. A typical source of temporal decorrelation is vegetation.
- Geometric decorrelation, caused by different incidence angles of the radar signal during the two acquisitions. The different incidence angles cause a shift between the data frequency spectra of the images involved, resulting in noise due to the non-overlapping parts of the range spectrum.
- Doppler centroid decorrelation, caused by different Doppler centroid frequencies during the two acquisitions
- Thermal or system decorrelation, caused by instrumental thermal noise during the acquisitions.
- Processing decorrelation, caused by the processing of the radar images to obtain interferograms, e.g., due to co-registration and interpolation errors.

To improve the interpretation, a number of additional processing steps can be applied (van Leijen, 2014):

- Spectral filtering. The geometric and Doppler centroid decorrelation can be reduced by filtering the non-overlapping parts of the spectra of the master and slave images before interferogram formation. The spectral filtering is applied separately in azimuth and range direction.
- Spatial filtering, remaining noise can be reduced by a spatial (smoothing) filter on the complex interferometric observations.
- Phase unwrapping, the interferogram obtained still contains phase values wrapped to the $[-\pi, +\pi]$ interval. To obtain absolute phase values, which can be translated to topographic height information or deformation values, the phase needs to be unwrapped.

If the objective of a radar interferometric analysis is to study the deformation, the deformation phase φ_{defo} should be isolated from the other phase contributors. In practice, especially the atmospheric signal, together with temporal and geometric decorrelation, are the limiting factors regarding interpretation in case of a single interferogram. To circumvent these disturbing factors, often radar interferometric time series analysis is performed.

Radar interferometric time series analysis

Radar interferometric time series analysis method starts with the detection of those pixels for which the deformation time series can be estimated with sufficient reliability. The reliability of the time series is directly related to the correct estimation of the phase ambiguities or phase unwrapping. Several characteristics of the dataset influence the ability to correctly estimate these ambiguities, particularly (van Leijen, 2014):

- The noise level of the observations, determined by the amount of geometric and/or temporal decorrelation.
- The spatio-temporal variability of the atmospheric signal delay. In all methods the ambiguities are resolved based on spatial (and temporal) phase differences. When strong spatial gradients in the atmospheric signal occur, correct ambiguity resolution becomes more difficult.
- The spatio-temporal smoothness of the actual deformation signal, sudden changes in space or in time, make the ambiguity resolution more difficult, particularly when a wavelength dependent threshold is exceeded. In addition, the spatial distance between coherent pixels and the acquisition repeat cycle determine the ability to estimate the correct solution.

Radar interferometric time series analysis methods are designed to account for these limitations. In the last decade various methods have been proposed. The methods can be distinguished based on:

- Baseline configuration determines the set of interferometric image pairs that is used in the time series analysis. The baseline is defined as the distance between the two SLC images involved, either in terms of antenna position (perpendicular baseline), acquisition time (temporal baseline), or Doppler centroid (Doppler baseline). The objective is to find a configuration that minimizes the noise level in the data set, hence to minimize the amount of decorrelation
- Image resolution used in the radar interferometric time series analysis is mainly dependent on the type of scattering that is expected or aimed to detect, i.e., primarily point scattering or distributed scattering. In both cases the aim of using a certain resolution is to reduce the amount of noise in the observations.
- Phase unwrapping is the critical step in any radar interferometric time series analysis, also known as ambiguity resolution. Unwrapping errors, i.e., phase jumps of 2 π, severely affect the quality of the results.
- A-priori selection of suitable pixels is the beginning of each radar interferometric time series analysis and is either based on amplitude or phase information. The main objectives are to improve the result by disqualifying low quality pixels which may influence the results in a negative manner and to reduce the computational efforts.
- A-posteriori pixel selection is applied is applied for some radar interferometric time series analysis. The objective is to detect the reliably estimated pixels in the total set of pixels analysed. This selection step is mainly applied where an independent solution for each pixel is obtained. Ideally, the a-posteriori selection is performed before the spatial integration step, to circumvent the influence of erroneous pixels in the final result.
- Atmospheric signal estimation/prediction method is based on the assumption that for each decomposition approach, the atmospheric delay due to turbulent mixing is uncorrelated in time. As a result, the expectation value of the differential atmospheric delay is zero.

D

Issuance level and planned maintenance for the city of Rotterdam

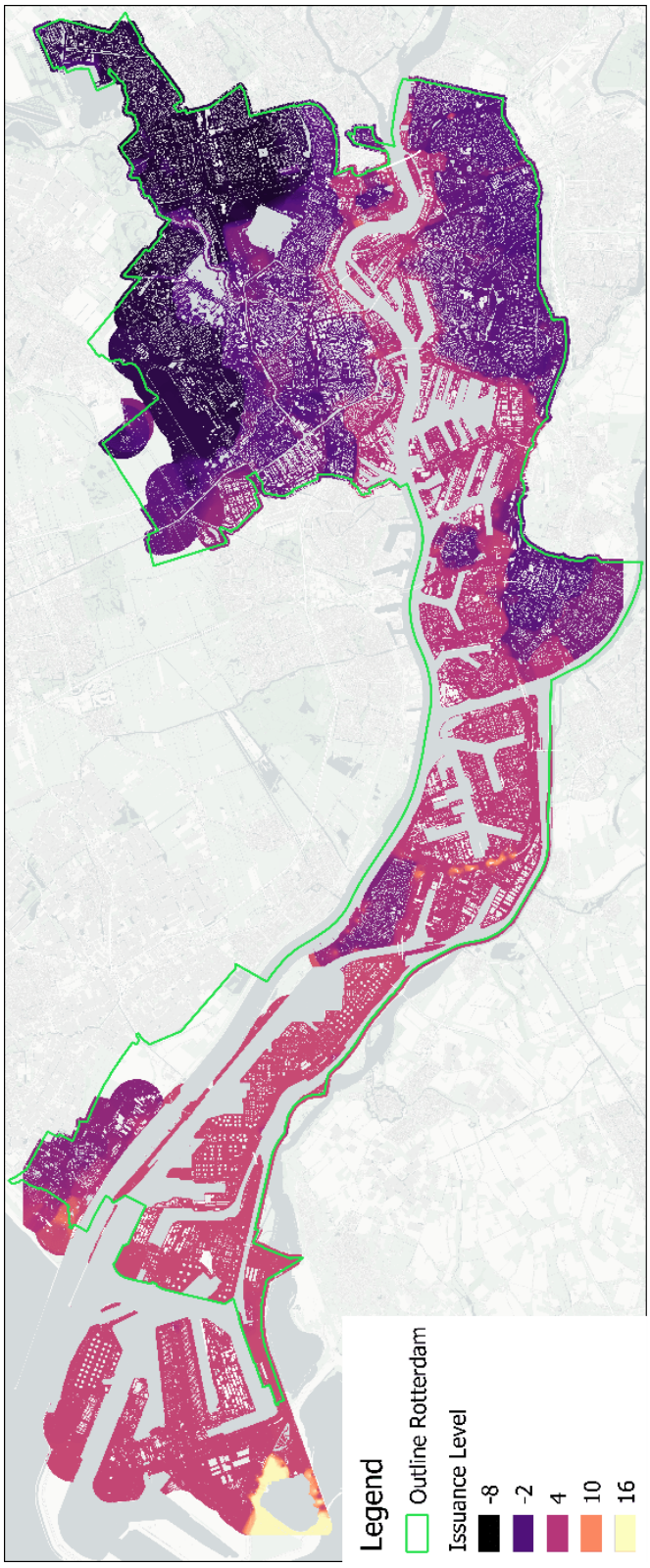

Figure D.1: Issuance Level Rotterdam

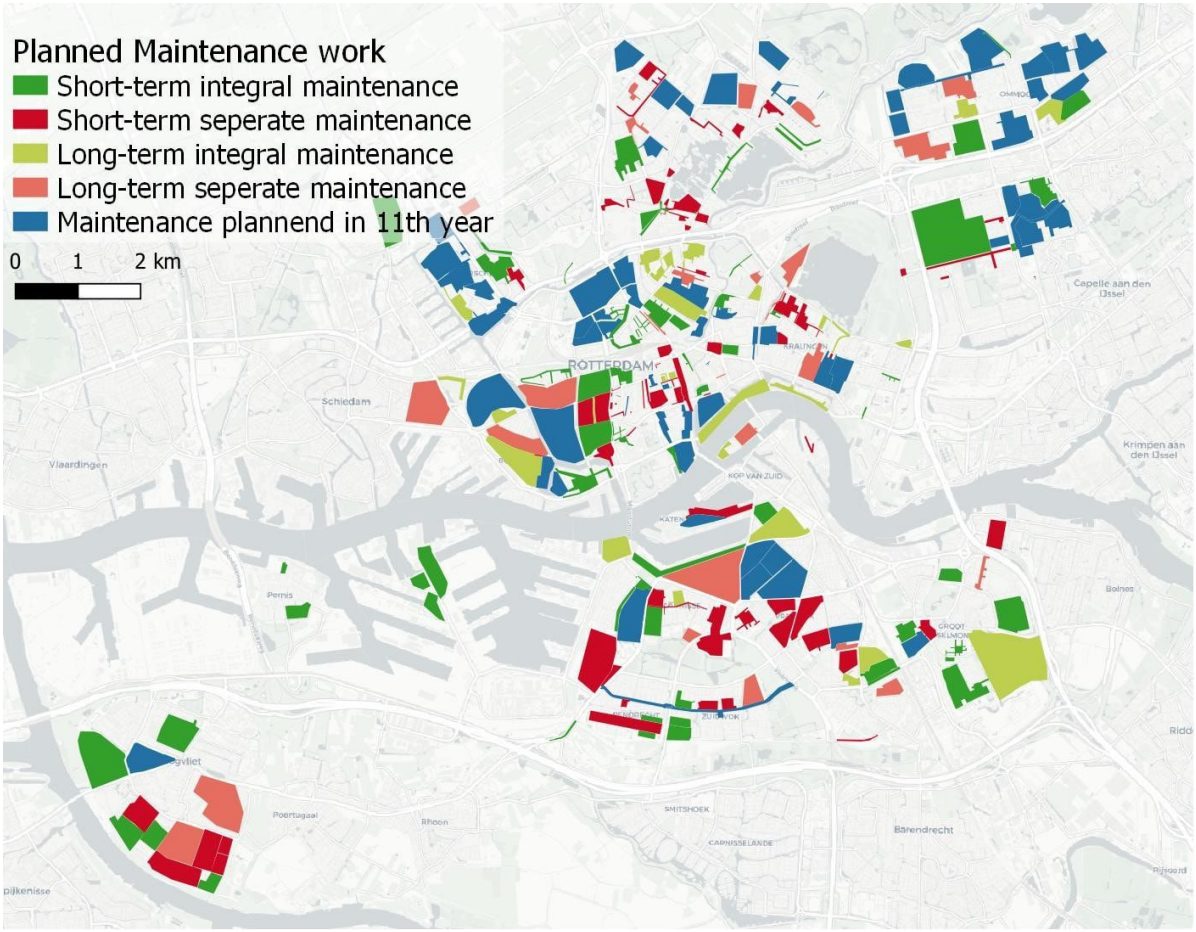

Figure D.2: Planned maintenance work by the city of Rotterdam on roads and sewer for the coming 10+ years

E

Subsidence rates per PS in Rotterdam

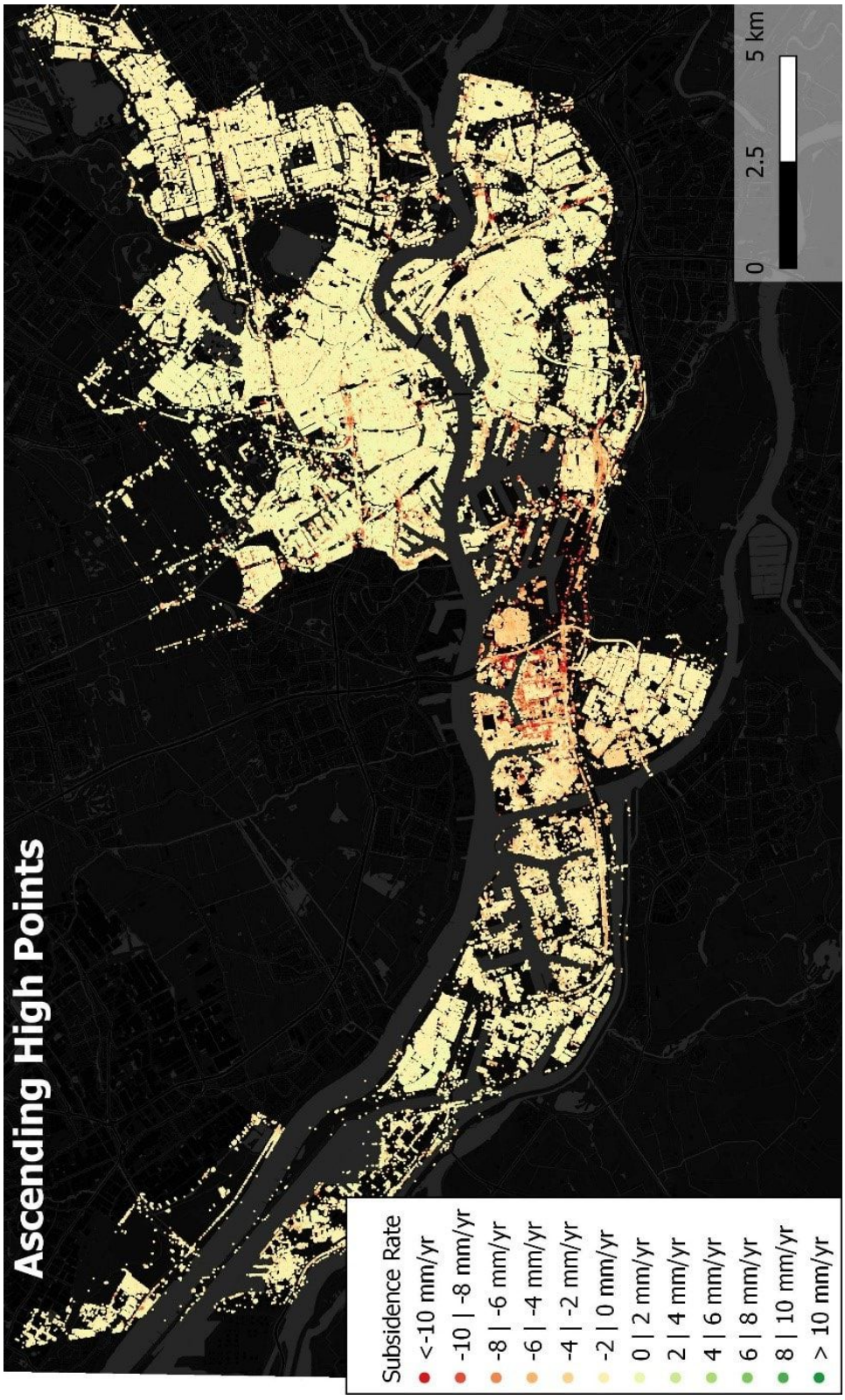

Figure E.1: InSAR high points based on the ascending TerraSAR-X orbit for the whole city of Rotterdam (Maccabiani, 2014)

Figure E.2: InSAR low points based on the ascending TerraSAR-X orbit for the whole city of Rotterdam (Maccabiani, 2014)

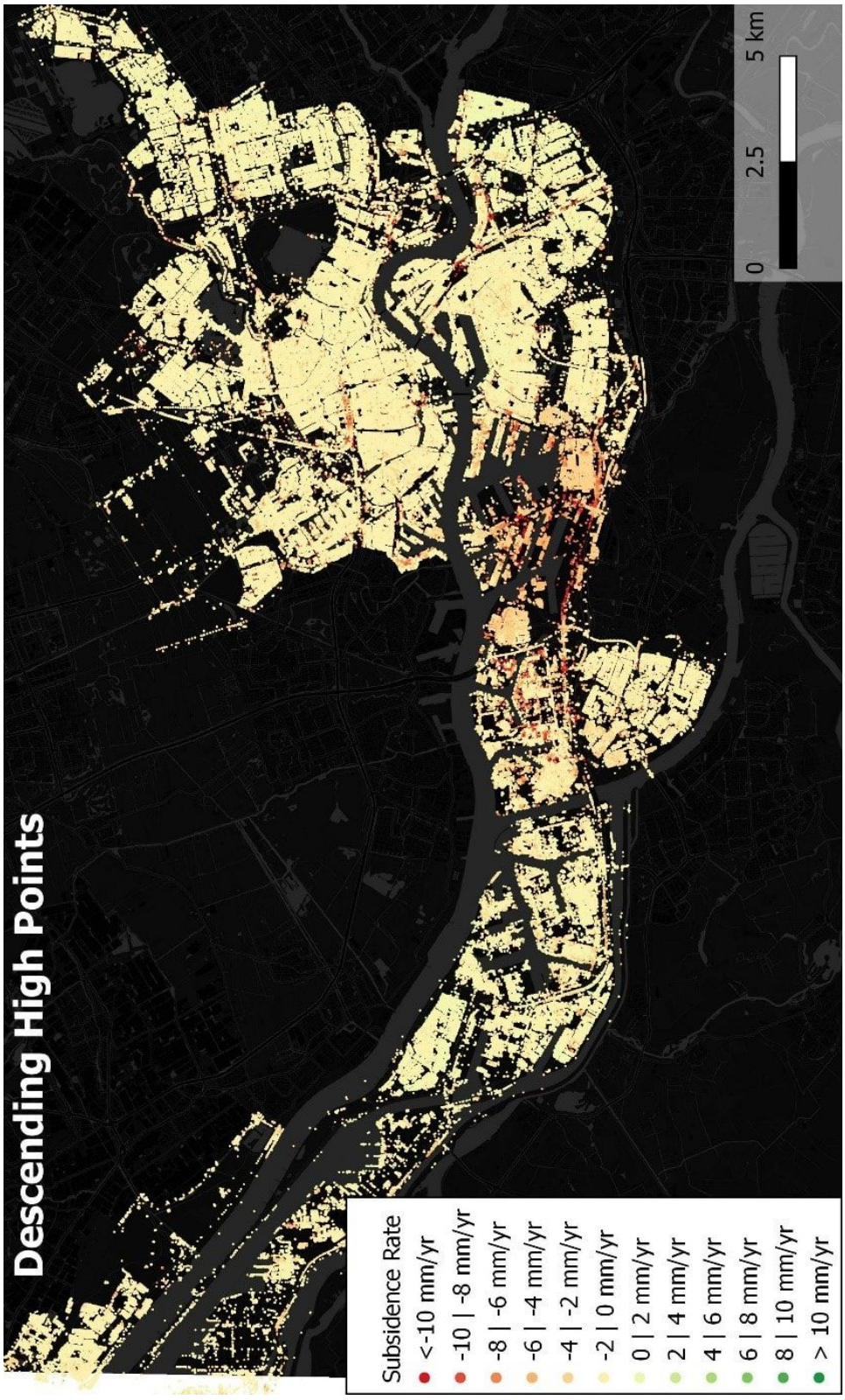

Figure E.3: InSAR high points based on the descending TerraSAR-X orbit for the whole city of Rotterdam (Maccabiani, 2014)

Figure E.4: InSAR low points based on the descending TerraSAR-X orbit for the whole city of Rotterdam (Maccabiani, 2014)

F

Determining the InSAR threshold value per building

Figure F.1 shows the standard deviation of all the mean subsidence rates per building based on a minimum number of points. As expected from figure 3.3, the standard deviation of the mean subsidence rates per building is higher if buildings are based on less points. Especially the subsidence rate of buildings based on less than 20 points is strongly influenced as a strong drop is observed. The same pattern is noted if the standard deviation of the individual standard deviations per building based on a minimum number of points is plotted in F.2. To determine a suitable threshold the drop in between the first 20 points is examined and it is noted that this drop levels out between 10 and 15 points per building. In addition, the standard deviation of buildings based on at least 200 points is plotted. It is assumed that buildings with at least 200 points show a representative spread of standard deviations and mean subsidence rates per building. Figure F.1 and F.2 show that the standard deviations of building based on at least 200 points, corresponds with the standard deviations of buildings with at least 11 points.

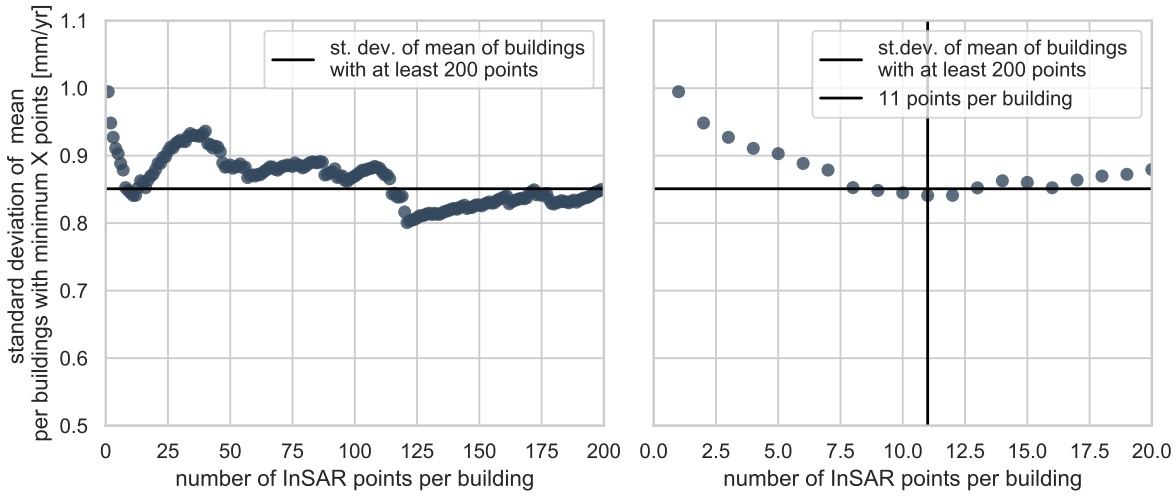

Figure F.1: Standard deviation of the mean of the subsidence rate of the high points per building based on at least X points

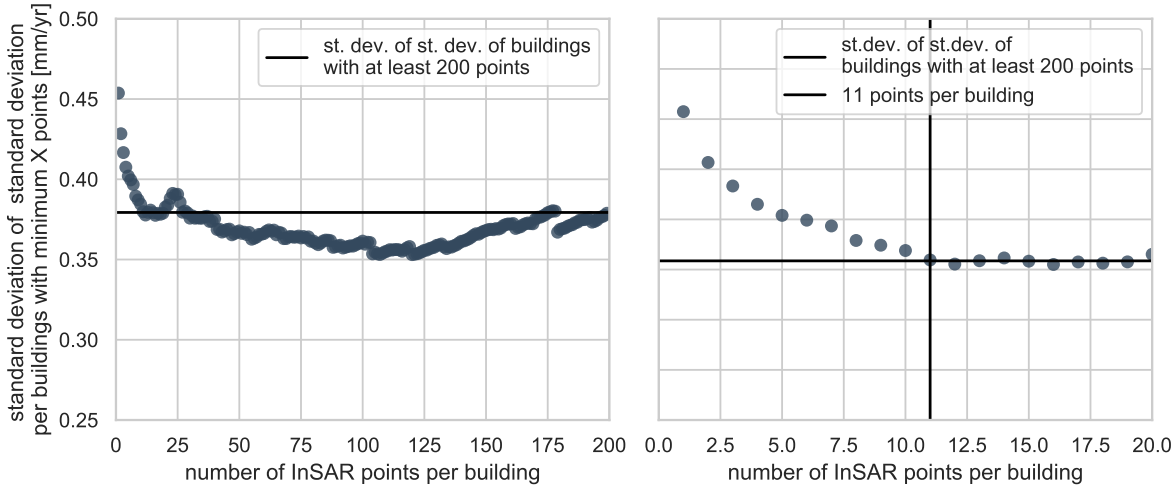

Figure F.2: Standard deviation of the standard deviation of the subsidence rate of the high points per building based on at least X points

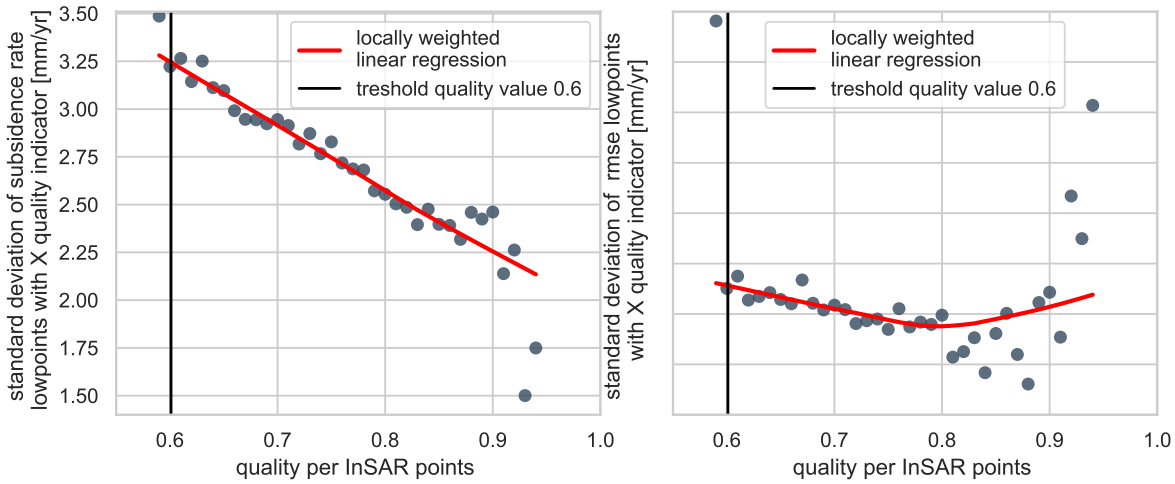

Figure E.3: Standard deviation of the subsidence rate (L) and the RMSE (R) per quality indicator)

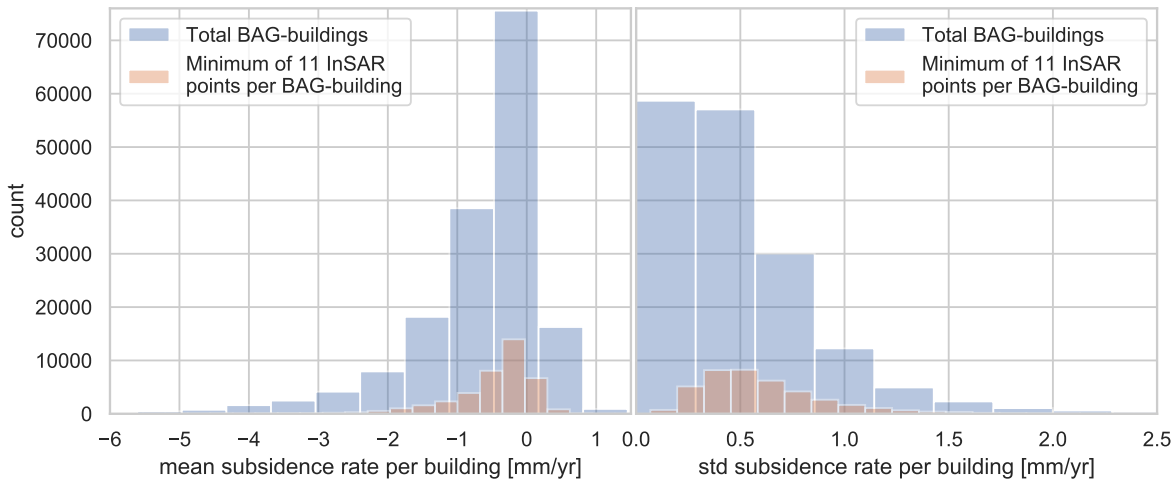

Figure E.4: Distribution of the mean (L) and the standard deviation(R) of the subsidence rate per building with and without a threshold

G

Foundation variety per neighbourhood and 3Di sub-model

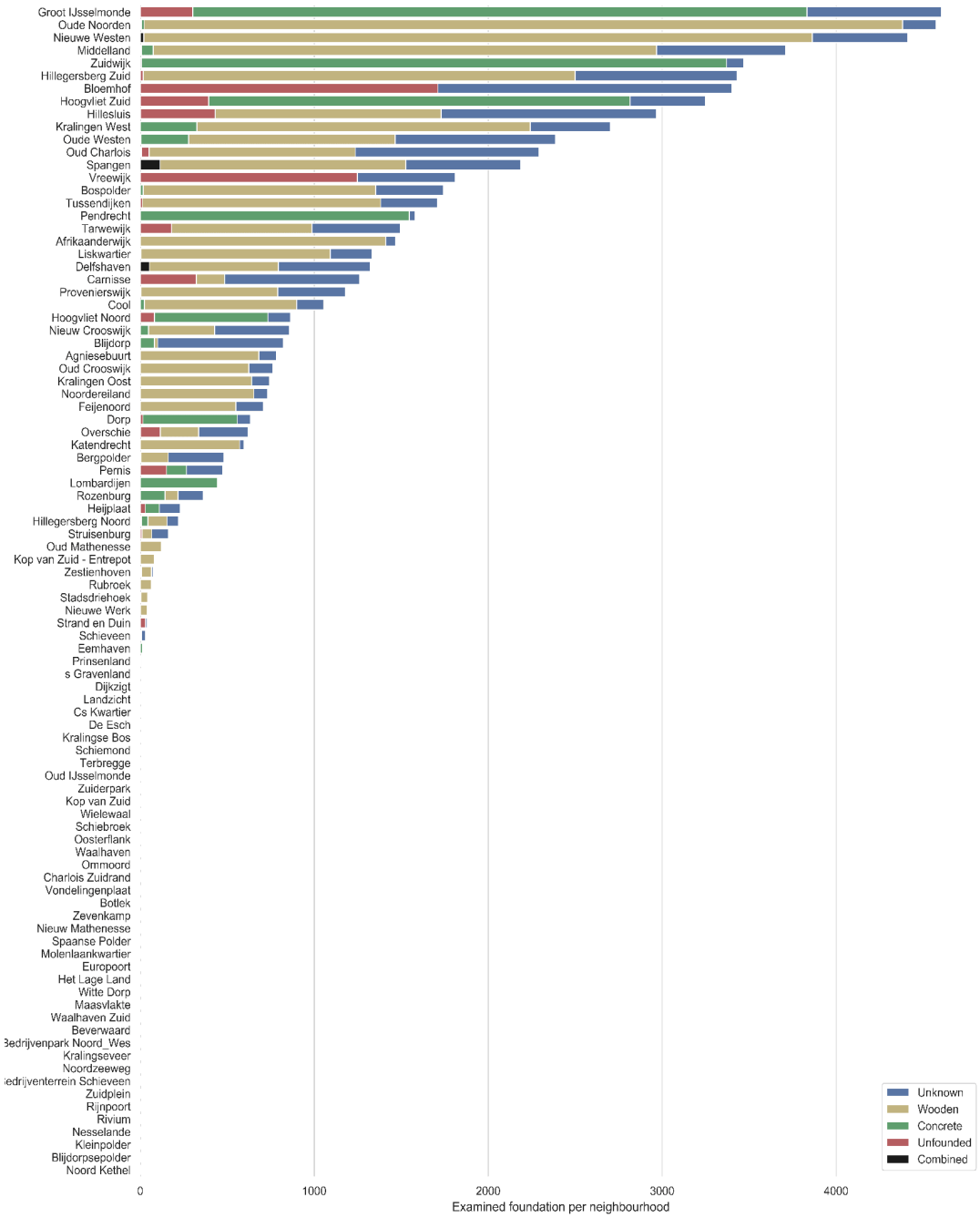

Figure G.1: Foundation types per neighbourhood in Rotterdam

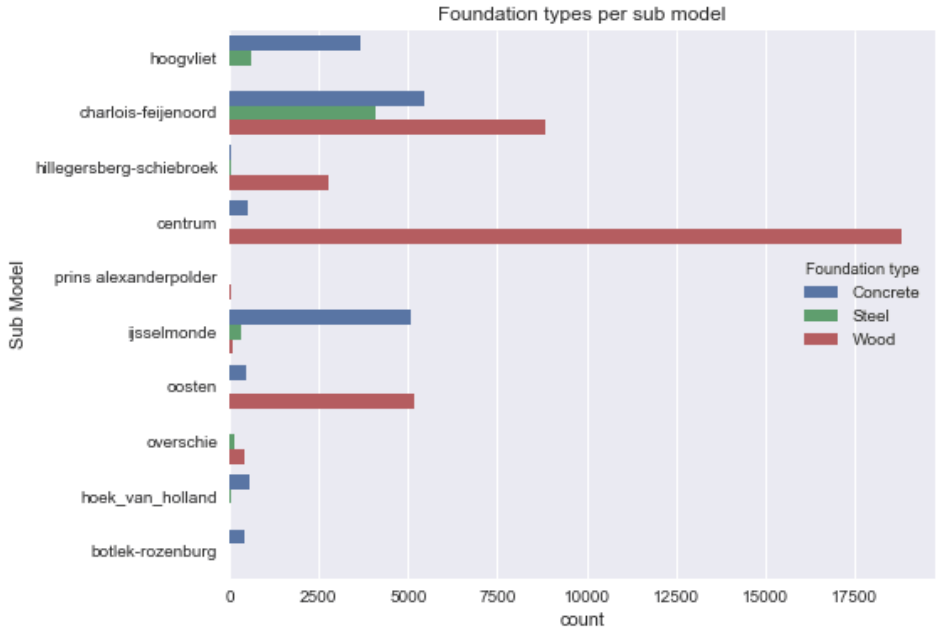

Figure G.2: Foundation types per sub model (Funderingsloket, 2019)

H

Subsurface structure of Rotterdam based on GeoTOP

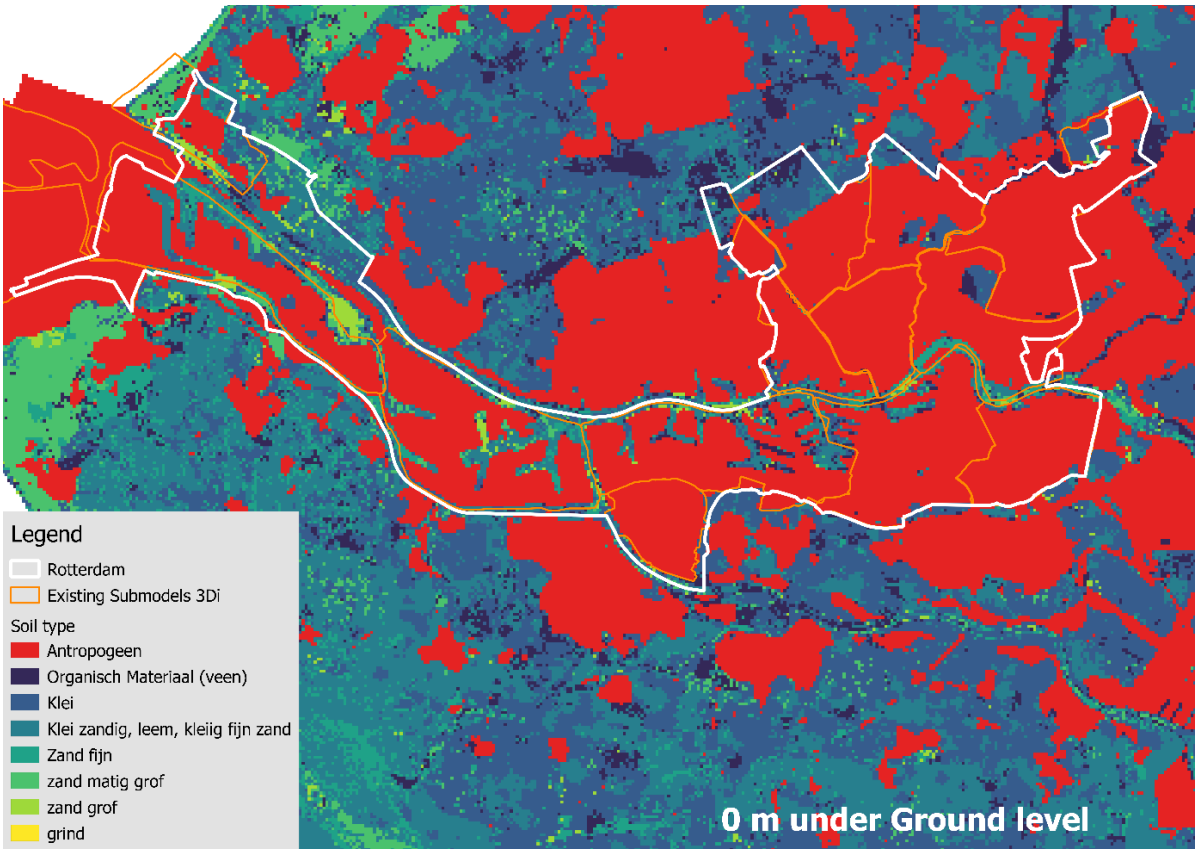

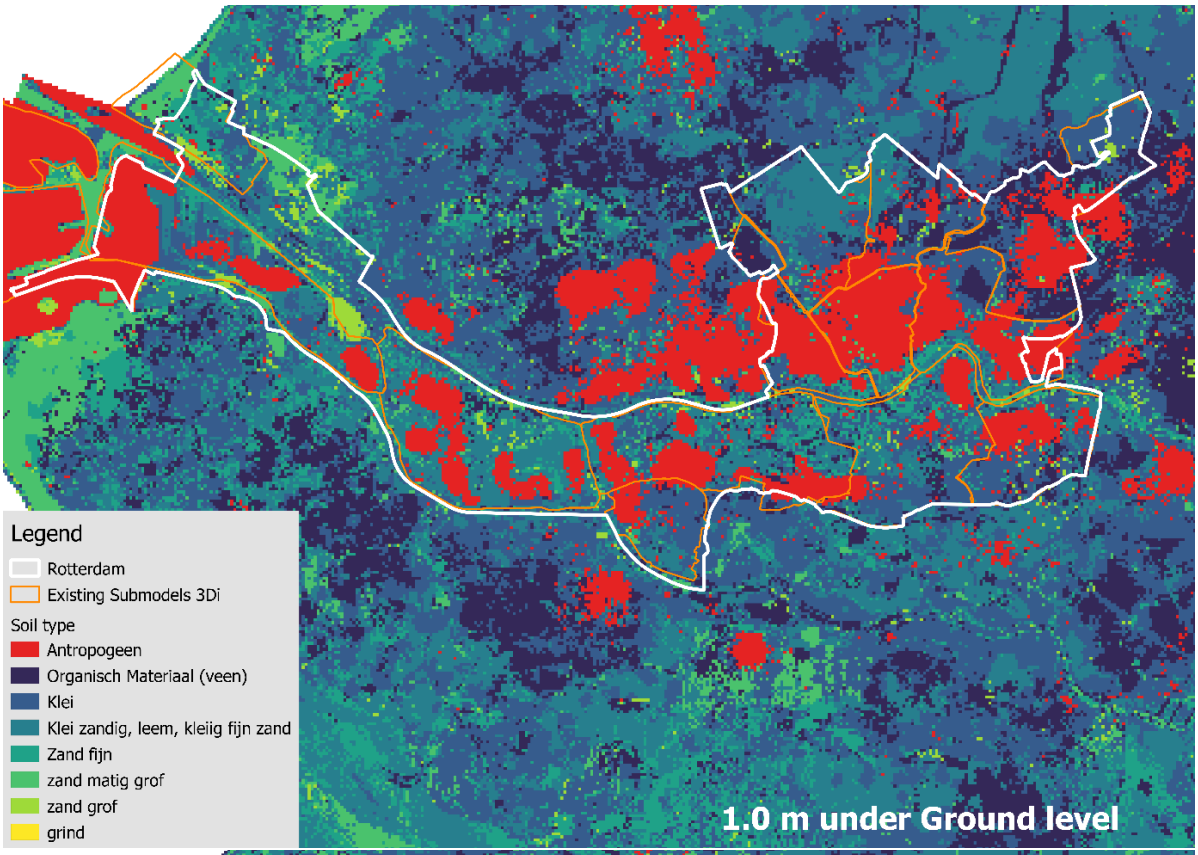
Legend
Rotterdam
Existing Submodels 3Di
Soil type
Antropogeen
Organisch Materiaal (veen)
Klei
Klei zandig, leem, kleiig fijn zand
Zand fijn
zand matig grof
zand grof
grind
1.0 m under Ground level

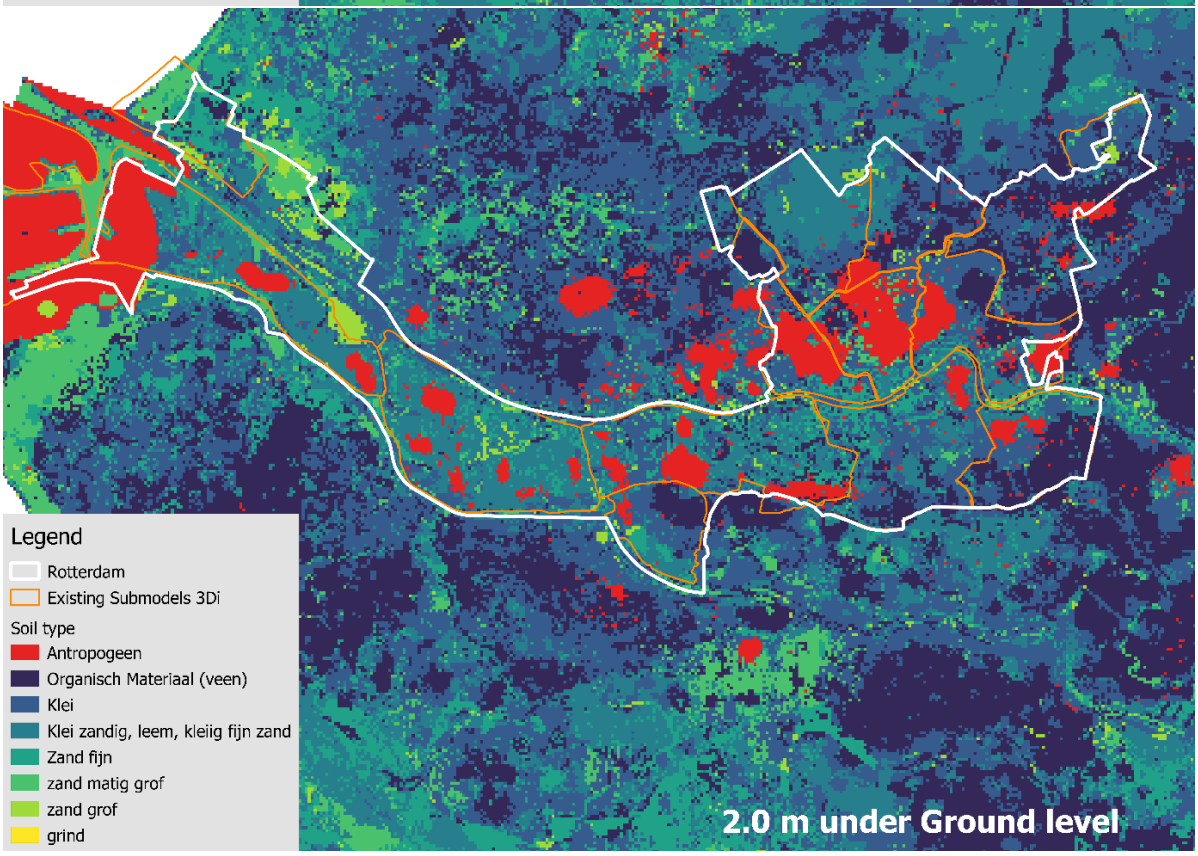
Legend
Rotterdam
Existing Submodels 3Di
Soil type
Antropogeen
Organisch Materiaal (veen)
Klei
Klei zandig, leem, kleiig fijn zand
Zand fijn
zand matig grof
zand grof
grind
2.0 m under Ground level

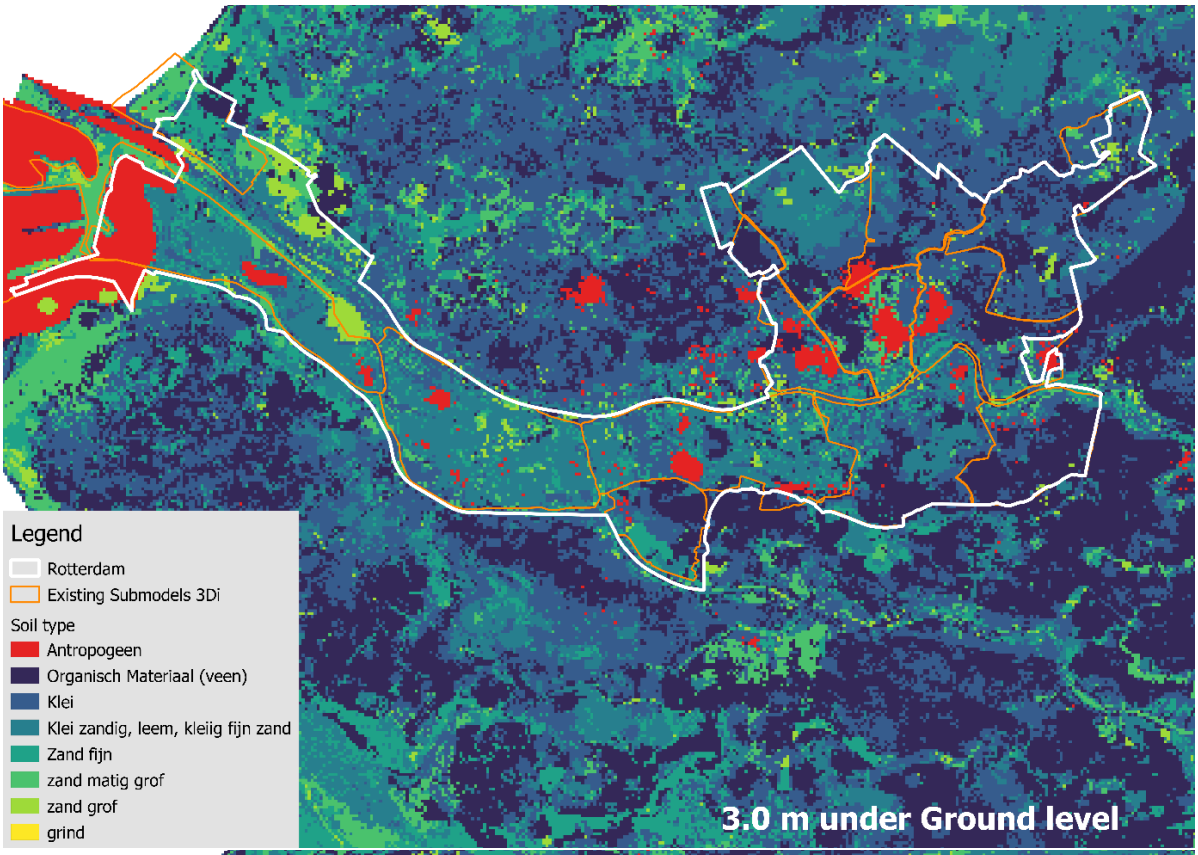
Legend
Rotterdam
Existing Submodels 3Di
Soil type
Antropogeen
Organisch Materiaal (veen)
Klei
Klei zandig, leem, kleiig fijn zand
Zand fijn
zand matig grof
zand grof
grind
3.0 m under Ground level

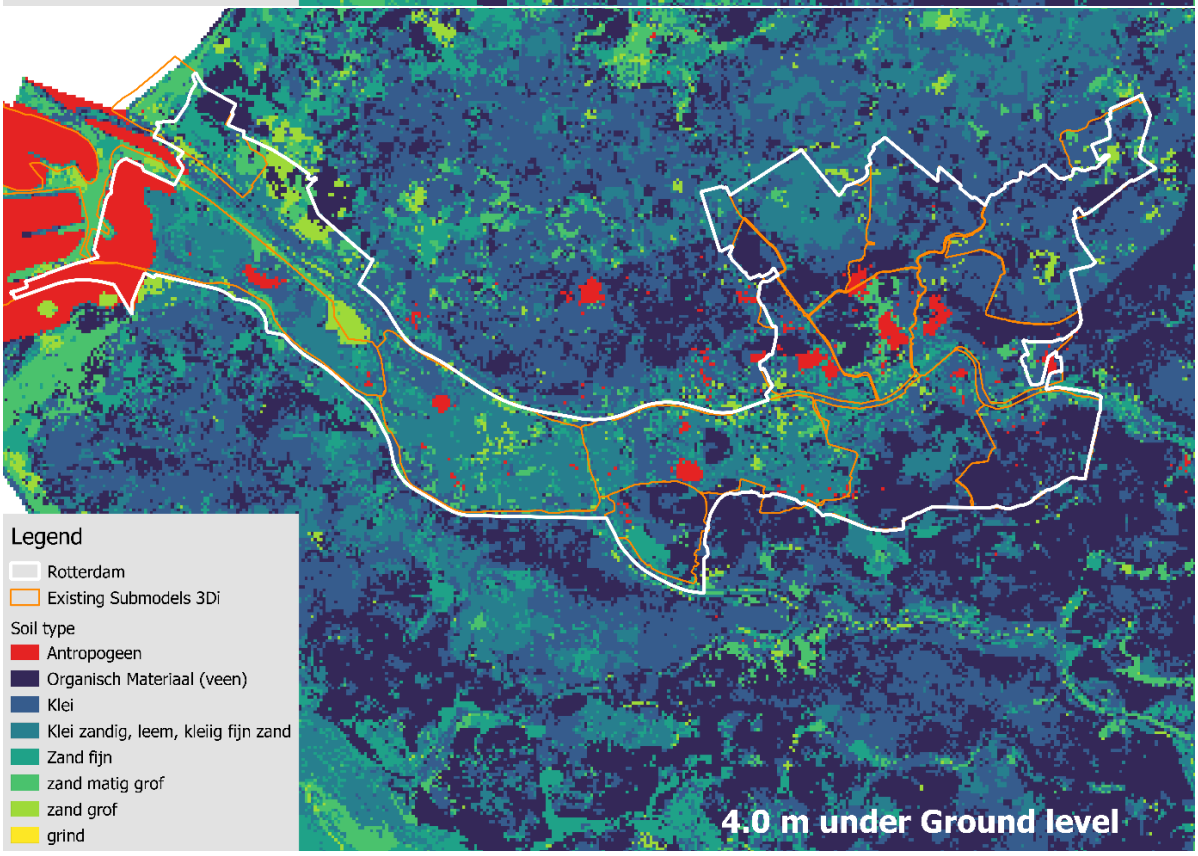
Legend
Rotterdam
Existing Submodels 3Di
Soil type
Antropogeen
Organisch Materiaal (veen)
Klei
Klei zandig, leem, kleiig fijn zand
Zand fijn
zand matig grof
zand grof
grind
4.0 m under Ground level

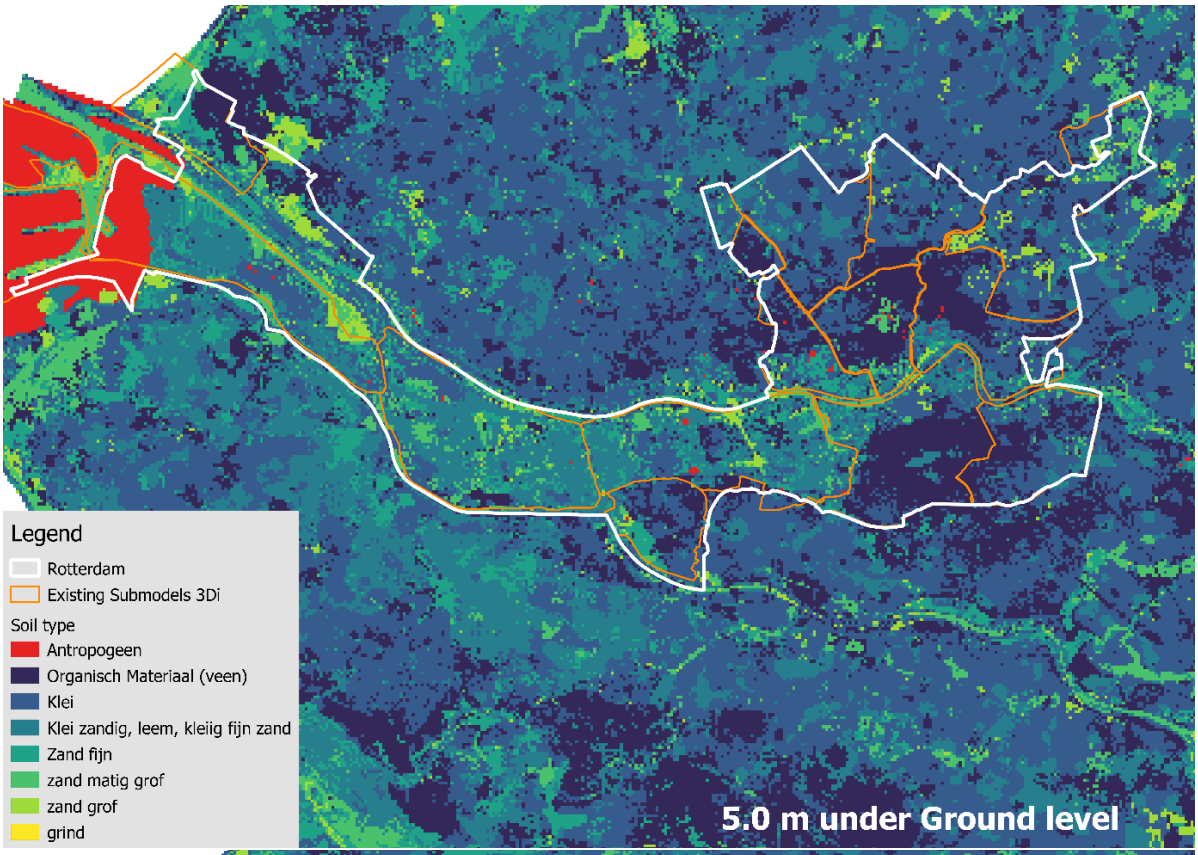
Legend
Rotterdam
Existing Submodels 3Di
Soil type
Antropogeen
Organisch Materiaal (veen)
Klei
Klei zandig, leem, kleiig fijn zand
Zand fijn
zand matig grof
zand grof
grind
5.0 m under Ground level

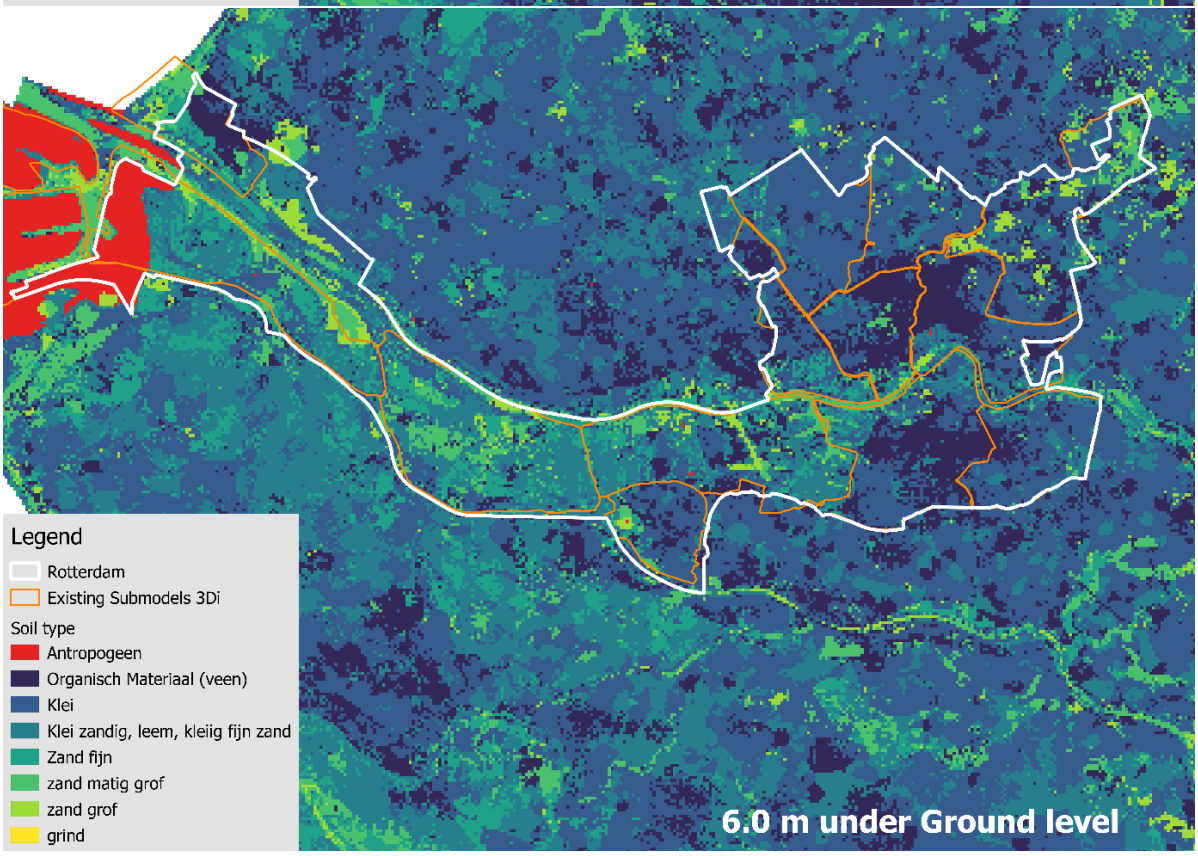
Legend
Rotterdam
Existing Submodels 3Di
Soil type
Antropogeen
Organisch Materiaal (veen)
Klei
Klei zandig, leem, kleiig fijn zand
Zand fijn
zand matig grof
zand grof
grind
6.0 m under Ground level

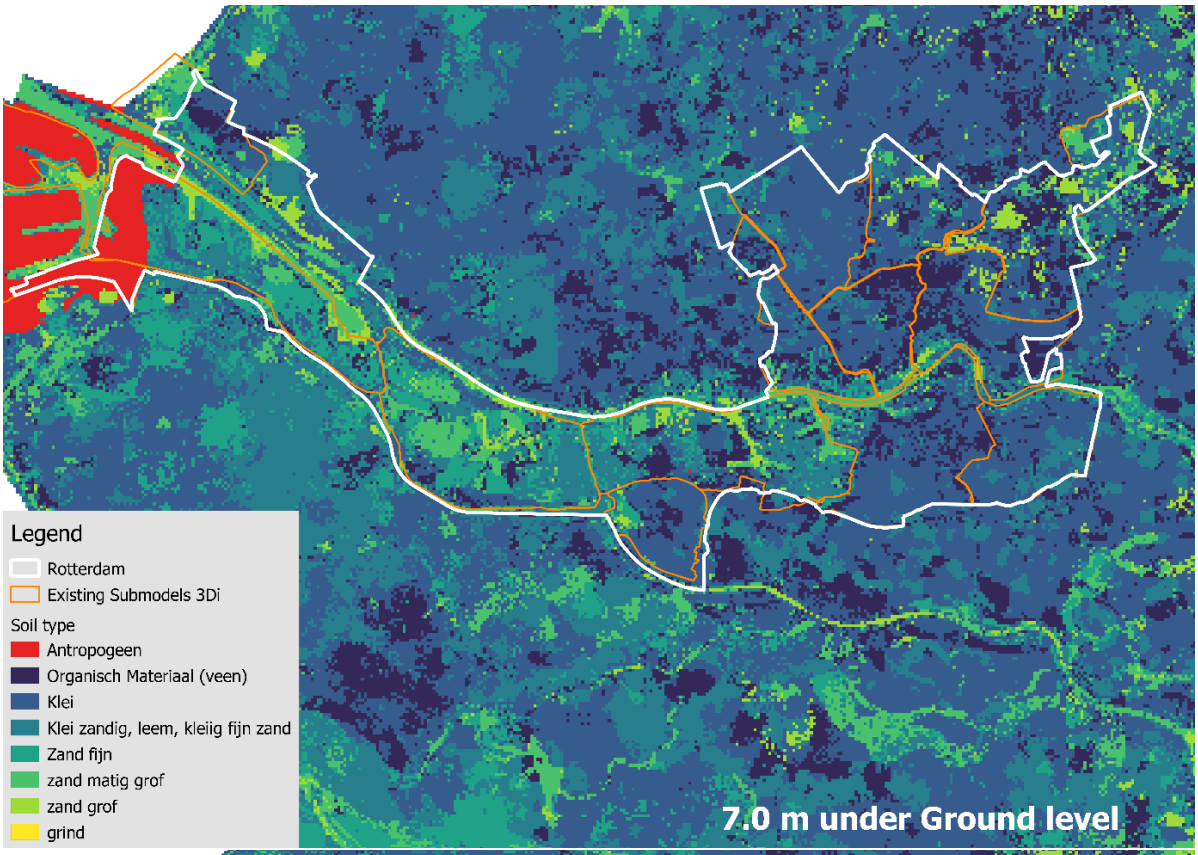
Legend
Rotterdam
Existing Submodels 3Di
Soil type
Antropogeen
Organisch Materiaal (veen)
Klei
Klei zandig, leem, kleiig fijn zand
Zand fijn
zand matig grof
zand grof
grind
7.0 m under Ground level

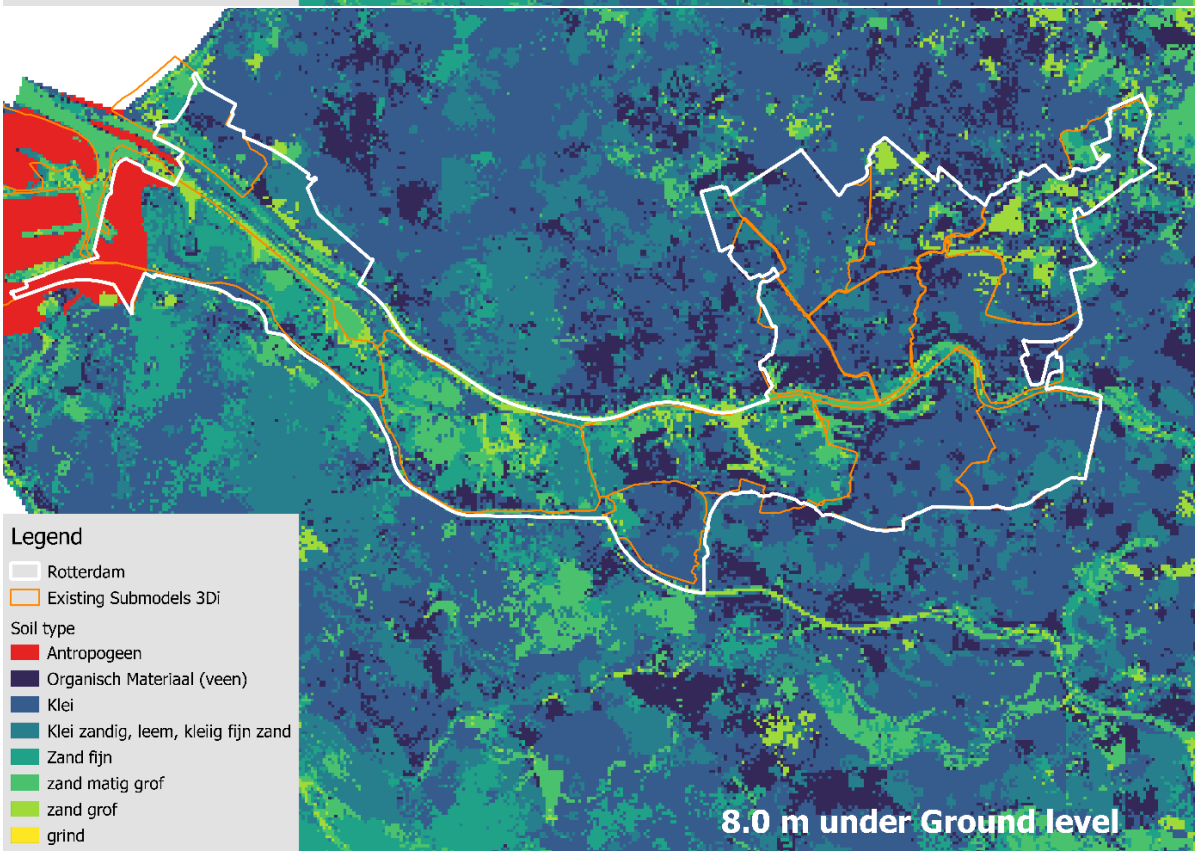
Legend
Rotterdam
Existing Submodels 3Di
Soil type
Antropogeen
Organisch Materiaal (veen)
Klei
Klei zandig, leem, kleiig fijn zand
Zand fijn
zand matig grof
zand grof
grind
8.0 m under Ground level

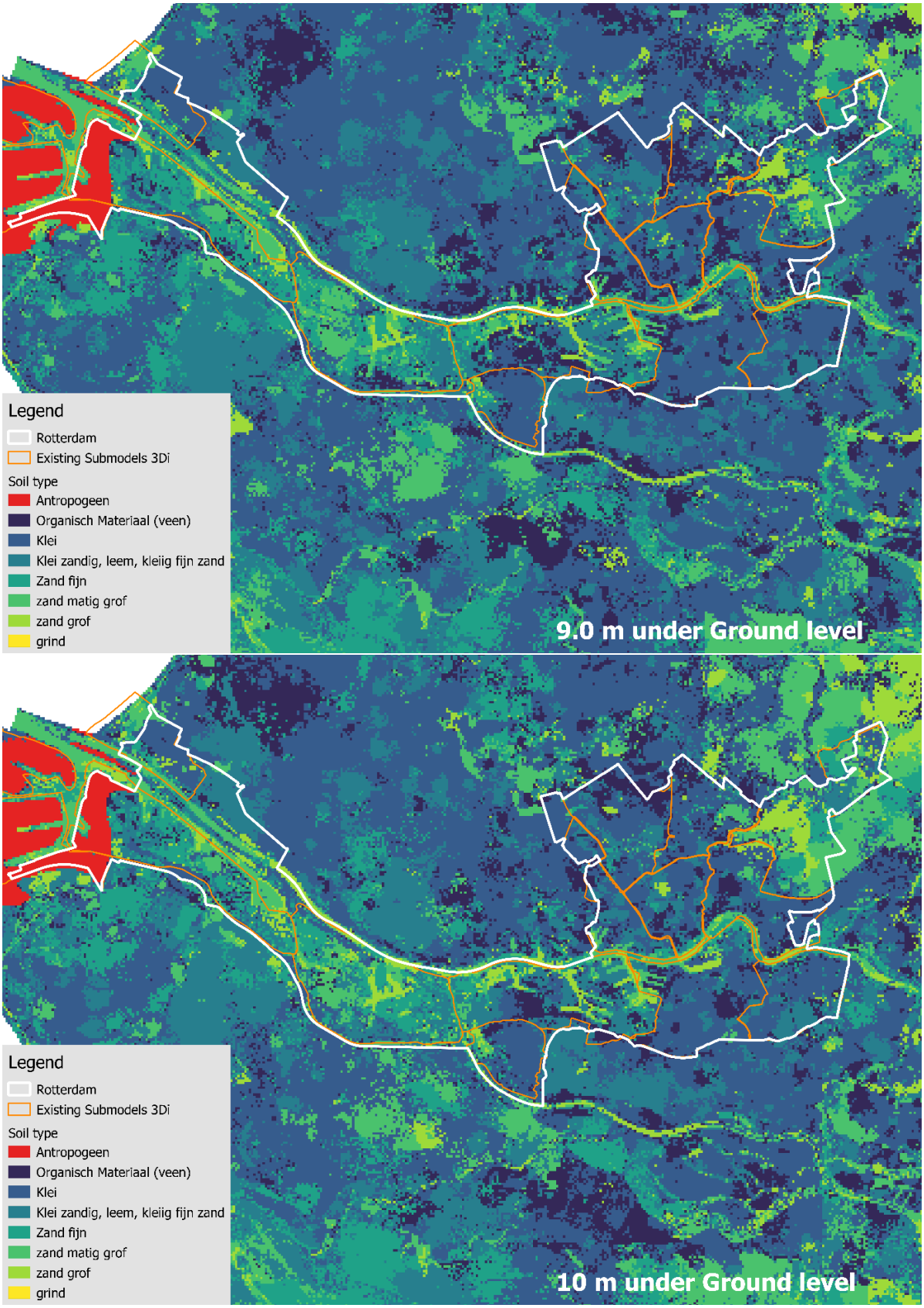

Figure H.1: Subsurface structure until 10 m under ground level of Rotterdam based on GeoTOP, received from Dinoloket (2019)

Subsurface structure of IJsselmonde sub-model based on GeoTOP

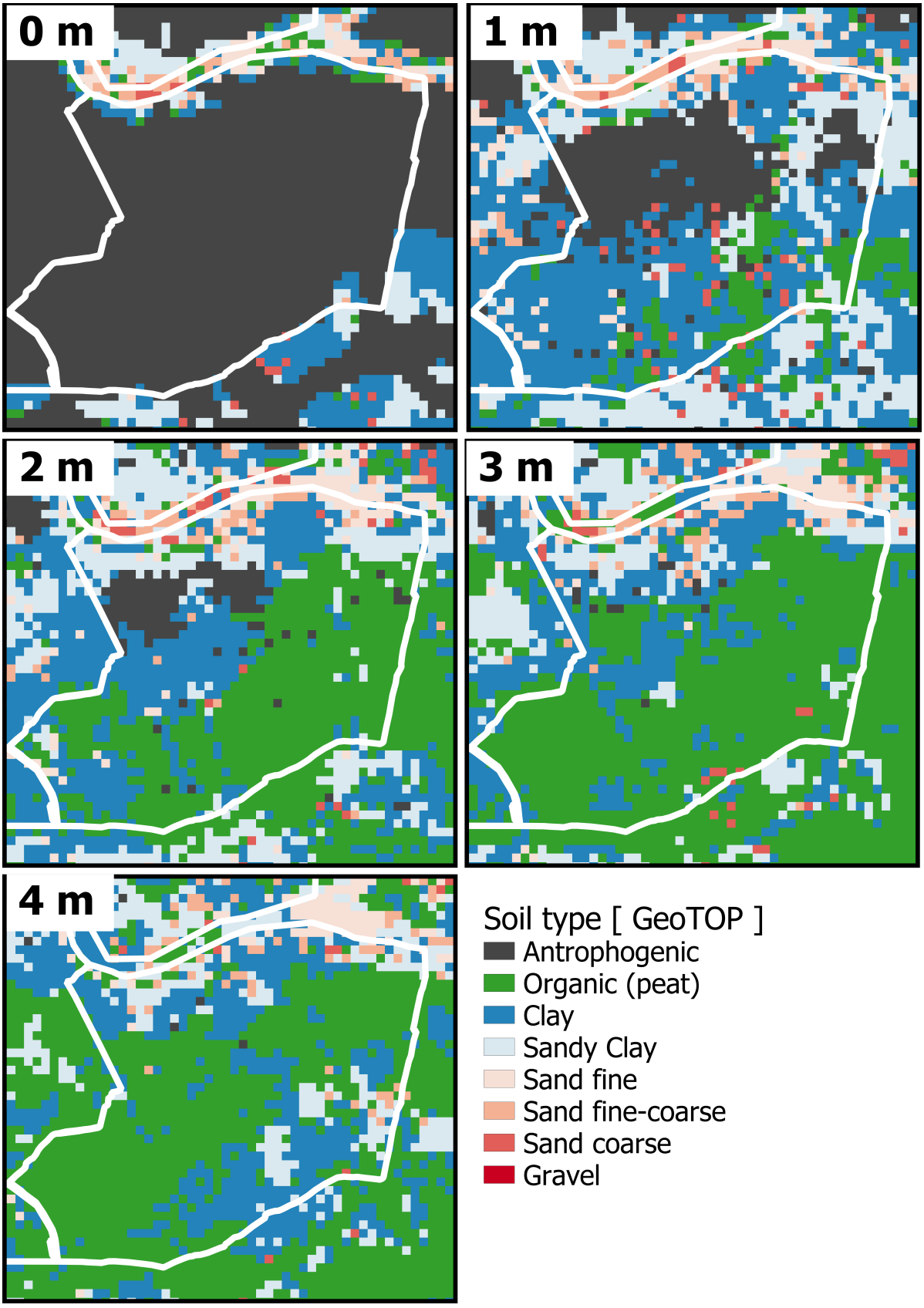
0 m
1 m
2 m
3 m
4 m
Soil type [GeoTOP]
Antrophogenic
Organic (peat)
Clay
Sandy Clay
Sand fine
Sand fine-coarse
Sand coarse
Gravel

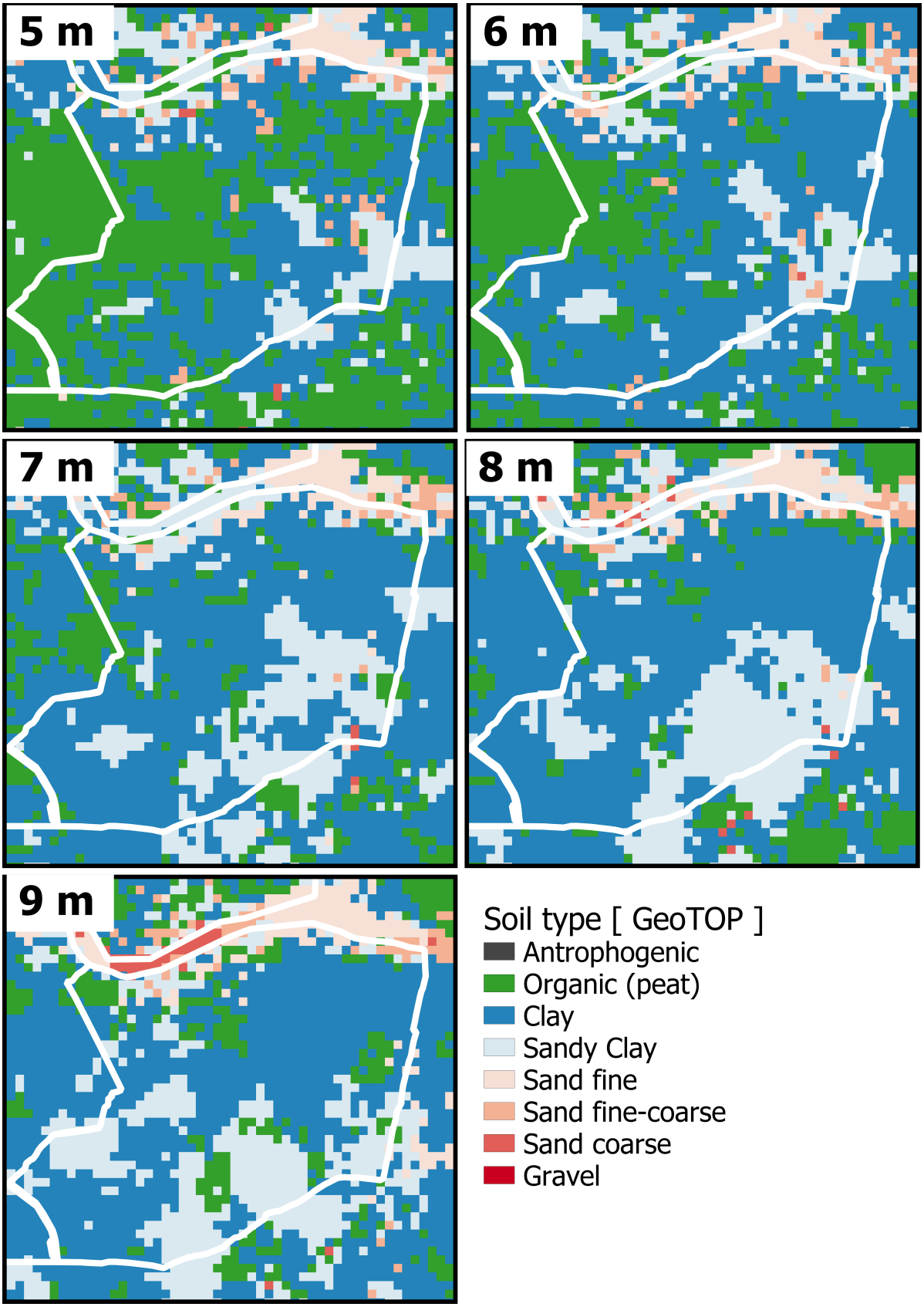
5 m
6 m
7 m
8 m
9 m
Soil type [GeoTOP]
Antrophogenic
Organic (peat)
Clay
Sandy Clay
Sand fine
Sand fine-coarse
Sand coarse
Gravel

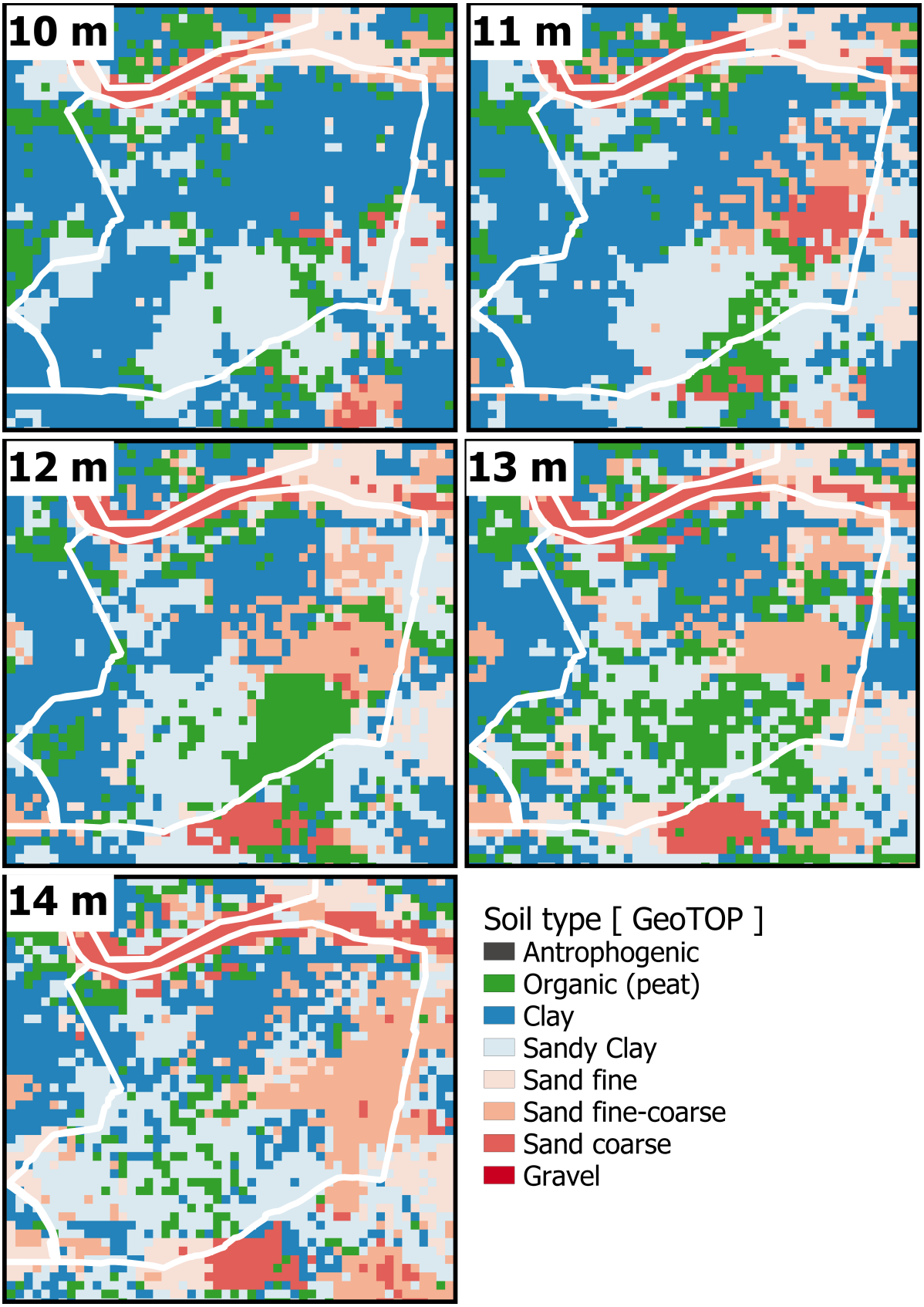
10 m
11 m
12 m
13 m
14 m
Soil type [GeoTOP]
Antrophogenic
Organic (peat)
Clay
Sandy Clay
Sand fine
Sand fine-coarse
Sand coarse
Gravel

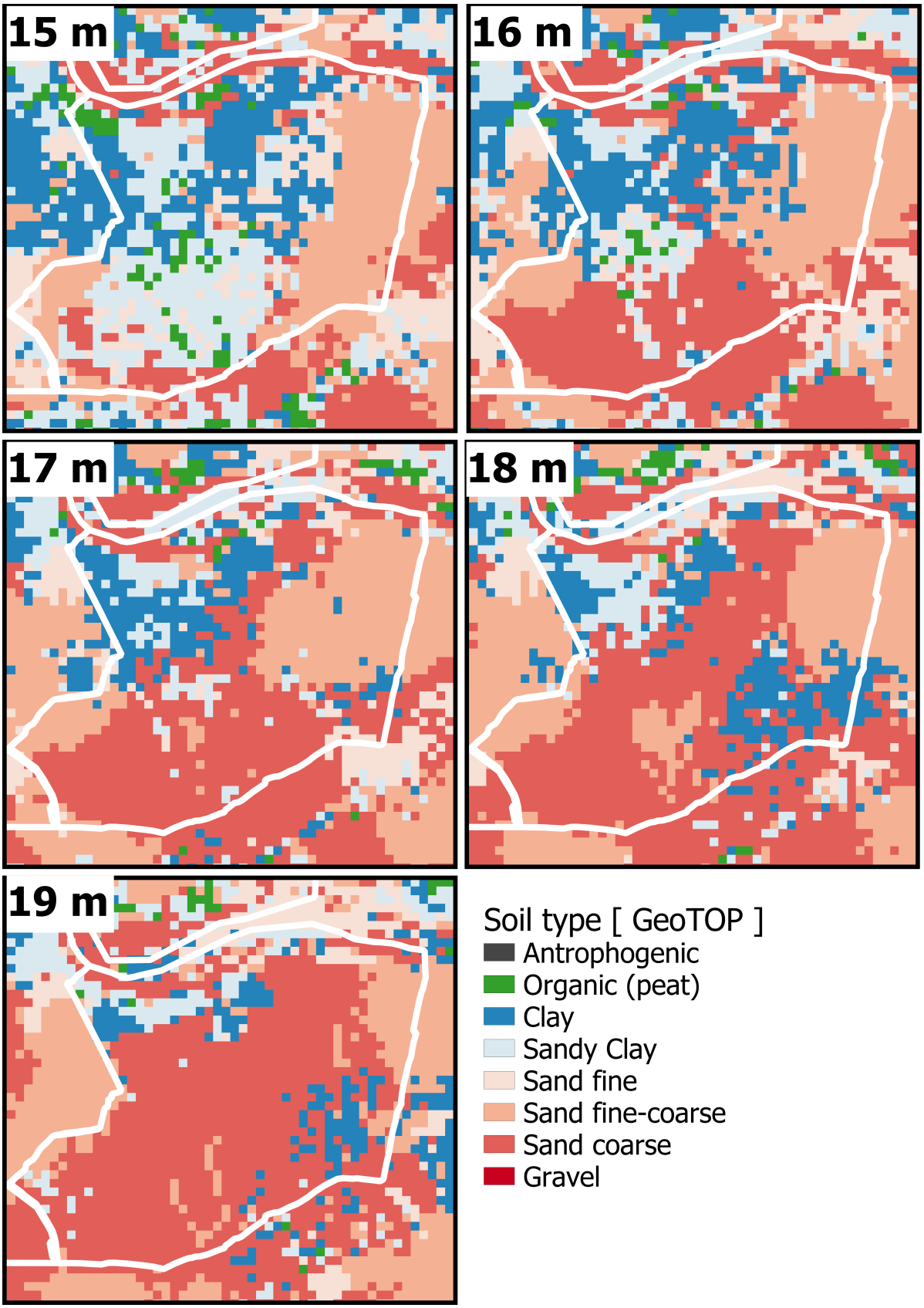

Figure I.1: Subsurface structure until 20 m under ground level of IJsselmonde based on GeoTOP, received from Dinoloket (2019)

J

Ground water monitoring wells in the IJsselmonde sub-model

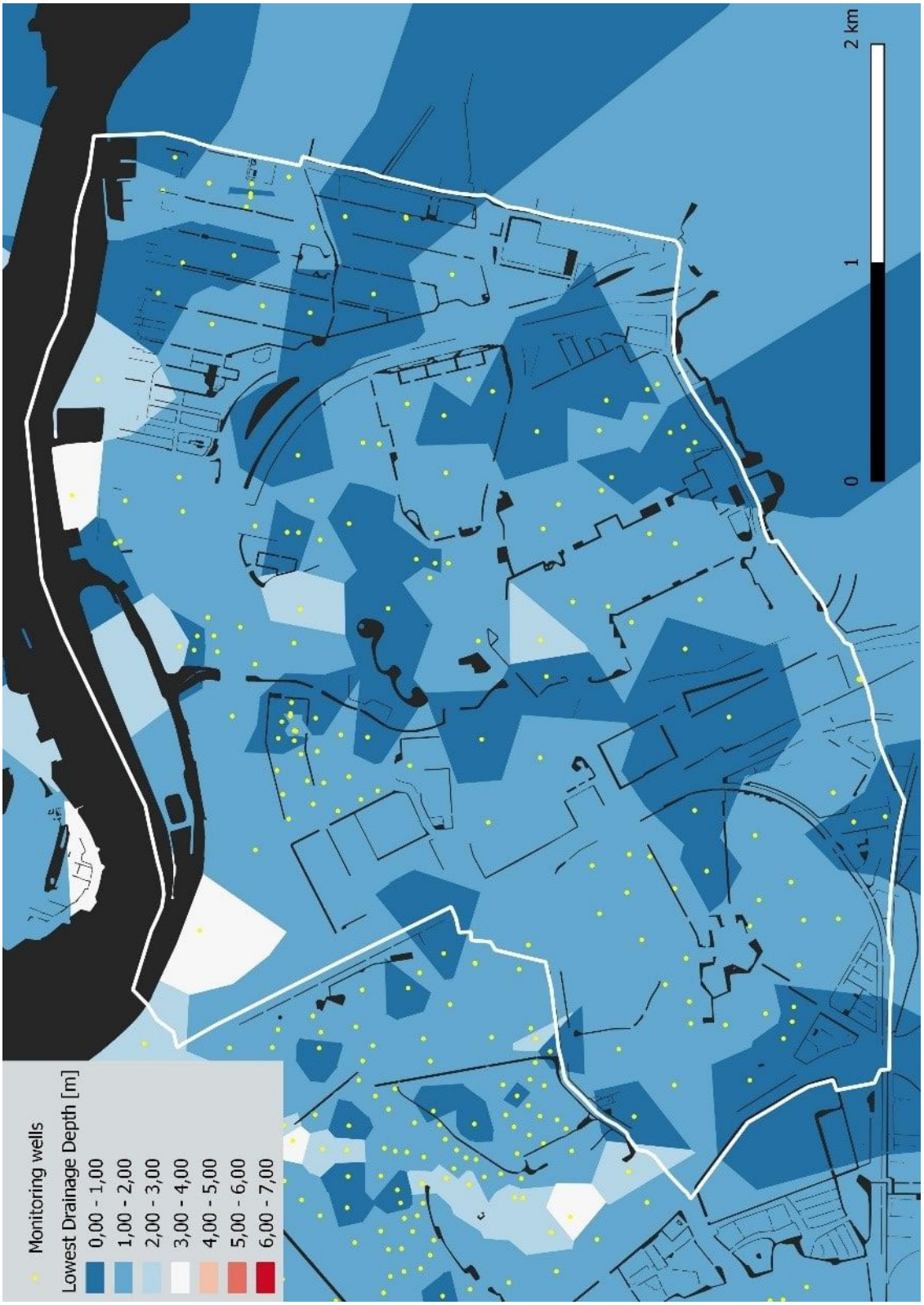

Figure J.1: Interpolated drainage depths in IJsselmonde

K

3Di model lay-out

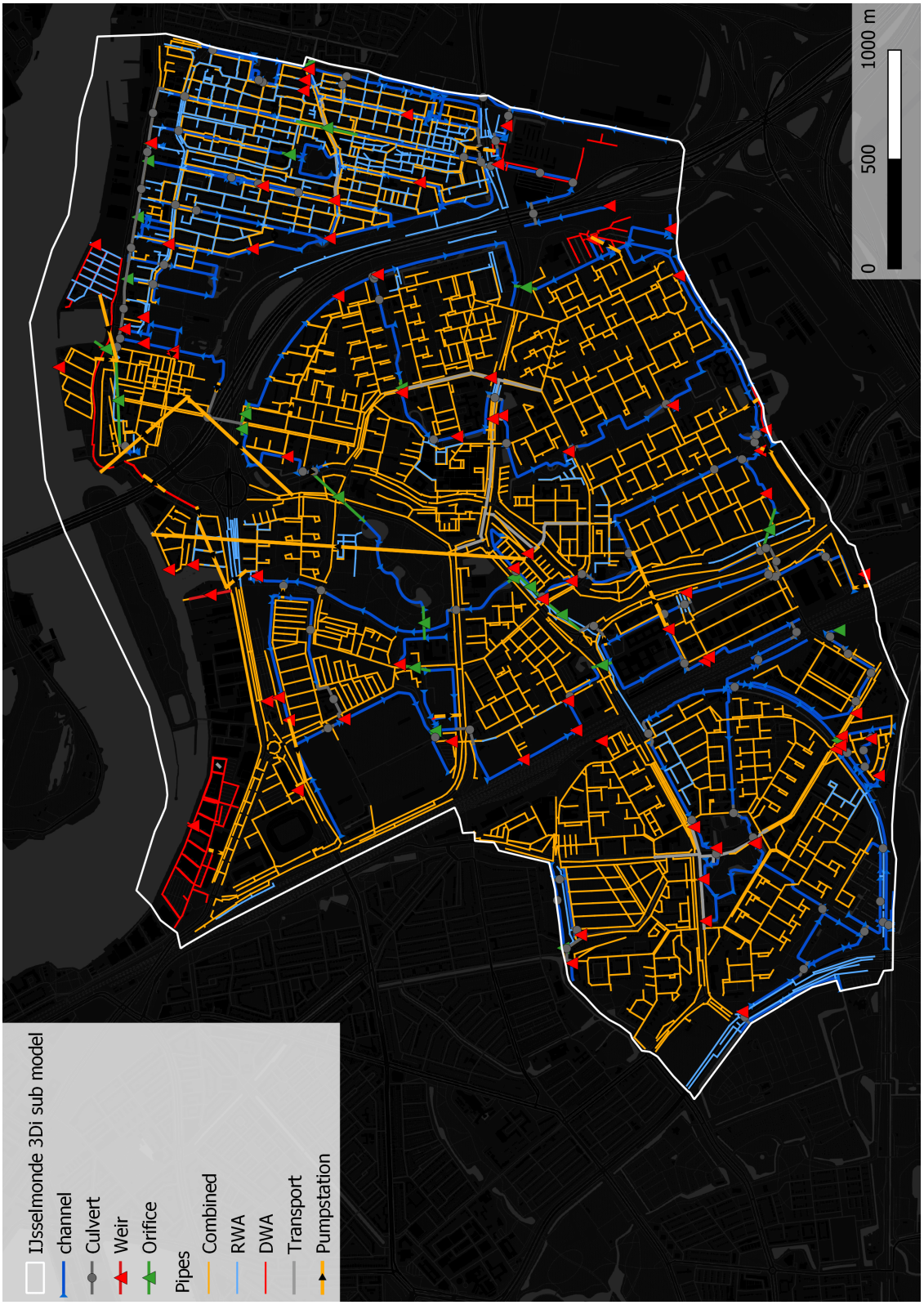

Figure K.1: IJsselmonde 3Di sub-model

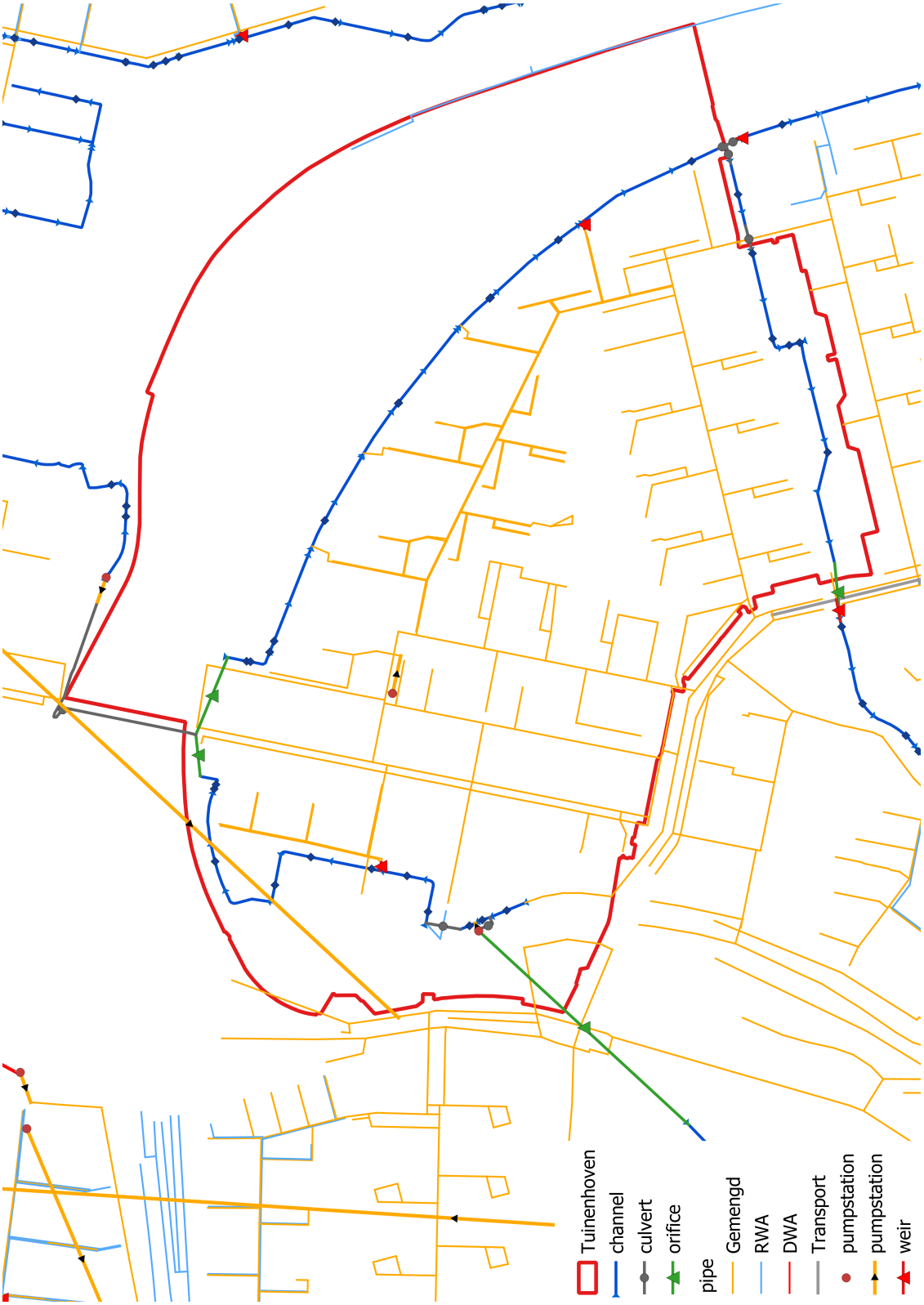

Figure K.2: Tuinenhoven 3Di sub-model

3Di results Tuinenhoven

Maps

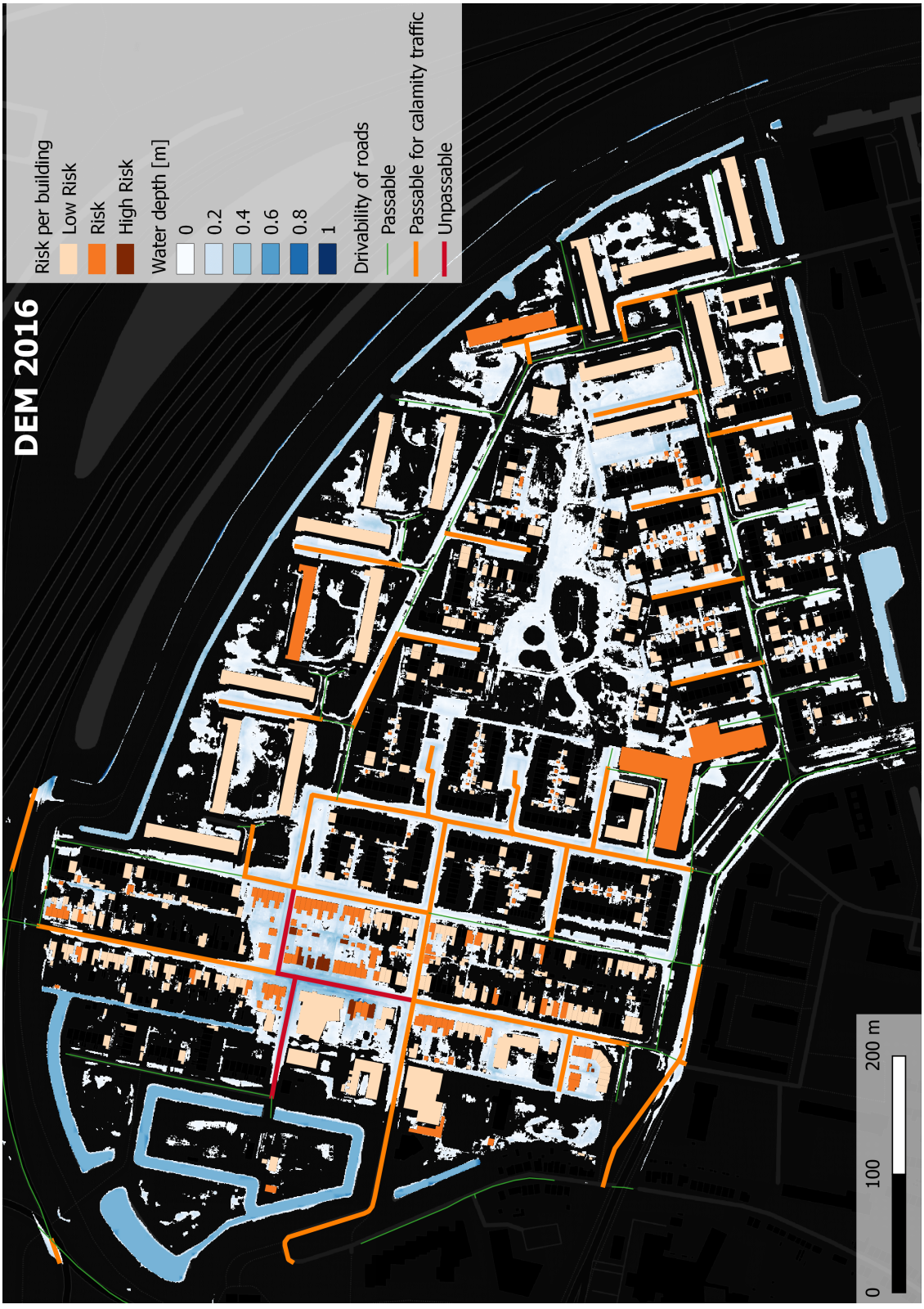

Figure L.1: Results for the 70 mm in one hour rain event simulation for the 3Di model Tuinenhoven based on the DEM of 2016

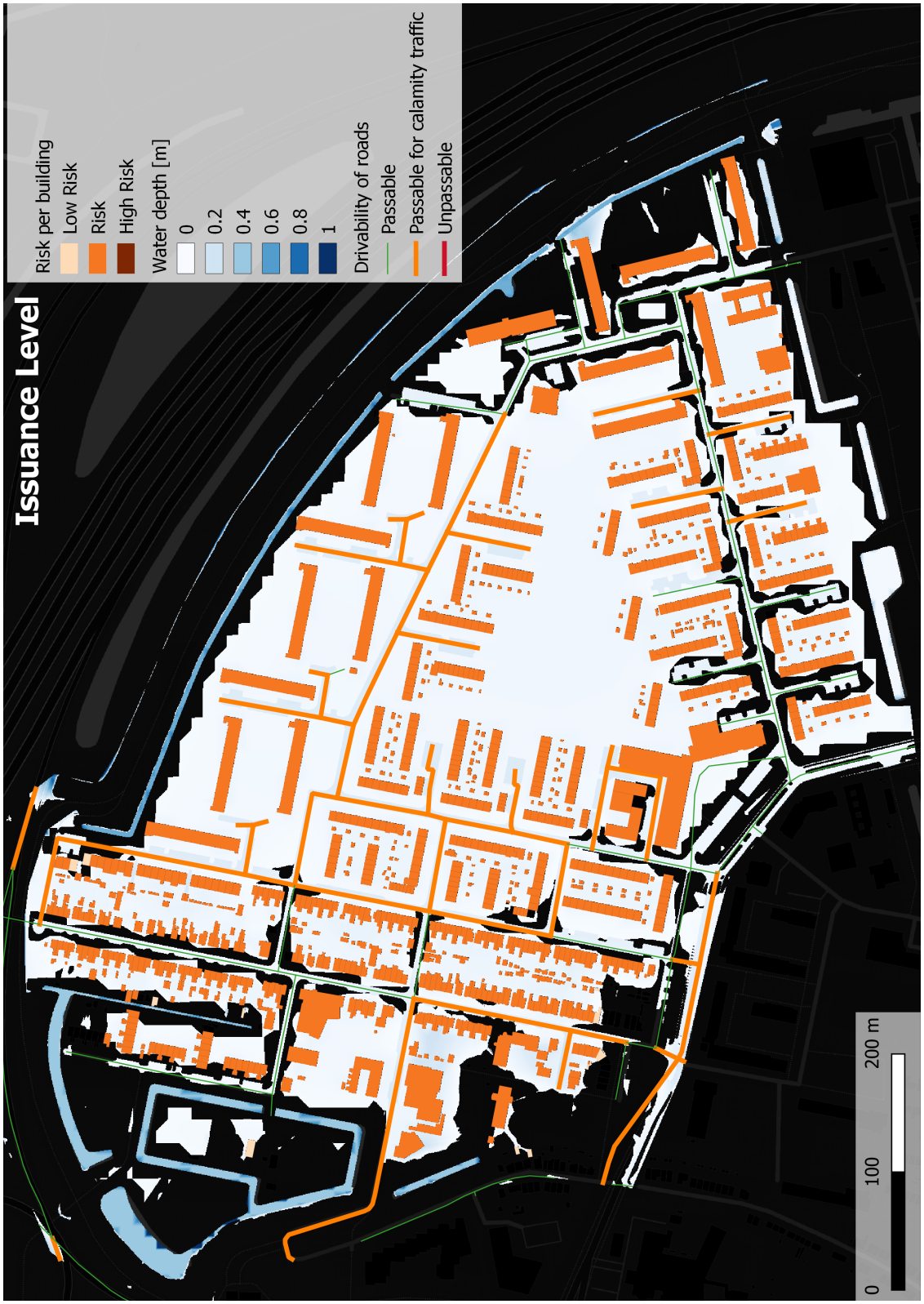

Figure L.2: Results for the 70 mm in one hour rain event simulation for the 3Di model Tuinenhoven based on a theoretical DEM based on issuance level

Overland flow

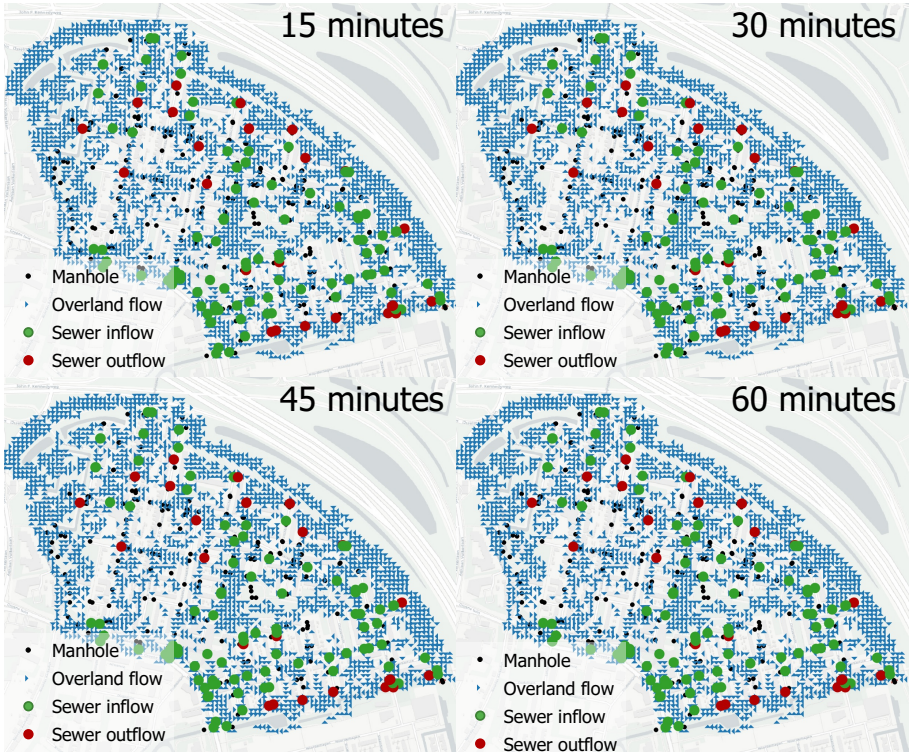

Figure L.3: 2D flow in a 3Di simulation of a 70 mm in one hour rain event simulation for the 3Di model Tuinenhoven based on the 2016 DEM

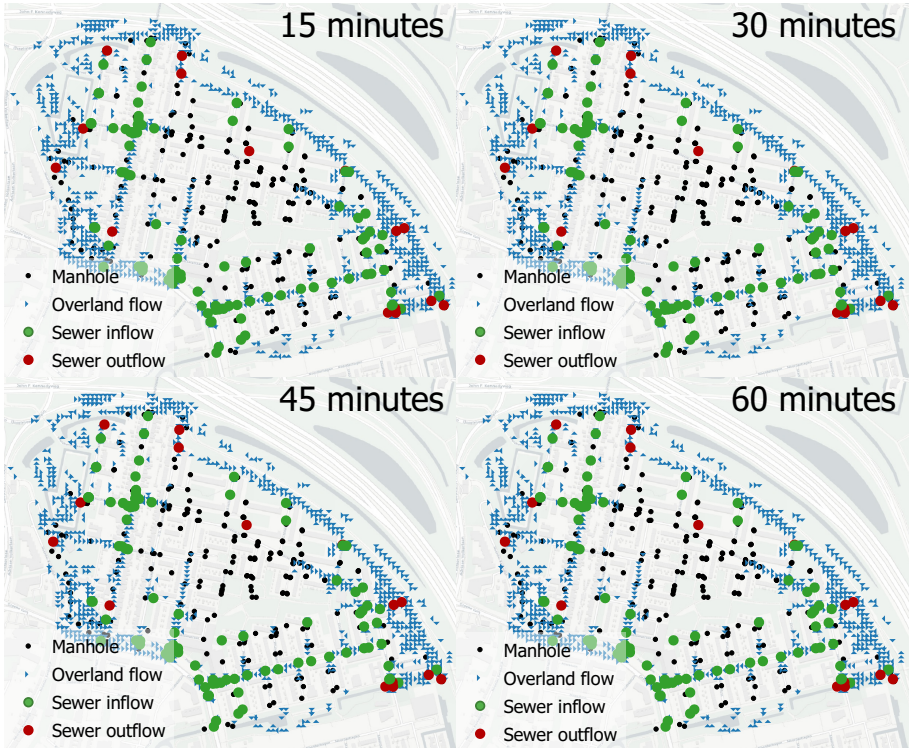

Figure L.4: 2D flow in a 3Di simulation of a 70 mm in one hour rain event simulation for the 3Di model Tuinenhoven based on the design DEM

Passability of Roads

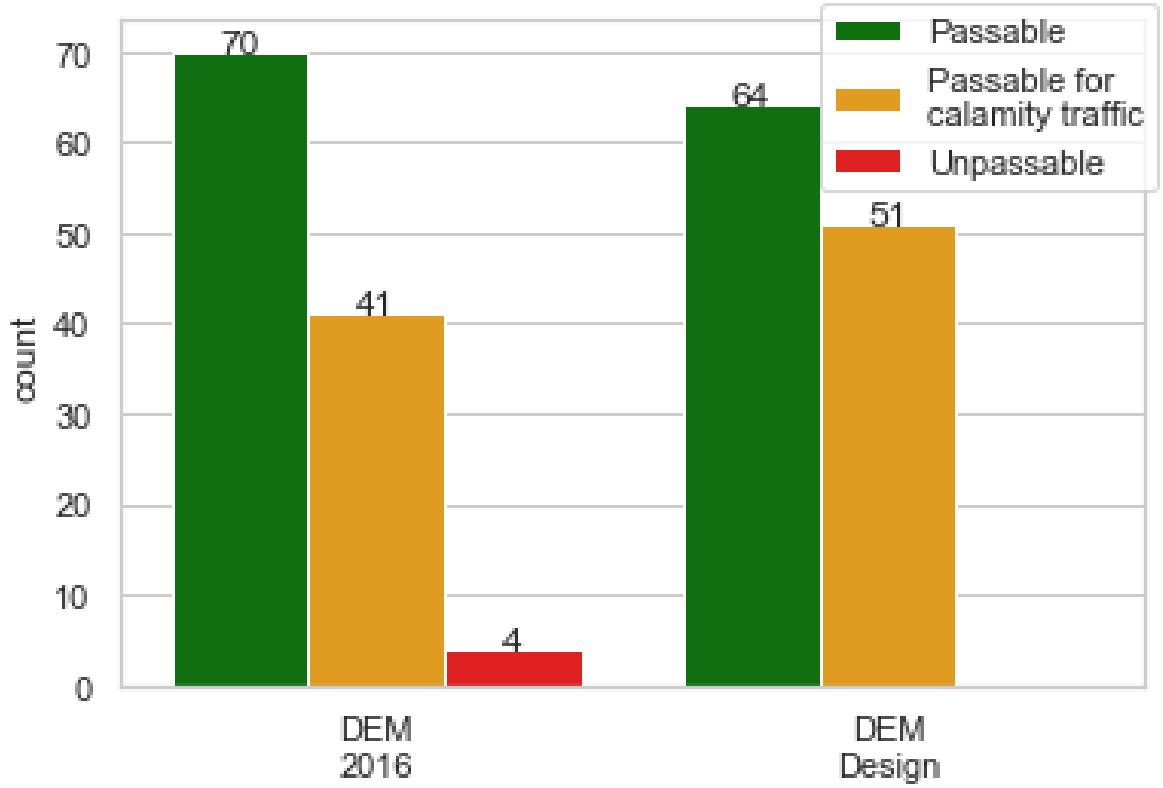

Figure L.5: Passability per road, based on two 3Di simulations of a 70 mm in one hour rain event for the Tuinenhoven sub-model. One simulation is based on a DEM of 2016 and one is based on the fictional DEM that approximates design level.

M

3Di results IJsselmonde

Maps

Figure M.1: Results for the 70 mm in one hour rain event simulation for the 3Di model IJsselmonde based on the DEM of 2016

Figure M.2: Results for the 70 mm in one hour rain event simulation for the 3Di model IJsselmonde based on the theoretical DEM of 2030 excluding maintenance

Figure M.3: Results for the 70 mm in one hour rain event simulation for the 3Di model IJsselmonde based on the theoretical DEM of 2030 including maintenance

Passability of Roads

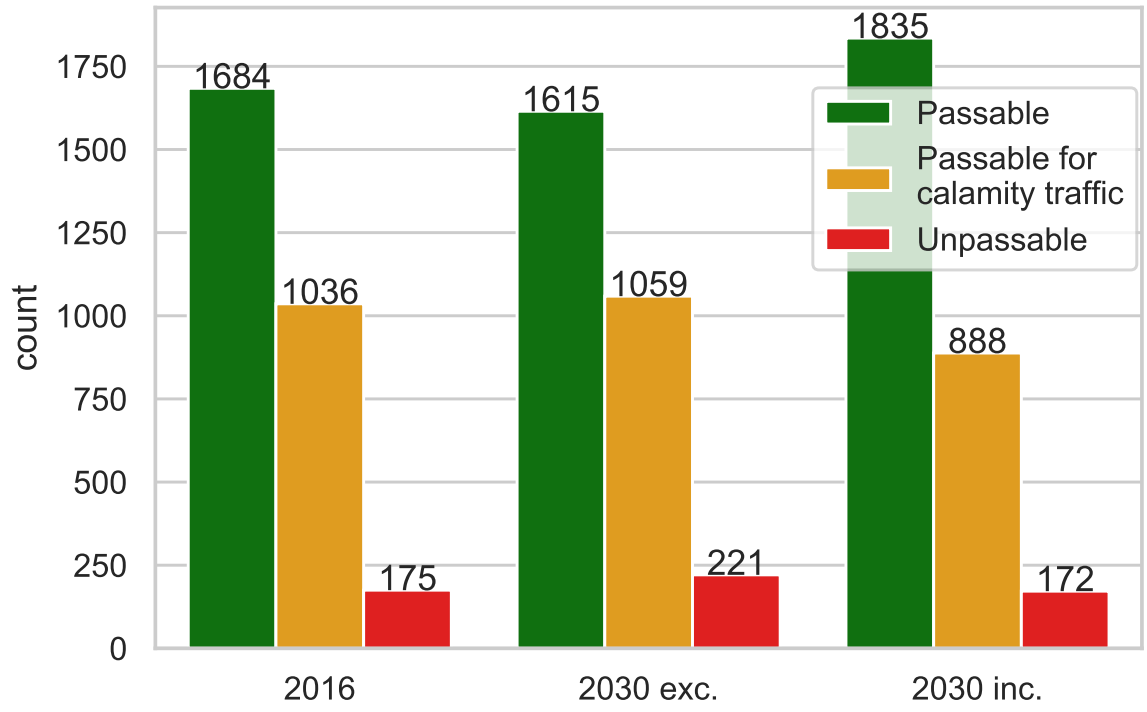

Figure M.4: Passability per roads based three 3Di simulations of a 70 mm in one hour rain event for the IJsselmonde sub-model. One simulation is based on a DEM of 2016, one on the prognosed 2030 DEM excluding maintenance and one on the prognosed 2030 DEM including maintenance.

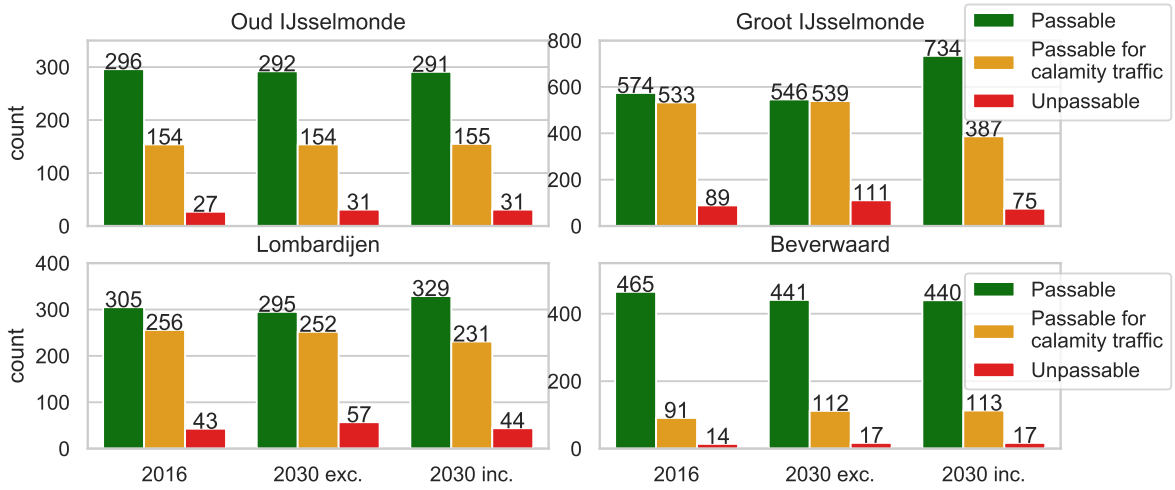

Figure M.5: Passability per roads based three 3Di simulations of a 70 mm in one hour rain event for the IJsselmonde sub-model subdivided per neighbourhood. One simulation is based on a DEM of 2016, one on the prognosed 2030 DEM excluding maintenance and one on the prognosed 2030 DEM including maintenance.

Bibliography

Ahern, M., Kovats, R. S., Wilkinson, P., Few, R., and Matthies, F. (2005). Global Health Impacts of Floods: Epidemiologic Evidence. *Epidemiologic Reviews*.

Allen, A. (1984). No Types of land subsidence. In *Guidebook to Studies of Land Subsidence due to Groundwater Withdrawal*, pages 133–142.

Ashley, R. M., Balmfort, D. J., Saul, A. J., and Blanskby, J. D. (2005). Flooding in the future - Predicting climate change, risks and responses in urban areas. *Water Science and Technology*.

Beckett, P. H. T. and Young, A. (2006). Tropical Soils and Soil Survey. *The Geographical Journal*.

Bunt, M. and Essing, P. O. (2015). Gemeentelijke rioleringsplan, planperiode 2016-2020. Technical report, City of Rotterdam.

Bunt, M. and Zondag, J. (2015). Notitie betreft: Toelichting kaart ontwateringsdieptes en risicofactoren grondwateroverlast. Technical report, City of Rotterdam.

Bürgmann, R., Rosen, P. A., and Fielding, E. J. (2000). Synthesis aperture Radar interferometry to measure Earth's measure earth's surface topology and its deformation. *Annu. Rev. Earth Planet. Sci.*

Casulli, V. (2009). A high-resolution wetting and drying algorithm for free-surface hydrodynamics. *International Journal for Numerical Methods in Fluids*.

Cebeon (2015). Meerkosten gemeenten met een slechte bodemgesteldheid, nadere verfijning maatstaven slappe bodem in gemeentefonds. Technical report.

Chan, F. k. S., Mitchell, G., and Mcdonald, A. (2012). Flood Risk in Asia's Urban Mega-deltas: Drivers, Impacts and Response. *Environment and Urbanization Asia*.

Chen, C. N. and Tfwala, S. S. (2018). Impacts of climate change and land subsidence on inundation risk. *Water (Switzerland)*.

City of Rotterdam (2019). Rotterdams weerwoord, urgentiedocument. Technical report.

Crosetto, M., Monserrat, O., Bremmer, C., Hanssen, R. F., Capes, R., and Marsh, S. (2008). Ground motion monitoring using SAR interferometry: quality assessment. *European Geologist*.

Dahm, R., Hsu, C.-T., Lien, H.-C., Chang, C.-H., and Prinsen, G. (2014). Next Generation Flood Modelling using 3Di: A Case Study in Taiwan. *DSD International Conference*.

Dekker, G., Nootenboom, T., Goedbloed, D., Kaptijn, R., Pieneman, J., Heideveld, M., Boomgaard, M., Kern, D., Heijkers, J., Peerdeman, K., Heijkers, F., GAstkemper, H., Buntrsma, J., and Roeling, A. (2018). Standaardisatie neerslaggebeurtenissen stresstest wateroverlast. Technical report, Ambient.

Delta Program (2017). Delta Programme 2018, Continuing the work on a sustainable and safe delta. Technical report, Ministry of Infrastructure and the Environment & the Ministry of Economic Affairs.

Delta Program (2018). Delta Programme 2019, Continuing the work the delta: adapting the Netherlands to climate change in time. Technical report, Ministry of Infrastructure and Water Management Ministry of Agriculture; Ministry of Interior and Kingdom Relations.

Dieters, M. and Groenendijk, J. (2010). Funderingsaanpak in zes gemeenten. Technical report, DPS group.

Dinoloket (2019). GeoTop model.

Elachi, C. (1988). Spaceborne radar remote sensing: applications and techniques. *IEEE Press, New York*, page 285.

Erkens, G., Bucx, T., Dam, R., De Lange, G., and Lambert, J. (2015). Sinking coastal cities. In *Proceedings of the International Association of Hydrological Sciences*.

Freedman, D. and Diaconis, P. (1981). On the histogram as a density estimator:L2 theory. *Zeitschrift für Wahrscheinlichkeitstheorie und Verwandte Gebiete*.

Funderingsloket (2019). Funderingstypekaart Rotterdam.

Gabriel, A. K., Goldstein, R. M., and Zebker, H. A. (1989). Mapping small elevation changes over large areas: differential radar interferometry. *Journal of Geophysical Research*.

Gaitan, S., van de Giesen, N. C., and ten Veldhuis, J. A. (2016). Can urban pluvial flooding be predicted by open spatial data and weather data? *Environmental Modelling and Software*.

Gambolati, G. and Teatini, P. (2015). Geomechanics of subsurface water withdrawal and injection. *Water Resources Research*.

Glopper, R. D. and Ritzema, H. (2006). Land subsidence. In *Drainage Principles and Applications*, pages 477–512.

Haan, E. D. (1994). *Vertical compression of soils*. Phd thesis, Delft University of Technology.

Hanssen, R. (2003). Subsidence Monitoring Using Contiguous and Ps-Insar : Quality Assessment Based on Precision and Reliability. In *11 th FIG Symposium on Deformation Measurements*.

Hanssen, R. F. (2001). *Radar Interferometry: Data Interpretation and Error Analysis*.

Hauke, J. and Kossowski, T. (2011). Comparison of Values of Pearson's and Spearman's Correlation Coefficients on the Same Sets of Data. *Quaestiones Geographicae*.

Heckens, G. and Engel, W. (2017). Benchmark Inundatiemodellen; Modelfunctionaliteiten en Testbank berekeningen. Technical report, STOWA.

Higgins, S. A. (2016). Review: Advances in delta-subsidence research using satellite methods. *Hydrogeology Journal*.

Hoogland, T., van den Akker, J. J., and Brus, D. J. (2012). Modeling the subsidence of peat soils in the Dutch coastal area. *Geoderma*.

Hoogvliet, M. and van de Ven, F. (2012). Schades door watertekorten en -overschotten in stedelijk gebied. Technical report, Deltares.

KCAF (2019). Over funderingsproblematiek.

Koster, K., Stafleu, J., and Stouthamer, E. (2018). Differential subsidence in the urbanised coastal-deltaic plain of the Netherlands. *Geologie en Mijnbouw/Netherlands Journal of Geosciences*.

Kruiver, P. P., Wiersma, A., Kloosterman, F. H., De Lange, G., Korff, M., Stafleu, J., Busschers, F. S., Harting, R., Gunnink, J. L., Green, R. A., Van Elk, J., and Doornhof, D. (2017). Characterisation of the Groningen subsurface for seismic hazard and risk modelling. *Geologie en Mijnbouw/Netherlands Journal of Geosciences*.

Lambert, J., van Meerten, J., Woning, M., and Eijbersen, M. (2014). Verbeterde onderhoud strategie infrastructuur in slappe bodemgebieden. Technical report, Deltares.

Maccabiani, J. (2014). Factual Report. Technical report, SkyGEO, Rotterdam.

Nelen & Schuurmans (2018). Stresstest extreme neerslag, eindrapportage. Technical report, City of Rotterdam.

Nelen & Schuurmans (2019). 3Di documentation.

O'kelly, B. C. (2005). Sewage sludge to landfill: Some pertinent engineering properties. *Journal of the Air and Waste Management Association*.

Revi, A., Satterthwaite, D. E., Aragón-Durand, F., Corfee-Morlot, J., Kiunsi, R., Pelling, M., Roberts, D., and Solecki, W. (2014). 8. Urban areas. In *Climate Change 2014: Impacts, Adaptation, and Vulnerability. Part A: Global and Sectoral Aspects. Contribution of Working Group II to the Fifth Assessment Report of the Intergovernmental Panel on Climate Change*.

Rhynsburger, D. (1973). Analytic Delineation of Thiessen Polygons. *Geographical Analysis*.

Ruxton, G. D. (2006). The unequal variance t-test is an underused alternative to Student's t-test and the Mann–Whitney U test. *Behavioral Ecology*.

Sampson, C. C., Fewtrell, T. J., Duncan, A., Shaad, K., Horritt, M. S., and Bates, P. D. (2012). Use of terrestrial laser scanning data to drive decimetric resolution urban inundation models. *Advances in Water Resources*.

SkyGEO (2018). InSAR Technical Background.

Spekkers, M. H., Clemens, F. H., and Ten Veldhuis, J. A. (2015). On the occurrence of rainstorm damage based on home insurance and weather data. *Natural Hazards and Earth System Sciences*.

Stafleu, J., Maljers, D., Busschers, F., Gunnink, J., Schokker, J., Damrink, R., and Schijf, M. (2012). GeoTop modellering. *TNO Report*, 10991.

Stelling, G. S. (2012). Quadtree flood simulations with sub-grid digital elevation models. *Proceedings of the Institution of Civil Engineers - Water Management*.

Stocker, T. F., Qin, D., Plattner, G. K., Tignor, M. M., Allen, S. K., Boschung, J., Nauels, A., Xia, Y., Bex, V., and Midgley, P. M. (2013). *Climate change 2013 the physical science basis: Working Group I contribution to the fifth assessment report of the intergovernmental panel on climate change*.

Streng, J. and Platteleeuw, R. (2008). Pernis, Effectenstudie bodemdaling extra Gaswinning. Technical report, Ingenieursbureau Rotterdam.

ten Veldhuis, J. A. (2011). How the choice of flood damage metrics influences urban flood risk assessment. *Journal of Flood Risk Management*.

ten Veldhuis, J. A., Clemens, F. H., and van Gelder, P. H. (2011). Quantitative fault tree analysis for urban water infrastructure flooding. *Structure and Infrastructure Engineering*.

Usai, S. and Hanssen, R. (1997). Long time scale INSAR by means of high coherence features. *European Space Agency, (Special Publication) ESA SP*.

USDI (1974). *Earth manual: a guide to the use of soils as foundations and as construction materials for hydraulic structures*. U.S. Dept. of the Interior, Bureau of Reclamation, 2 edition.

van den Born, G., Kragt, F., Henkens, D., Rijken, B., van Bemmel, B., and van der Sluis, S. (2016). Subsiding soils, rising costs: Possible measures against peatland subsidence in rural and urban areas: English summary and Findings. Technical report, PBL Netherlands Environmental Assessment Agency.

van den Brink, L., van Eekelen, H., and Reuvers, M. (2013). Basisregistratie grootschalige topografie Gegevenscatalogus IMGeo 2.1.1. Technical report, Ministry of Infrastructure and Environment.

Van den Hurk, B., Siegmund, P., Klein, A., Eds, T., Attema, J., Bakker, A., Beersma, J., Bessembinder, J., Boers, R., Brandsma, T., Brink, H. V. D., Drijfhout, S., Eskes, H., Haarsma, R., Hazeleger, W., Jilderda, R., Katsman, C., Lenderink, G., Loriaux, J., Meijgaard, E. V., Noije, T. V., Van Oldenborgh, G. J., Selten, F., Siebesma, P., Sterl, A., and De Vries, H. (2014). KNMI ' 14 : Climate Change scenarios for the 21st Century. *Scientific Report WR2014-01, KNMI, De Bilt, The Netherlands. www.climatescenarios.nl*.

van der Meer, W. and van Herck, O. (2016). Op weg naar een water & wegen strategie. Technical report, City of Rotterdam.

van Haaren, B., Veld, A. v. t., and Kemeling, A. (2018). *Effect straatkolken op berekende wateroverlast*. Bsc., Utrecht University.

van Leeuwen, E. (2019). Interview project leader land- and water soil at Gemeente Rotterdam Ingenieursbureau.

van Leijen, F. (2014). *Persistent scatterer interferometry based on geodetic estimation theory*. Phd, Delft Univesity of Technology.

van Wolfswinkel, L. (2019). RasterCaster – Detailed elevation maps in design situations.

van Workum, R., Visser, W., and de Jong, D. (2016). Handleiding funderingsproblematiek voor gemeenten. Technical report, KCAF.

Verruijt, A. (2009). *Grondmechanica*. VSSD Delft, 7 edition.

Volp, N. D., Van Prooijen, B. C., and Stelling, G. S. (2013). A finite volume approach for shallow water flow accounting for high-resolution bathymetry and roughness data. *Water Resources Research*.

Weissgerber, F., Colin-Koeniguer, E., Nicolas, J. M., and Trouvé, N. (2017). 3D monitoring of buildings using TerraSAR-X InSAR, DInSAR and PolSAR capacities. *Remote Sensing*.

Westra, S., Fowler, H. J., Evans, J. P., Alexander, L. V., Berg, P., Johnson, F., Kendon, E. J., Lenderink, G., and Roberts, N. M. (2014). Future changes to the intensity and frequency of short-duration extreme rainfall.

Wezenberg, S., Leicher, M., and Karssenberg, D. (2016). *Pluvial flood damage estimation in the urban context , assessment of the Waterschadeschatter*. Msc., University Utrecht.

Willems, P. (2013). Revision of urban drainage design rules after assessment of climate change impacts on precipitation extremes at Uccle, Belgium. *Journal of Hydrology*.

Yin, J., Yu, D., and Wilby, R. (2016). Modelling the impact of land subsidence on urban pluvial flooding: A case study of downtown Shanghai, China. *Science of the Total Environment*.

Zimmerman, D. W. and Zumbo, B. D. (2007). Rank transformations and the power of the Student t test and Welch t' test for non-normal populations with unequal variances. *Canadian Journal of Experimental Psychology/Revue canadienne de psychologie expérimentale*.

Zweers, S. (2019). Label voor wateroverlast. *Civiele Techniek*, 1/2:p2–3.